

2014

ACTIVITY REPORT



2014
ACTIVITY REPORT

© 2015 ALBA SYNCHROTRON. All rights reserved.

ALBA Synchrotron
Ctra. BP 1413, km. 3,3 08290
Cerdanyola del Vallès (Barcelona)
Spain
Tel. +34 93 592 4300
www.albasynchrotron.es

Graphic design: Lucas Wainer

INDEX

06	FOREWORD
08	THE ALBA SYNCHROTRON
10	2014 IN ALBA
12	PHASE-II BEAMLINES
	SCIENTIFIC RESULTS
14	BIOSCIENCES
21	CATALYSIS
24	MAGNETISM
31	MATERIALS SCIENCE
39	INDUSTRIAL LIAISON OFFICE
	ACTIVITY REPORTS
42	ACCELERATOR
47	ENGINEERING
52	COMPUTING AND CONTROLS
57	HEALTH AND SAFETY
61	COLLABORATION WITH EXTERNAL INSTITUTIONS
64	STUDENT TRAINING ACTIVITIES
66	WORKSHOPS AND SEMINARS
68	COMMUNICATIONS AND OUTREACH
72	FACTS & FIGURES

FOREWORD

Dear reader,

Let me introduce you to the ALBA Activity Report dedicated to 2014, a year in which the main activity of our staff has been the consolidation of the user operation visiting our day-one beamlines, together with the start-up of the Phase II beamlines, and the definition of the Phase III which draws the near future of the facility.

ALBA is nowadays offering Photoemission Spectroscopy, including a NAPP station, Soft X-ray full-field Microscopy, Macromolecular Crystallography Diffraction, High Resolution SAXS and WAXS, Powder Diffraction including High Pressure Station, EXAFS and XANES, Circular Magnetic Dichroism and Resonant Magnetic Diffraction. In the report you can read through a few of the main scientific highlights chosen among the many results hereon obtained.

A single user call has been opened this year, as we have done since the start-up of the operation in 2012, while from 2015 on we are offering biannual user calls. We have increased the number of operating hours to 5700, with a good availability, over 96%. The number of proposals has increased with respect to last year, and especially the international percentage is constantly growing, trend confirmed also in the first user call for 2015, which was closed last autumn. This behaviour confirms us that our instruments are competitive in the synchrotron radiation community, and that the user services have become mature. The original technical and strategic choices, together with the development and consolidation of instrumentation and services, and the maintenance plans are the reason for these excellent results. Special attention has also been paid to keep improving all aspects of Health and Safety in our activity, promoting awareness on the importance of engaging everybody.

Our Industrial Liaison office activity has focused on providing support to usual and new users, on communicating to industrial representatives the opportunities that ALBA instruments can offer in terms of R&D (the first industrial workshop, dedicated to the chemistry industry, was a success in terms of participation, well above the expectations), and on assisting all divisions in their technology transfer activities.

Top-up injection mode has been implemented and offered to users since June. This is an important step which provides excellent stability both in the accelerator systems and in the beamlines, with constant photon flux and thermal load. The electron beam current has not yet reached the nominal value since we have privileged beam availability over peak current, while waiting for the completion of the critical elements review, in particular the

radio frequency powering system. We expect to be able to increase the current by next year.

The Phase II Beamline programme started in 2014 with the construction of MIRAS, a beamline dedicated to infrared spectro-imaging, and LOREA, dedicated to low-energy angular resolved photoemission with ultra-high resolution. This programme had suffered a delay of a few years in coincidence with the austerity policies, which are now slowly changing.

The Phase III process, already initiated in autumn 2013 with a user interest survey, has produced during 2014 six excellent proposals for new beamlines, which, together with other infrastructure upgrades, shape the ALBA Phase III programme. The proposals have been positively evaluated by the Scientific Advisory Committee. At the time of writing this, negotiations with the administrations are under way in order to secure the needed funding.

Explaining our activities to the society is one of our tasks, which we all accomplish with enthusiasm. Our Communication Office, sheltered by a significant part of the staff, is spreading the principles of our science, and its repercussion in everyday life in different environments. An example is the outreach activity organised on the occasion of the International Year of Crystallography for the European Researchers' Night, and of course the Open Day, when the number of visitors is limited only by our reception capacity.

Our staff is multicultural, with people from all over the world, and the international representation is particularly high among the scientists dedicated to the different beamlines. This fact, together with the collaboration with several national and foreign research institutions and universities, creates an international and open environment, stimulating and interesting, for the development of new technologies and the advancement of new ideas.

CATERINA BISCARI
Director





THE ALBA SYNCHROTRON

ALBA IS THE SPANISH 3RD GENERATION SYNCHROTRON LIGHT SOURCE, LOCATED IN Cerdanyola del Vallès, near Barcelona, and constitutes the largest scientific infrastructure in the country. The facility consists of the accelerator systems providing a 3 GeV electron beam and several experimental beamlines, with photon energy currently ranging from UV to hard X rays of tens of keV. Different techniques of synchrotron radiation utilization are available including diffraction, spectroscopy and imaging.

The ALBA project was approved in 2003 and funded in equal parts by the Spanish and Catalan governments. It is governed by CELLS (Consortium for the Construction, Equipping and Exploitation of the Synchrotron Light Source).

ALBA was built on a green field next to the Universitat Autònoma de Barcelona and several research centres. The construction began in 2006, after a few years dedicated to the design and to the training of a new team of experts, coming from Spain and abroad. The building and the services were ready by 2009, when the accelerator installation started. The whole accelerator was ready and commissioned by 2011, and the seven first beamlines were installed and commissioned in 2011-12. First official users were hosted in 2012, and in 2013 all the Phase I beamlines were operational.

THE ACCELERATORS

The accelerator system consists of a linear accelerator (Linac), where electrons reach 100 MeV, a low-emittance, full-energy Booster, where electrons are accelerated to 3 GeV, and the Storage Ring, where electrons are injected in top-up operation mode. The Booster (250 m of circumference) and the Storage Ring (269 m) are both

hosted in the same tunnel. The lattice is optimized for high photon flux density, with a nominal current of 250 mA. There is a large number of straight sections (24) available, despite the relatively short circumference, thanks to the very compact lattice design, which incorporates quadrupolar field component in the dipoles.

The vacuum chamber has up to 34 windows for light extraction. Eleven of them are presently used (2 for accelerator diagnostics, 9 for the Phase I and Phase II beamlines), and the others witness the great potentiality of ALBA for the future.

THE BEAMLINES

ALBA is in operation since May 2012 with seven beamlines dedicated to different scientific fields, namely physics, chemistry, life sciences, materials science, cultural heritage, biology and nanotechnology. Two new beamlines have been initiated in 2014, devoted to infrared and microspectroscopy with angular resolution. These beamlines are expected to receive friendly users by the end of 2016 and 2018, respectively.

ALBA beamlines can be divided into three groups, according to their scientific applications.

Port	Beamline	Endstations	Experimental techniques	Scientific applications
4	MSPD	2	High-resolution powder diffraction High-pressure diffraction	Structure of materials, Time-resolved diffraction
9	MISTRAL	1	Soft X-ray full-field transmission X-ray microscope. Optimized on the 'water window'	Cryogenic tomography of biological objects. Spatially-resolved spectroscopy
11	NCD	1	High-resolution small- and high-angle X-ray scattering/diffraction	Structure and phase transformations of biological fibres, polymers, solutions. Time-resolved X-ray studies
13	XALOC	1	X-ray diffraction from crystals of biological macromolecules	Macromolecular crystallography, with particular emphasis on large unit cell crystals
22	CLÆSS	1	EXAFS, XANES, Quick-EXAFS	Material science, chemistry, time-resolved studies
24	CIRCE	2	Photoemission microscopy (PEEM) Near-atmospheric-pressure photoemission (NAPP)	Nano-science and magnetic domain imaging (PEEM). Surface chemistry (NAPP)
29	BOREAS	2	Circular Magnetic Dichroism Resonant Magnetic Diffraction	Magnetism, surface magnetism and magnetic structures
01	MIRAS	1	Infrared microspectroscopy	Life sciences, Food sciences, Materials science
20	LOREA	1	Angle-resolved photoemission spectroscopy	Polarized electron spectroscopies, band structure determination

Tab. I List of Phase-I and Phase-II beamlines.

BIOSCIENCES

- MISTRAL, X-ray full-field transmission microscope for cryo-tomography of biological material of high spatial resolution, producing 3D images of complete cells without the need of sample slicing.
- NCD (non-crystalline diffraction) is a SAXS-WAXS (small- and wide-angle X-ray diffraction) dedicated mostly to research of biomaterials, polymers and solutions.
- XALOC is devoted to protein structure determination through X-ray crystallography.
- MIRAS, infrared microspectroscopy beamline, is under construction and will allow studying the vibrational modes of a variety of samples such as organic tissues or cells with lateral resolution.

CONDENSED MATTER, especially magnetic and electronic properties and nanoscience.

- CIRCE, photoemission microscopy for chemical and magnetic imaging of surfaces (PEEM) and photoemission spectroscopy (NAPP) with samples at pressures up to 20 mbar for investigating surface chemical reactions and surfaces of liquid samples.
- BOREAS has two endstations. The first one is dedicated to X-ray magnetic circular dichroism (XMCD) and X-ray magnetic linear dichroism (XMLD) techniques for the study of advanced magnetic materials. The 2nd experimental endstation is dedicated to soft X-ray resonant scattering (SXRS).
- LOREA, Low-energy ultrahigh-resolution angular

photoemission beamline, for the understanding of the electronic structure of advanced materials such as topological insulators, graphene or magnetic surfaces. This beamline is currently at the design stage and will be available for friendly users at the end of 2018.

MATERIALS SCIENCE, with applications in chemistry, environment and cultural heritage, among others.

- MSPD, powder diffraction beamline with two endstations: diffraction under high pressure for analyzing the crystalline structure of matter under extreme pressure (up to 100 GPa) and high resolution to investigate complex crystal structures and high-speed diffraction to study kinetics and phase transformations in materials.
- CLÆSS has two endstations. One is dedicated to absorption spectroscopy (XANES, EXAFS) for analyzing solid samples. The beamline allows acquiring spectra while running catalytic reactions. The second endstation is devoted to X-ray emission spectroscopy and is currently under commissioning.

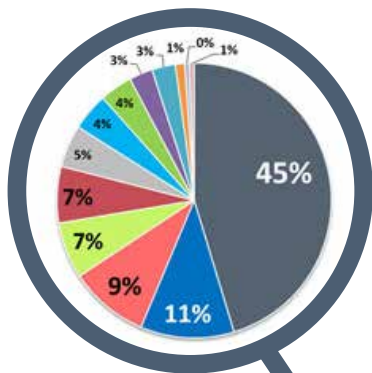
Six additional beamlines have been positively evaluated by the Scientific Advisory Committee: a microfocus beamline for macromolecular crystallography, an instrument-development and innovation beamline, a fast X-ray tomography & radioscopy beamline, a beamline for advanced chiroptical spectroscopies, a submicrometer-beam diffraction, fluorescence and absorption beamline and a surface, interface and resonant diffraction beamline.

2014 IN ALBA

SYNCHROTRON USERS' SURVEY RESULTS

JANUARY

A survey amongst researchers was launched by ALBA and the Spanish Association of Synchrotron Users (AUSE) to know their opinion about the present and future scientific fields of interest of synchrotron-based research.



SELECTING PHASE-III BEAMLINES

MARCH

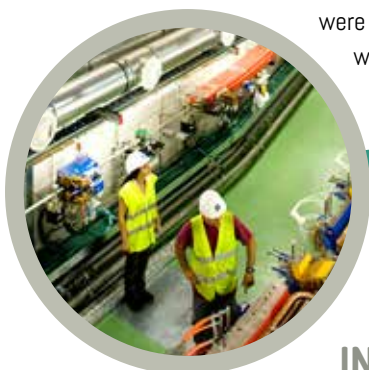
Once the results of the survey were analysed, a workshop with the scientific community was organized to present new proposals for phase-III beamlines. A total of nine proposals were presented during the workshop.



INCREASING NUMBER OF PROPOSALS

FEBRUARY

In the 2014 call for proposals, ALBA received 34% more proposals than in the previous one. 128 proposals out of 250 were granted on the basis of scientific excellence criteria. Most of the accepted experiments belong to Spanish institutions (73%), followed by European ones (25%) and international organizations (2%).



UNDERGRADUATE STUDENT INTERNSHIP PROGRAMME

MAY

ALBA launched a new internship programme for undergraduate students from varied academic profiles: physics and accelerator technologies, scientific applications of synchrotron light, mechanics design, vacuum technologies, electronics, communications and outreach, health and safety, etc.

30 COMPANIES AT THE INDUSTRY WORKSHOP

APRIL

The aim of the workshop was to illustrate the industrial applications of ALBA in the field of Chemistry and Materials Science to the almost 50 registered participants, including renowned companies like CEPSA, ERCROS or AC MARCA group.



ALBA REACHES ITS 1,000TH USER

JUNE

The ALBA Synchrotron welcomed its 1,000th user, Manuel Vázquez, and his colleagues from the Institute of Materials Science of Madrid (CSIC) and the University of Barcelona (UB), who studied the magnetic properties of nanowires to determine their spin configuration at the CIRCE beamline.



ALBA EXPERIMENTS AWARDS

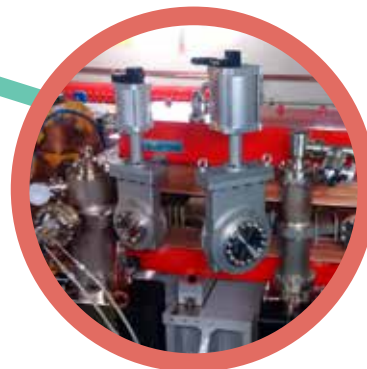
JULY

Second edition of the ALBA Experiments Awards to the best experiment, the best instrumental development and the best publication. The award winners were CIRCE beamline (PEEM endstation), MSPD (powder diffraction endstation) and CIRCE beamline (NAPP endstation), respectively. A ceremony with ALBA staff is to be organized to highlight this recognition.

THE CONSTRUCTION OF PHASE-II BEAMLINES BEGINS

AUGUST

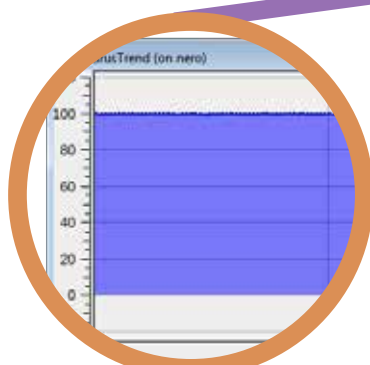
In August 2014, the construction of phase-II beamlines was initiated with the installation of a vacuum chamber with a special aperture for infrared light at the dipole magnet for MIRAS. During the winter shutdown, a tunnel drilling was done to accommodate the emission port of MIRAS while several beamline components were selected. Also, LOREA design works were performed.



ALBA CELEBRATES THE EUROPEAN RESEARCHERS' NIGHT

SEPTEMBER

On September 26th the ALBA Synchrotron organized free outreach activities for all ages to explain what a synchrotron is and which its main applications are. The event was held at the Museum of Art of Cerdanyola del Vallès.



100% BEAM AVAILABILITY IN TOP-UP

OCTOBER

From 28th October to 2nd November, ALBA operated continuously in top-up mode. That was the first week free of trips since ALBA started operating in top-up mode in September.

EVALUATION OF PHASE-III BEAMLINES

DECEMBER

On the 3rd and 4th of December, members of the ALBA Scientific Advisory Committee met at ALBA's premises. In the 19th session of the SAC, the meeting was dedicated to the presentation and evaluation of six beamline proposals to be constructed in phase-III. All six proposals were positively evaluated.





PHASE-II BEAMLINES

IN 2014 ALBA PHASE-II BEAMLINES – MIRAS AND LOREA – HAVE STARTED THEIR CONSTRUCTION AND DESIGN, RESPECTIVELY. THE INFRARED MICROSCOPY BEAMLINE (MIRAS), DEDICATED TO INFRARED SPECTRO-IMAGING, WILL BE A VALUABLE TOOL TO IDENTIFY THE CHEMICAL COMPOSITION OF MATERIALS AT THE MOLECULAR LEVEL. THE LOW-ENERGY ULTRAHIGH-RESOLUTION ANGULAR PHOTOEMISSION BEAMLINE (LOREA) WILL LET US UNDERSTAND THE ELECTRONIC STRUCTURE OF GRAPHENE-BASED MATERIALS, TOPOLOGICAL INSULATORS AND OTHER ADVANCED MATERIALS.

MIRAS

MIRAS, currently at the design and construction stage, will provide ALBA users with a modern infrared microscopy facility covering a wavelength range from 04 to 100 μm , optimized for work in the mid-IR region. However, the design of the beamline will provide significantly enhanced efficiency, compared to a conventional source, in both far-IR and mid-IR regions.

The scientific applications of MIRAS will cover a wide range of research fields, including materials science, archaeology, microanalysis, biochemistry, biomedical diagnostics, etc. The discipline of life sciences will represent the main body of research, with direct impact on the study of disease states. This technique will also be helpful in surface science applications, in particular, the analysis and chemical imaging of thin films and protection layers. In addition, high-pressure studies using diamond anvil cells like those performed in geology, environmental sciences and astrophysics will also benefit from this technique.

The MIRAS project at ALBA was started in 2009. Experimental options in both the far-IR and mid-IR regions were projected with the capacity to address the present and future requirements of the scientific community not only in Spain but

also in the whole of Europe. The project was formally approved in 2010, but was frozen due to the difficult economic situation in the country. However, by the end of 2013 the project was reactivated again, thanks to a close collaboration between staff from ALBA, SOLEIL and the CSIC.

Several actions have been performed during its design and initial construction. Bending magnet 04 of the ALBA Storage Ring was selected, after careful analysis, to become the IR radiation source for the MIRAS beamline. A modified dipole chamber enabling the collection of the IR beam with an acceptance angle of $43 \times 25.17 \text{ mrad}^2$ was installed during the summer shutdown of 2014. The dipole chamber design implements horizontal IR beam extraction geometry using a laterally-inserted flat mirror with a horizontal transverse slot in order to avoid interaction with the central high-energy core of the dipole emissions and thus avoid thermal loading. Only the IR and visible light fraction of the dipole radiation emissions is collected by the mirror and redirected towards the emission port. A high-stability XYZ positioning system for M1 mirror, designed by ALBA engineers in collaboration with colleagues at the SOLEIL SMIS beamline, allows for a crucially accurate positioning of M1 mirror with respect to the dipole emission fan and electron beam (see Fig. 1).

All hardware parts of M1 Extraction will be manufactured in 2015, planning to have them delivered and tested during the

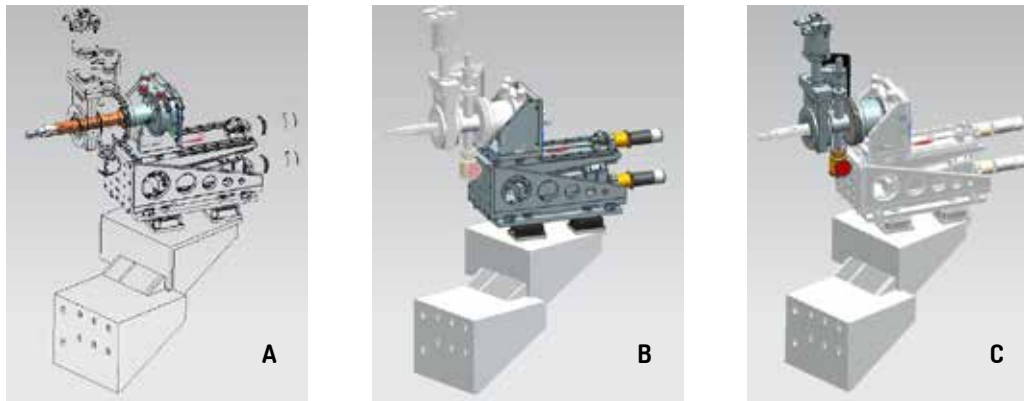


Figure 1. 3D model of the IR extraction mirror assembly for the MIRAS beamline, highlighting, from left to right, the extraction mirror itself (a), XYZ positioning stage (b), and the vacuum interface with the dipole magnet chamber (c).

first half of the 2015 summer with subsequent installation in the dipole chamber during the summer shutdown period.

After its extraction, the IR beam is transported through an optical train of 1:1 symmetrical imaging scheme to the first endstation inside the MIRAS experimental hutch in the hall. It is scheduled to have the MIRAS experimental hutch erected and functional during 2015. The design of the experimental hutch foresees two more downstream endstations as a near-future upgrade of the MIRAS beamline. One of them is projected as a customizable platform for the experiments with user-supplied equipment under the BYOD (Bring Your Own Device) policy.

The optical design of MIRAS includes the option for splitting IR beam in two parts, separating the dipole emission and edge radiation fractions of the IR beam. This allows either to use them separately at different endstations or to deliver both fractions to the same endstation. At the end of the transport chain, a confocal scanning system will deliver a beam of approximately 1000x the brightness of a conventional infrared source into a diffraction-limited spot size of 5-12 μm^2 at the sample location in a commercial FTIR microscope.

Ray-tracing and optical simulations have been carried out using SRW, RAY, SpotX and ART codes in order to simulate IR beam propagation and verify the optical layout. The specifications for the mechanics of the main optical elements, including the beam transport system, as well as the mechanical designs, have been completed and are about to be manufactured, with planned delivery by the end of 2015.

The target is to have the beamline entering the commissioning phase in 2016 and first official users visiting us within the first half of 2017.

LOREA for ARPES

The new beamline LOREA will deliver photons in the energy range 10-600eV with a high energy resolution to permit angle-resolved photoemission spectroscopy (ARPES) experiments on a large variety of samples. The synchrotron

light will be either linearly polarized in any direction or circularly polarized, and the option of having the electron analyzer equipped with a spin detector to perform spin-resolved ARPES (S-ARPES) experiments is being evaluated.

Similarly to the case of MIRAS, the project was started in 2009, approved in 2010 and kept in standby due to the lack of funding to proceed with it. Finally, funding for the project was allocated in 2014 and the process to have an updated conceptual design of the BL was started. The field had evolved during the last few years, so some decisions were made, like shifting the whole energy range to higher energies to reach 600 eV with good flux. Design work started in 2014 and is planned to proceed during 2015, with the aim of starting the contracting phase, having the different subsystems produced during 2016 and having most of the installation work done in 2017. The period 2018-19 should see commissioning activity and the first official users.

LOREA will be a valuable tool for most fields of solid state physics: superconductivity, magnetism and phase transitions, strongly correlated electron systems, nanoscale systems and emerging complex materials. The latter include novel unconventional superconductors, alloys, intermetallic compounds, magnetic semiconductors, f-electron systems and low-dimensional (like topological insulators) as well as self-organized systems.

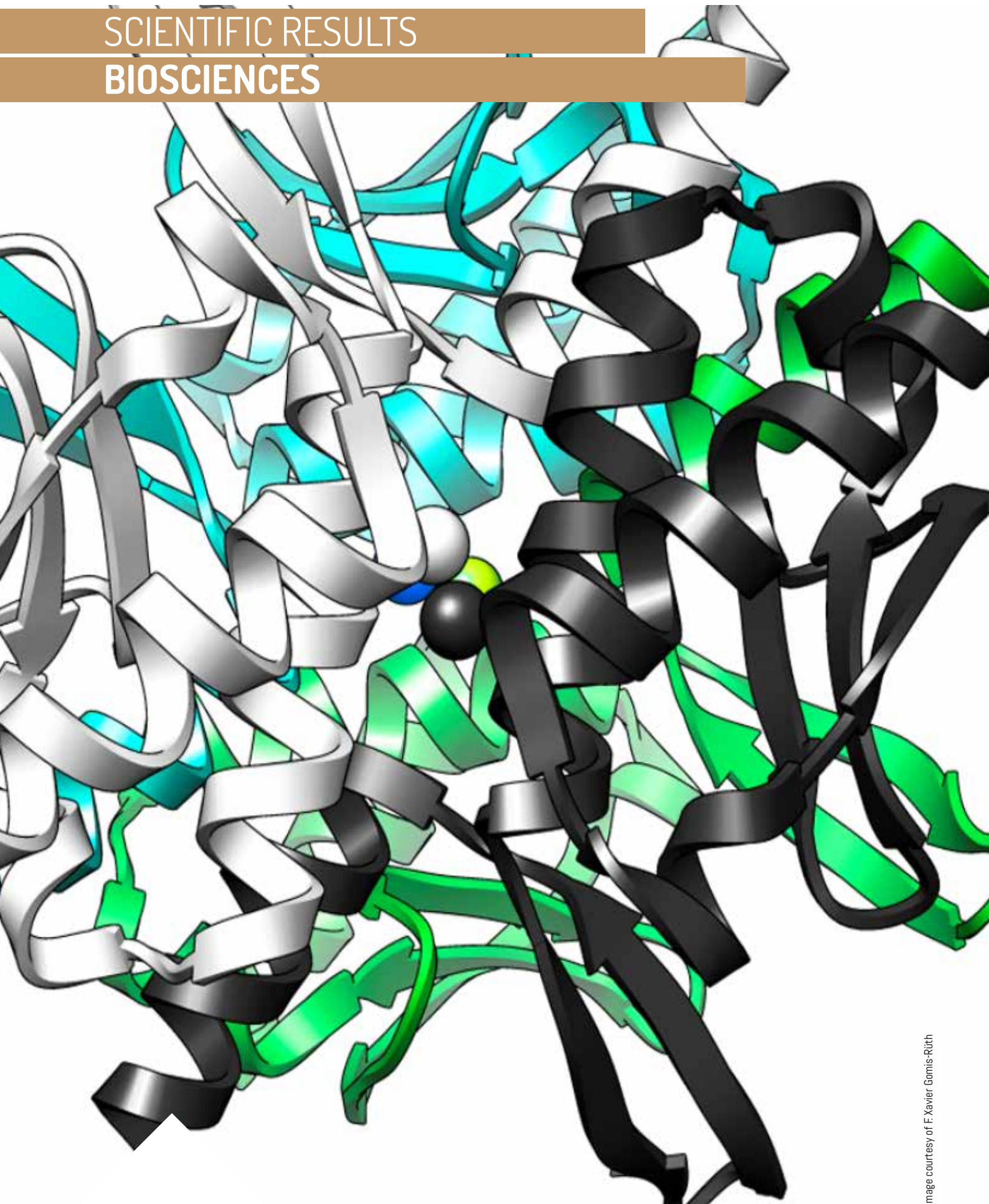
LOREA beamline specifications

- Insertion Device: Aperiodic permanent magnet, undulator UE125
- Flux through a 1x1 μrad^2 slit: $>10^{14}$ Ph/s/0.1%BW
- Energy range: 10-600eV
- Resolving power: 10^4
- Polarization: horizontal, vertical, diagonal, circular

LOREA experimental capabilities

- High resolution ARPES and spin-ARPES
- Low-temperature cryostat, T~7K
- *In situ* characterization with STM and LEED
- *In situ* film preparation with Molecular Beam Epitaxy, Chemical Vapor Deposition and Atomic Layer Deposition

SCIENTIFIC RESULTS
BIOSCIENCES



MOLECULAR PLASTICITY CONTROLS PROTEOLYTIC ACTIVITY

Multiple Stable Conformations Account for Reversible Concentration-Dependent Oligomerization and Autoinhibition of a Metamorphic Metallopeptidase. *Angew. Chem. Int. Ed.* 53, 10624-10630, (2014)

MAR LÓPEZ-PELEGRÍN¹, NÚRIA CERDÀ-COSTA¹, ANNA CINTAS-PEDROLA¹, FÁTIMA HERRANZ-TRILLO², PAU BERNADÓ², JUAN R. PEINADO¹, JOAN L. AROLAS¹, AND F. XAVIER GOMIS-RÜTH^{1*}

Proteolytic enzymes, also known as peptidases or proteases, are responsible for the hydrolysis of the peptide bonds that link amino acids together in a polypeptide chain. They occur in all organisms, from prokaryotes to eukaryotes and viruses, and they are essential for life, participating not only in broad spectrum degradation of peptides and proteins but also in highly selective cleavage of specific substrates. Their diverse catalytic properties make them invaluable tools in industry and pharmacy. Peptidases are exquisitely regulated as excessive or diminished activity may lead to disease. Therefore, a better understanding of the structure and working mechanism of these players at the molecular level is a requisite for the development of therapeutic strategies and biotechnological applications. This article describes a minimal selective and specific caseinolytic metallopeptidase, which reversibly transits between competent and incompetent conformations for proteolysis due to autoinhibition by simple concentration/dilution.

The authors discovered a mature, fully active metallopeptidase with very narrow and selective substrate specificity that cleaved bovine milk casein at a single site. The protein, called selecace, is a novel member of the minigluzincin family¹. Selecace was extremely soluble in aqueous buffer and, surprisingly, showed a progressive decrease in proteolytic activity upon protein concentration. Most interestingly, this inactive concentrated protein regained maximal activity following simple dilution with buffer. Accordingly, the enzymatic activity of selecace was reversibly autoinhibited due to changes in concentration and not to inhibition by the substrate or any other reagent, which is novel for peptidases.

It was subsequently explored the oligomerization of selecace in solution over a wide concentration range using several biophysical techniques, namely size-exclusion chromatography coupled to multi-angle laser scattering, analytical ultracentrifugation, chemical crosslinking, and small-angle X-ray scattering in a joint work with researchers from the Université Montpellier in France. These analyses in solution revealed the presence of mixtures of monomers, dimers, tetramers, and octamers, with larger protein concentrations leading to higher oligomerization orders. The concentrations at which monomeric selecace was predominant coincided with those of maximal enzymatic activity, thus suggesting that the monomer was the active species and that oligomers corresponded to self-inhibiting species in all cases. This correlated with higher enzyme concentrations yielding lower activity. Most interestingly, simple dilution with buffer reversed oligomerization to render monomers and restore activity.

To identify the molecular determinants of this behaviour, the structures of monomeric, dimeric, and tetrameric forms of selecace were solved using data collected at ALBA and ESRF

AFFILIATION

¹ Institut de Biologia Molecular de Barcelona (IBMB-CSIC), 08028 Barcelona (Spain); ² Centre de Biochimie Structurale, Université de Montpellier, 34090 Montpellier (France)

REFERENCES

- 1 M. López-Pelegrín et al., A novel family of soluble minimal scaffolds provides structural insight into the catalytic domains of integral-membrane metallopeptidases. *J. Biol. Chem.* 2013, 288, 21279-21294
- 2 A. G. Murzin, Metamorphic proteins. *Science* 2008, 320, 1725-1726

ACKNOWLEDGEMENTS

The authors are grateful to Joan Pous and Xandra Kreplin from the joint IBMB/IRB Automated Crystallography Platform for assistance during crystallization experiments and to the local contacts at ESRF and ALBA synchrotrons. This study was financially supported in part by grants from European, Spanish, and Catalan agencies (FP7-PEOPLE-2011-ITN-290246 "RAPID"; FP7-HEALTH-2012-306029-2 "TRIGGER"; BFU2012-32862; BIO2013-49320-EXP; MDM-2014-0435; and 2014SGR9). MLP acknowledges an FPI-fellowship (BES-2010-035767) from the former Spanish Ministry for Education, Culture and Sport. The Department of Structural Biology of IBMB is a "María de Maeztu" Unit of Excellence from the Ministry of Economy and Competitiveness.

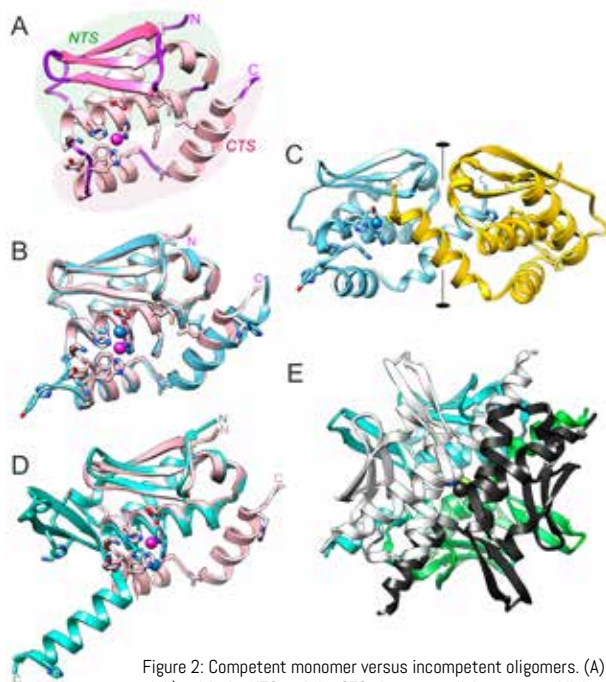


Figure 2: Competent monomer versus incompetent oligomers. (A) Structure of monomeric selease (in pink), with the NTS and the CTS shown over light green and light purple background, respectively, and the catalytic metal ion as a sphere. (B) Superposition of monomeric (in pink) and one protomer of dimeric (in cyan) selease. (C) Structure of symmetric dimeric selease (chains in cyan and gold). (D) Superposition of monomeric (in pink) and one protomer of tetrameric (in turquoise) selease. (E) Structure of tetrameric selease, with two dimers in turquoise/light green and white/dark gray, which associate face to face under a relative rotation to yield the overall particle.

Synchrotrons. With only 13.1 kDa, selease is the smallest active peptidase structurally characterized to date, and it displayed a compact globular shape that consisted of an upper N-terminal subdomain (NTS) and a lower C-terminal subdomain (CTS), which were separated by a horizontal central active-site cleft (Fig. 2). Dimeric selease showed only minor differences within the NTS compared to monomeric selease. However, major metamorphic rearrangement (see reference 2 for terminology) was observed around the metal-binding site and at the beginning of CTS (Fig. 2), which was consistent with an inactive species in solution. As in dimeric selease, the protomer of the tetrameric form showed good overall fit with monomeric selease within the NTS. However, both major displacement and drastic conformational rearrangement were observed in the CTS, which diverged from those found in the dimeric form (Fig. 2). Overall, this metamorphic structural transition of selease was stabilized by the association of four monomers in the crystal, which would explain tetrameric oligomerization in solution. The oligomer was a compact, almost spherical self-inhibitory particle, which altered the structural segments that shape the active-site cleft in competent selease and, thus, corresponded to an inactive species in solution. Finally, selease proved to be highly resistant to potentially deleterious mutagenesis, which together with the structural data proved that this protein is highly plastic.

The research was successful in identifying and probing for the first time the structural transitions of a natural metamorphic protein. One conformer is catalytically competent and the others are incompetent but they coexist in equilibrium. These transitions between folding variants are triggered by major rearrangement at the NTS–CTS interface, and they mainly affect the CTS. This is consistent with each subdomain corresponding to a distinct folding unit and the subdomain interface acting as a reversible zipper. Results also provide the first evidence for a peptidase with a reversible, strictly concentration-dependent reduction of activity at higher concentrations, which is triggered by the sequestering of the competent conformation in incompetent but structured oligomers. This system affords a switch that provides a unique and reversible mechanism of control of catalytic activity in nature.

STRUCTURAL EVALUATION OF ANIONIC LIPID/DOPE/CA²⁺-PLASMID DNA LIPOPLEXES: A SAXS STUDY

Ca²⁺-Mediated Anionic Lipid-Plasmid DNA Lipoplexes. Electrochemical, Structural and Biochemical Studies. *Langmuir* 30 (39), 11704-11713, (2014)

ANA L. BARRÁN-BERDÓN¹, BELÉN YÉLAMOS², MARC MALFOIS³, EMILIO AICART¹ AND ELENA JUNQUERA^{1*}

The treatment of human disease by gene therapy is a real promise in the medicine field, because it is possible to revert the effects of many genetic disorders through the introduction of recombinant DNA into the cell with the aim of producing the necessary biologically active proteins to repair the cell damage. However, DNA internalization requires that the biopolymer must be firstly compacted by vectors and then protected from degradation. The non-viral vectors based in cationic lipid formulations have been revealed as one of the most adequate methods to transfect DNA to a wide variety of cells. However, the use of cationic lipids (CLs) presents moderate cytotoxicity levels. At this respect, anionic lipids (ALs) are more biocompatible, and may be pointed as potentially safer DNA delivery systems. Their interaction with negatively charged DNA helixes has to be mediated by divalent cations, such as calcium, which may act as effective cationic bridges between the anionic liposomes and DNA. Small-angle X-ray diffraction (SAXS) has been used to obtain information about the lipoplex structures, with the aim of correlating them with their capabilities as gene transfecting agents in order to clarify if lipofection protocols involving ALs in the presence of divalent cations may be considered as a promising alternative in gene therapy.

Preparation of Mixed Liposomes and Lipoplexes. Appropriate amounts of anionic lipid (AL) and DOPE were dissolved in chloroform to obtain the desired AL composition, α , of the mixed liposomes. After briefly vortexing, chloroform was removed by evaporation under high vacuum to yield a dry lipid film. The films were then hydrated with HEPES 10 mM, pH = 7.4, and homogenized with the help of alternating cycles of vigorous vortexing, sonication and moderate heat yielding MLVs, which were transformed into the desired unilamellar liposomes, LUVs, by a sequential extrusion procedure. This process consisted in subjecting the hydrated solution through polycarbonate membranes: 5, 5 and least 10 passes through 400, 200 and 100 nm pore size, respectively. The liposomes were left to rest during 24 hours before their use. A stock solution of pDNA was prepared one day before the mixing with mixed lipids. Appropriate amounts of this pDNA solution were firstly mixed with adequate volumes of Ca²⁺ solution, and added to liposomal suspensions in order to obtain the lipoplexes with the desired final [Ca²⁺] and AL/pDNA ratios. The mixing process was done at an addition speed of 0.2 mL/min, with continuous, constant, and vigorous magnetic stirring. The pDNA concentration was 10 μ g/capillar for SAXS.

AFFILIATION

¹ Grupo de Química Coloidal y Supramolecular, Departamento de Química Física I, ² Departamento de Bioquímica y Biología Molecular I, Facultad de Ciencias Químicas, Universidad Complutense de Madrid, 28040 Madrid, Spain and ³ALBA Synchrotron, 08290 Cerdanyola del Vallès, Barcelona, Spain

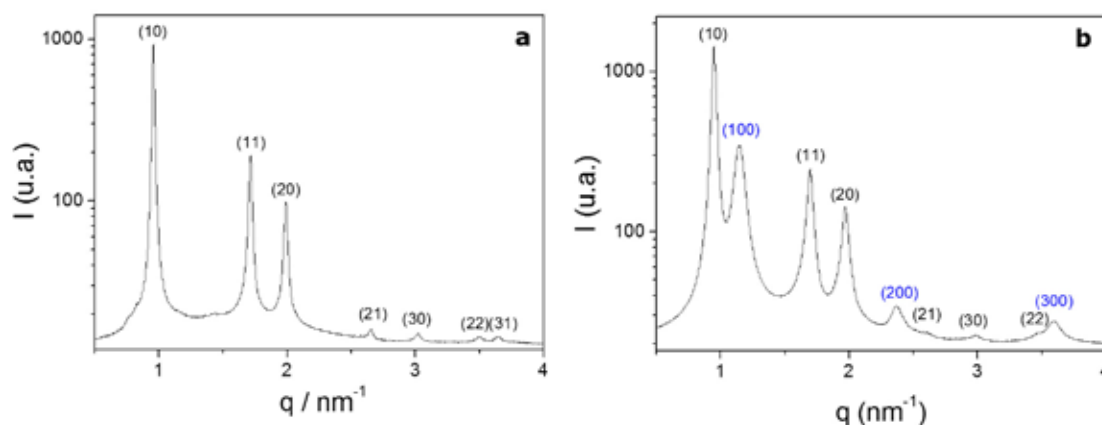
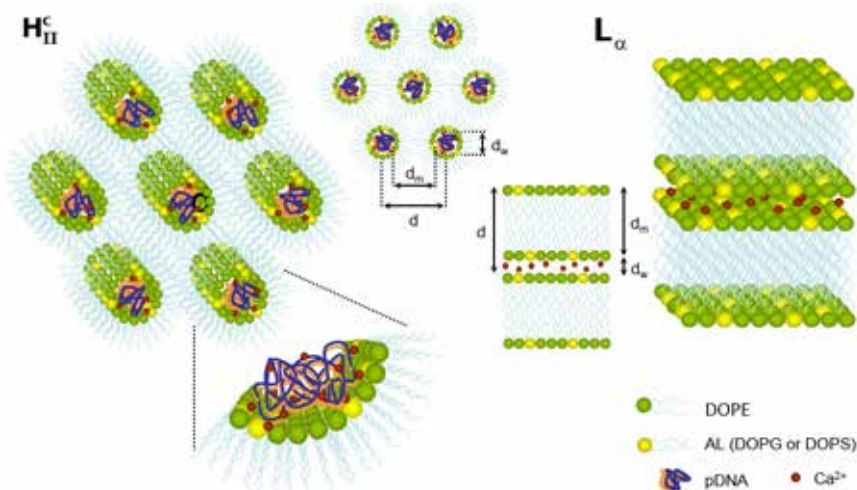


Figure 3: SAXS diffractograms of (a) DOPG/DOPE-Ca²⁺-pDNA lipoplexes and (b) DOPS/DOPE-Ca²⁺-pDNA lipoplexes at $\alpha = 0.20$, AL/pDNA mole ratio = 20 and [Ca²⁺] = 25 mM, showing an inverted hexagonal H_{II}^c structure in (a), and the coexistence of inverted hexagonal H_{II}^c (black) and lamellar L_{α} (blue) structures in (b).

Figure 4: Schematic drawings of 3D and 2D views of H_{II}^c and L_{α} phases of AL/DOPE-Ca²⁺-pDNA lipoplexes, where AL may be DOPG or DOPS. Values of d were obtained from q values of Figure 3 as follows: for H_{II}^c the phase, $d = 4\pi/\sqrt{3}q_{10}$, and for the L_{α} phase, $d = 2\pi/q_{100}$. The value of d_m was estimated from the length of the mixed lipids, and $d_w = d - d_m$.



ACKNOWLEDGEMENTS

Authors thank MICINN of Spain, project no. CTQ2012-30821. Authors also thank C. Aicart-Ramos for carrying on amplification of plasmid DNA at the Departamento de Bioquímica y Biología Molecular I (UCM, Spain).

Small-angle X-ray Scattering. SAXS experiments were carried out on the beamline BL11-NCD at ALBA Synchrotron. The energy of the incident beam was 12.6 KeV ($\lambda = 0.995 \text{ \AA}$). Samples were placed in sealed glass capillaries purchased from Hilgenberg with an outside diameter of 1.5 mm and wall thickness of 0.01 mm. The scattered X-ray was detected on CCD detector Quantum 210r (4096 x 4096 pixels highest achievable resolution - pixel size 51 microns), converted to one-dimensional scattering by radial averaging, and represented as a function of the momentum transfer vector $q (= 4\pi\sin\theta/\lambda)$, in which θ is half the scattering angle and λ is the wavelength of the incident X-ray beam. The sample-to-detector distance was maintained at 1.4 m. Measurements on each sample were collected over 5 to 20 s each. SAXS experiments were run at different cationic lipid compositions, α , for the lipoplexes formed with pDNA. Solutions were prepared using deionized water buffered with HEPES 10 mM, at pH = 7.4.

Small-angle X-ray scattering (SAXS) experimental methods have been used to analyse the potential of anionic lipids (AL) as effective non-toxic and non-viral DNA vectors, assisted by divalent cations. The lipoplexes studied are those constituted by the green fluorescent protein-encoding plasmid DNA pEGFP-C3, an anionic lipid as 1,2-dioleoyl-*sn*-glycero-3-phospho-(1'-*rac*-glycerol) (DOPG) or 1,2-dioleoyl-*sn*-glycero-3-phospho-L-serine (DOPS), and a zwitterionic lipid, the 1,2-dioleoyl-*sn*-glycero-3-phosphatidylethanolamine

(DOPE, not charged at physiological pH). The studies have been carried on at different liposome and lipoplex compositions and in the presence of a variety of [Ca²⁺]. From a structural standpoint, DOPG/DOPE-Ca²⁺-pDNA lipoplexes are self-assembled into a H_{II}^c phase (inverted cylindrical micelles in hexagonal ordering with plasmid supercoils inside the cylinders), while DOPS/DOPE-Ca²⁺-pDNA lipoplexes show two phases in coexistence: one classical H_{II}^c phase which contains pDNA supercoils and one L_{α} phase without pDNA among the lamellae, i.e. a lamellar stack of lipidic bilayers held together by Ca²⁺-bridges (Figures 3 and 4). Transfection and cell viability studies were done with HEK293T and HeLa cells in the presence of serum. Lipoplexes herein studied show moderate-to-low transfection levels combined with moderate-to-high cell viability, comparable to those yielded by Lipofectamine2000*.

UNCOVERING THE MOLECULAR MECHANISM OF HOW GalNAc-TRANSFERASES LECTIN DOMAINS MODULATE O-GLYCOSYLATION

Dynamic interplay between catalytic and lectin domains of GalNAc-transferases modulates protein O-glycosylation *Nature Communications*. May 5; 6:6937 (2015)

ERANDI LIRA-NAVARRETE¹, MATILDE DE LAS RIVAS¹, ISMAEL COMPAÑÓN², MARÍA CARMEN PALLARÉS³, YUN KONG⁴, JAVIER IGLESIAS-FERNÁNDEZ⁵, GONÇALO J. L. BERNARDES^{6,7}, JESÚS M. PEREGRINA², CARMÉ ROVIRA^{5,8}, PAU BERNADÓ⁹, PIERPAOLO BRUSCOLINI^{1,10}, HENRIK CLAUSEN⁴, ANABEL LOSTAÓ^{3,11}, FRANCISCO CORZANA² & RAMON HURTADO-GUERRERO^{1,11*}

GalNAc-transferases (GalNAc-Ts) are unique enzymes that glycosylate (that is to say, transfer sugars to) important proteins such as mucins. Mucins are highly glycosylated proteins that are key for cell signaling and forming chemical barriers. In fact, the anomalous glycosylation of these proteins cause cancer and is also linked to metastasis. GalNAc-Ts contain a catalytic domain connected to a lectin domain through a flexible linker. One of the longstanding questions about these enzymes is how they glycosylate mucins and how the lectin domains contribute to this glycosylation. In this article, the authors discover that the dynamic interplay between both domains is essential for the glycosylation profile occurring in mucins. Furthermore, these findings might guide the rational design of future inhibitors against these enzymes and in turn for the potential treatment of some type of cancers.

At ALBA (XALOC beamline), the authors managed to get very good data of one of our GalNAc-T2 crystals in complex with the glycopeptide MUC5AC-Cys13. This experiment at high resolution allowed them to solve and interpret the density maps without problems (Fig. 5). Furthermore,

AFFILIATION

¹ BIFI, University of Zaragoza, BIFI-IQFR (CSIC) Joint Unit, Mariano Esquillor s/n, Campus Rio Ebro, Edificio I+D, Zaragoza 50018, Spain.

² Departamento de Química, Universidad de La Rioja, Centro de Investigación en Síntesis Química, E-26006 Logroño, Spain.

³ LMA, INA, Universidad de Zaragoza, 50018 Zaragoza, Spain.

⁴ Copenhagen Center for Glycomics, Department of Cellular and Molecular Medicine, School of Dentistry, University of Copenhagen, Copenhagen DK-2200, Denmark.

⁵ Departament de Química Orgànica i IQTCUB, Universitat de Barcelona, Martí i Franquès 1, 08028 Barcelona, Spain.

⁶ Department of Chemistry, University of Cambridge, Lensfield Road, Cambridge CB2 1EW, UK.

⁷ Instituto de Medicina Molecular, Faculdade de Medicina, Universidade de Lisboa, Av Prof Egas Moniz, 1649-028 Lisboa, Portugal.

⁸ ICREA, Passeig Lluís Companys 23, 08020 Barcelona, Spain.

⁹ Centre de Biochimie Structurale, INSERM U1054, CNRS UMR 5048, Université Montpellier 1 and 2, 29 rue de Navacelles, 34090 Montpellier, France.

¹⁰ Departamento de Física Teórica, Universidad de Zaragoza, Zaragoza 50009, Spain.

¹¹ Fundación ARAID, 50018 Zaragoza, Spain.

ACKNOWLEDGEMENTS

The authors thank synchrotron radiation sources DLS (Oxford), ALBA (Barcelona) and PETRA-III (DESY/Hamburg), and in particular beamlines I03 (experiment number MX8035-21 and MX8035-24), I04-1 (experiment number MX8035-17), XALOC and P12 (SAXS-172), respectively. The authors also thank ARAID, the MEC (BFU2010-19504, CTQ2013-44367-C2-2-P, CTQ2011-25871, BIO2010-14983, CTQ2012-36365 and MAT2012-38318), the DNERF (DNERF107), the DGA (B89 and B18), the Generalitat de Catalunya (2014SGR-987), ANR-CHEX-2011 and ATIP-Avenir (PB) for their financial support. The research leading to these results has also received funding from the FP7 (2007-2013) under BioStruct-X (grant agreement N°283570 and BIOSTRUCTX_5186). It is also acknowledged the computer support, technical expertise, and assistance provided by the Barcelona Supercomputing Center-Centro Nacional de Supercomputación (BSC-CNS).

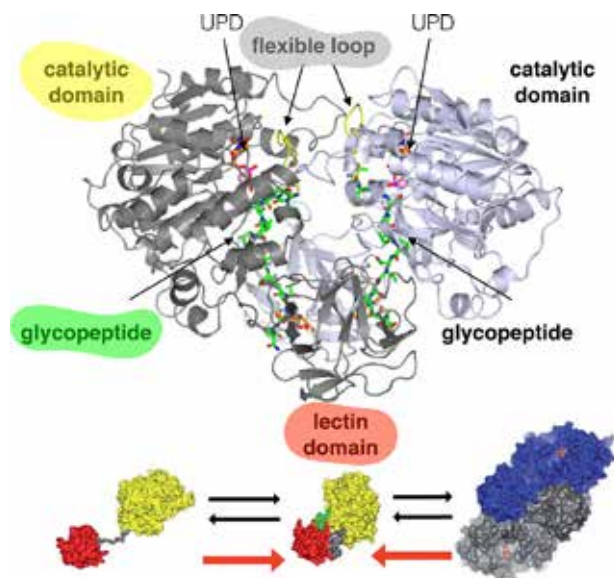


Figure 5: Polypeptide GalNAc-transferases decorate proteins with dense arrays of O-glycans, which in the case of mucins are essential for their barrier functions. (Upper panel) Cartoon representation of the overall dimeric structure of GalNAc-T2 in complex with UDP-MUC5AC-13. The monomers are coloured in grey and blue-white, respectively. UDP, MUC5AC-13 and flexible loop in yellow are indicated by arrows. The nucleotide and the glycopeptide are depicted as orange and green carbon atoms, respectively. The GalNAc moiety covalently bound to Thr13 is depicted as orange carbon atoms. (Lower panel) GalNAc-T2 is in equilibrium with an ensemble of compact and extended structures, and dimeric forms. This equilibrium is partly shifted towards the ensemble of compact structures in the presence of peptides and mainly glycopeptides.

this structure showed for the first time that GalNAc-Ts are enzymes capable of binding to glycopeptides in their inactive states. This is an important discovery because it might be helpful not only to design rational glycopeptides binding to their active form but also to the inactive form.

Here, the authors present the first crystal structures of complexes of GalNAc-T2 with glycopeptides that, together with enhanced sampling molecular dynamics simulations, demonstrate a cooperative mechanism by which the lectin domain enables free acceptor sites binding of glycopeptides into the catalytic domain. Atomic force microscopy and small-angle X-ray scattering experiments further reveal a dynamic conformational landscape of GalNAc-T2 and a prominent role of compact structures that are both required for efficient catalysis.

The model indicates that the activity profile of GalNAc-T2 is dictated by conformational heterogeneity and relies on a flexible linker located between the catalytic and the lectin domains. The results also shed light on how GalNAc-Ts generate dense decoration of proteins with O-glycans.

Finally, these findings may guide the rational design of mechanism-based modulators for this relevant family of enzymes. The finding of inactive and active conformational states in GalNAc-Ts together with the motion of the flexible loop and its association with activity somehow resemble similar features found for the large family of protein kinases. In general, similar states and an activation flexible loop, marked by conserved DFG and APE motifs, are also found in protein kinases and these structural features have been exploited to discover protein kinase inhibitors. The authors believe that modulators for this particular family of GalNAc-Ts can be developed using similar approaches that will also include the targeting of the lectin domains.

REFERENCES

- 1 Substrate-guided front-face reaction revealed by combined structural snapshots and metadynamics for the polypeptide N-acetylgalactosaminyltransferase Lira-Navarrete E, Iglesias-Fernández J, Zandberg WF, Compañón I, Kong Y, Corzana F, Pinto BM, Clausen H, Peregrina JM, Vocadlo DJ, Rovira C, Hurtado-Guerrero R. *Angew Chem Int Ed Engl.* 2014 Jul 28;53(31):8206-10. doi: 10.1002/anie.201402781.

SCIENTIFIC RESULTS
CATALYSIS

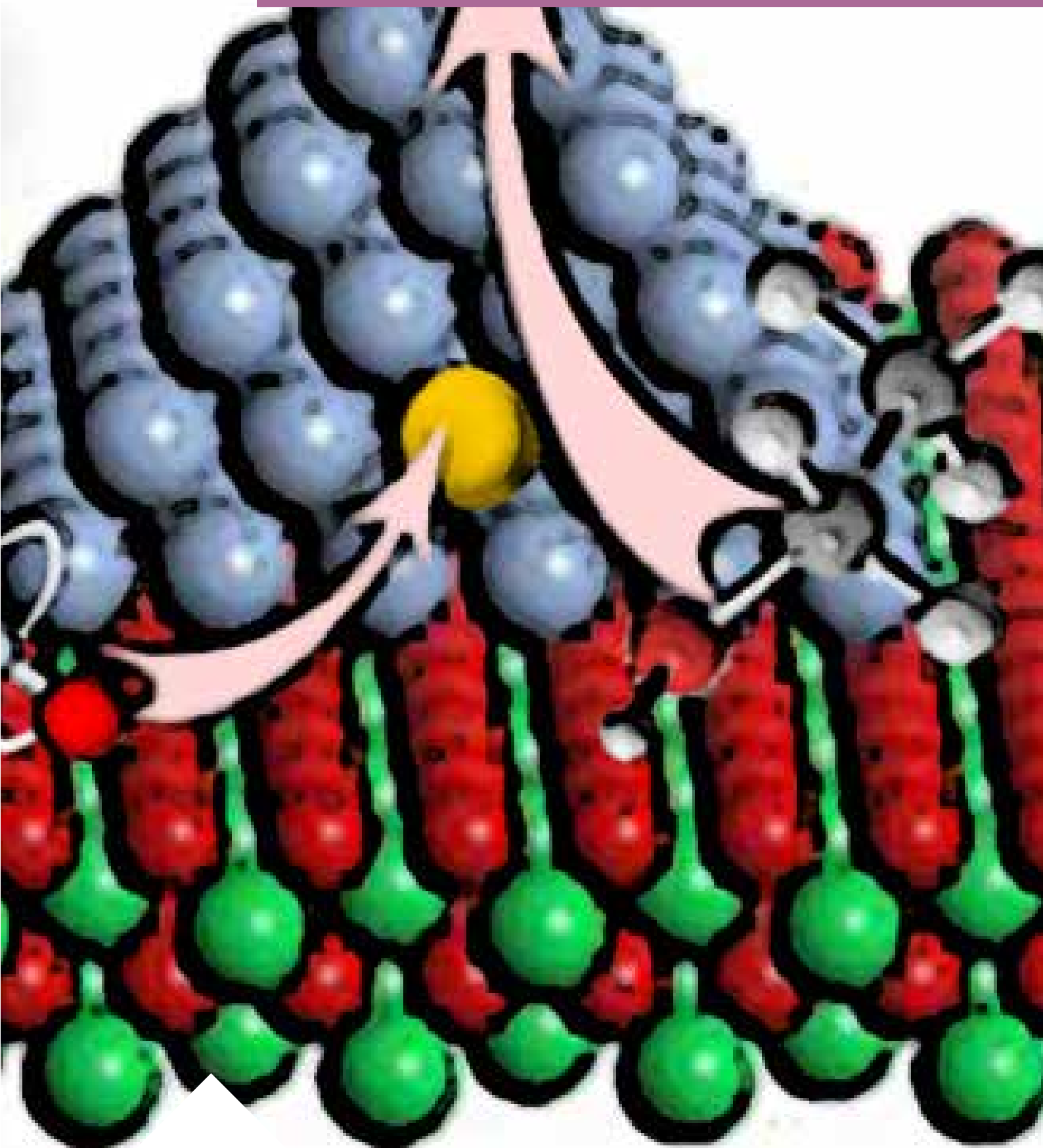


Image courtesy of Jordi Llorca

UNRAVELLING THE WORKING ARCHITECTURE OF REAL CATALYSTS BY NEAR-AMBIENT X-RAY PHOTOELECTRON SPECTROSCOPY

Influence of the support on surface rearrangements of bimetallic nanoparticles in real catalysts, *Science* 346, 620–623 (2014).

N.J. DIVINS¹, I. ANGURELL², C. ESCUDERO³, V. PÉREZ-DIESTE³, J. LLORCA^{1*}

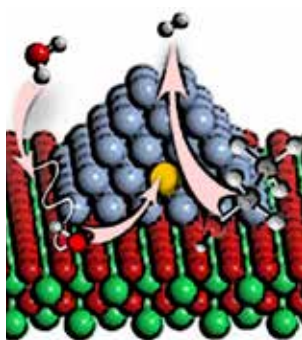


Figure 6: Drawing of a ceria-supported metal rhodium-palladium nanoparticle. The ethanol and water molecules are adsorbed at the interface between the nanoparticles and the support and they generate new reactive chemical species that make the rhodium and palladium atoms reorganise on the surface, change their oxidation state and thus facilitate the production of hydrogen.

A catalyst is a substance that accelerates a chemical reaction without itself being affected. A heterogeneous catalyst is in a different phase to the reactants and products, and is often favoured in industry, being easily separated from the products. The components of a heterogeneous catalyst are usually the catalytic particles (metal, oxide or sulfide), the support (stabilizing the catalytic particles) and the promoters (enhancing the catalytic performance or structural effects). A testimony to the importance of heterogeneous catalysis today is the award of the Nobel Prize in Chemistry in 2007 to Gerhard Ertl. However, only the active sites of a heterogeneous catalyst directly catalyze a reaction. Knowledge of the structure and composition of the active sites is crucial for understanding and improving the properties of catalysts. The high mobility of both surface metal atoms and adsorbed molecules during the catalytic process brings into focus the dynamic nature of active sites as they form and disassemble. The advent of *operando* surface science techniques has led to important advances in probing the active sites of catalysts, in which interactions between the active metals and the oxide supports are highly synergistic and sensitive to the environmental and reaction conditions.

The authors have carried out an *operando* near-ambient-pressure X-ray photoelectron spectroscopy (AP-XPS) study, in the CIRCE beamline (NAPP endstation) at ALBA Synchrotron, of bimetallic rhodium-palladium nanoparticles supported over cerium dioxide (RhPd/CeO₂), see Fig. 6. This catalyst has an excellent performance for producing hydrogen through the ethanol steam reforming reaction (ESR), $C_2H_5OH + 3H_2O \rightarrow 6H_2 + 2CO_2$, which represents an attractive route for renewable hydrogen generation for energy applications. The authors have monitored both the surface restructuring and chemical state of two systems: (i) unsupported model Rh_{0.5}Pd_{0.5} nanoparticles (4±1 nm) and (ii) model Rh_{0.5}Pd_{0.5} nanoparticles supported on CeO₂ powder (which constitutes a real catalyst). Both systems were exposed at 0.05 mbar to oxidizing, reducing and ESR conditions at 823 K to produce hydrogen. The photon beam spot size at the sample was about 100 x 20 μm² (horizontal x vertical) and the resolving power measured at 400 eV was $E/\Delta E = 8600$. The ethanol-water mixture was prepared in a bubbler connected to the analysis chamber by a UHV leak valve. The sample temperature was controlled by using an infrared laser ($\lambda = 808$ nm) focused on a W plate on top of which the samples were mounted.

AFFILIATION

¹ Institute of Energy Technologies and Centre for Research in Nanoengineering. Technical University of Catalonia (UPC), Barcelona, Spain.

² Dendrimers and Molecular Polygons Group, Universitat de Barcelona (UB), Barcelona, Spain.

³ ALBA Synchrotron, Cerdanyola del Vallès, Spain.

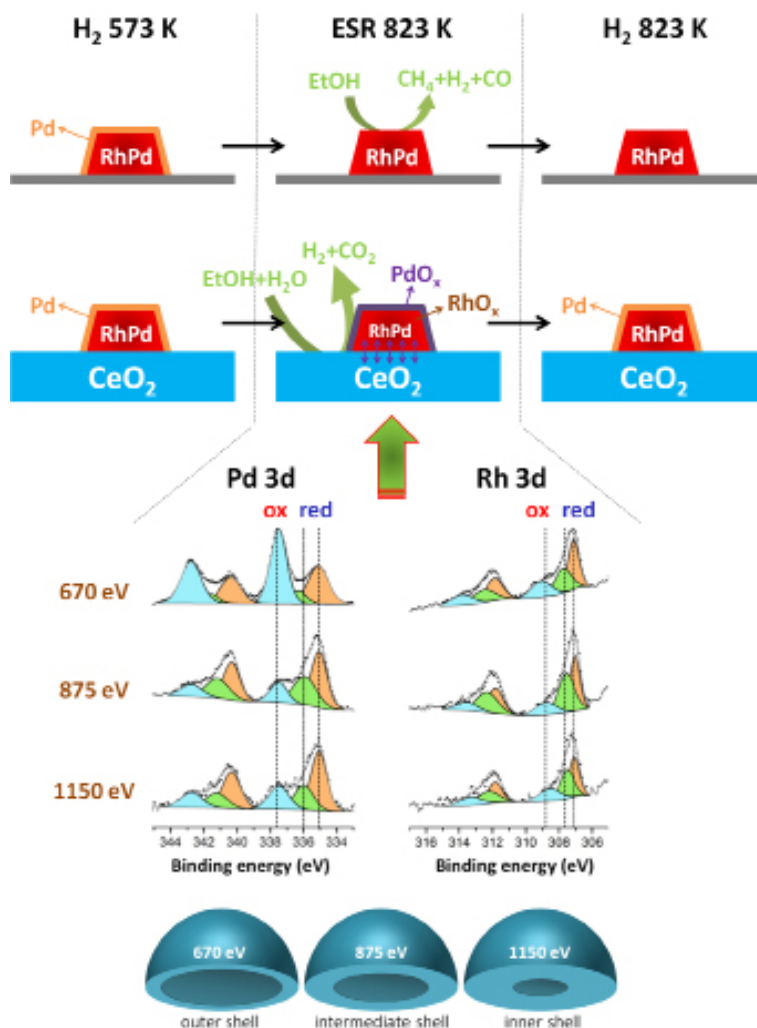


Figure 7: Recording XP spectra at different photon energies (the spectra shown in the figure corresponds to the RhPd/CeO₂ sample under ethanol steam reforming) allows reconstructing the structure and oxidation state of the nanoparticles. Initially, under reducing conditions, both unsupported RhPd and RhPd nanoparticles supported on CeO₂ are essentially reduced and Pd is segregated at the surface. Under reaction, unsupported RhPd nanoparticles reduce and Rh segregates toward the surface, whereas RhPd nanoparticles supported on CeO₂ undergo oxidation and are much more active for producing hydrogen. This transformation is reversible only over RhPd/CeO₂.

ACKNOWLEDGEMENTS

Jordi Llorca is a Serra Hünter Fellow and is grateful to the ICREA Academia programme. Funding from MINECO ENE2012-36368 is acknowledged.

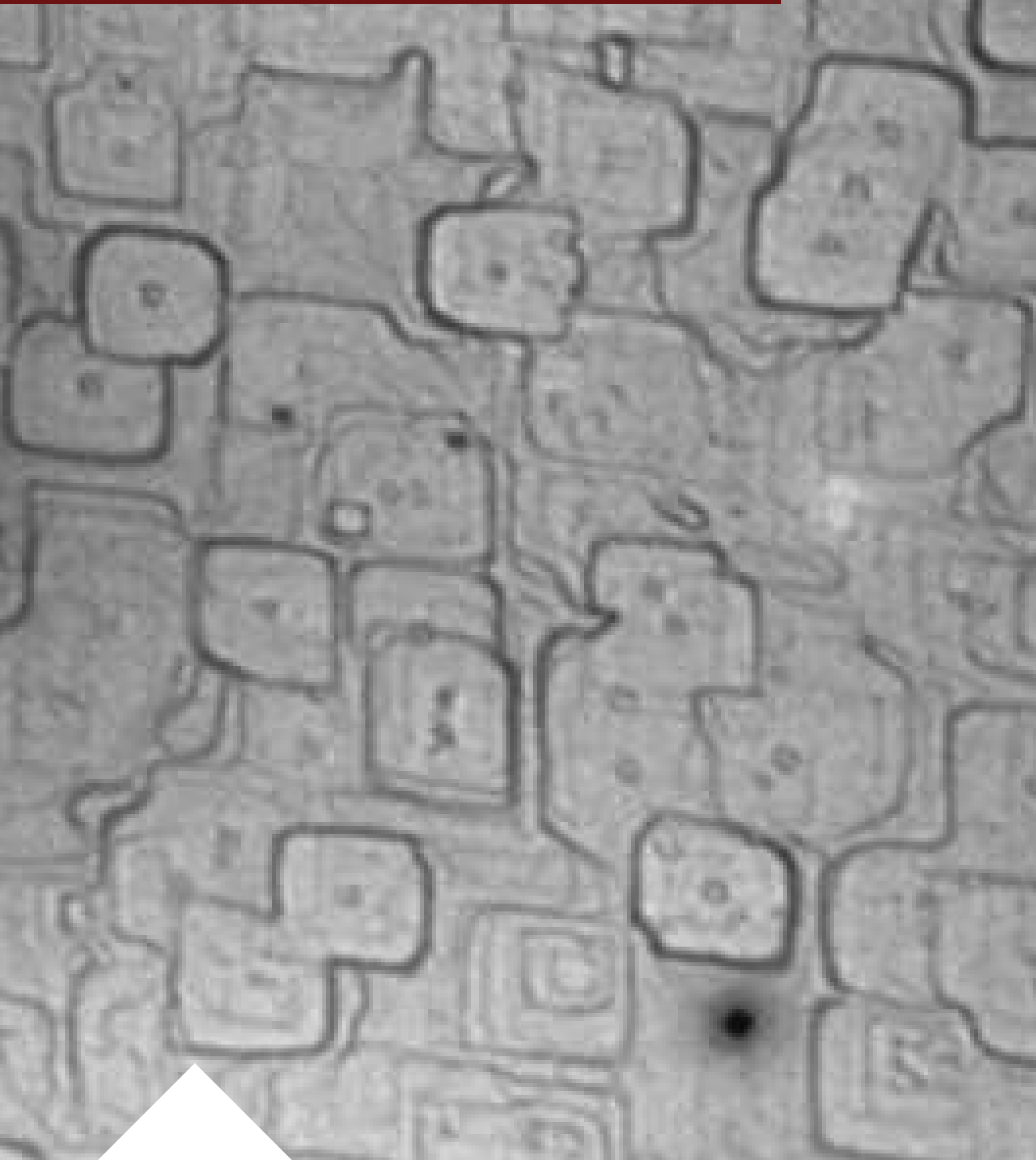
Three photon energies were chosen in order to perform a depth-profile study of both systems to infer the environment-induced rearrangement and the development of a core-shell structure of oxidation states. The selected photon energies were 670, 875 and 1150 eV, which accounted for inelastic mean free paths (IMFPs) of 0.7, 0.9 and 1.2 nm (Fig. 7). These IMFPs defined three different volumes in the nanoparticles and were calculated as the volume enclosed within one IMFP from the surface inside a sphere of diameter 4 nm. The regions defined from these three depths accounted for approximately 25, 34 and 44% of the total volume of the nanoparticles for 670, 875 and 1150 eV photon energies, respectively.

In the absence of the support, the model Rh_{0.5}Pd_{0.5} nanoparticles decomposed ethanol and the yield of hydrogen was low. The model nanoparticles were strongly reduced for all the environments tested and the reduction temperature affected the amount of metallic phase found in Rh and Pd. In contrast, the capability of CeO₂ as a support to activate water and to donate oxygen atoms determined the oxidation states of the noble metals under the same reaction conditions, and ESR was effective to produce hydrogen over RhPd/CeO₂.

The structure of heterogeneous catalysts is dynamic and depends on the composition of the surrounding environment. Both their surface structure and composition are modified when the gaseous conditions change in order to adapt their electronic properties and geometry to the new atmosphere. Some structures and active phases only exist under reaction conditions and differ from those identified under UHV conditions. Thus, the study of catalytic systems under real operating conditions is essential to identify the active species at work, as the restructuring driven by the environment may induce strong changes in both their properties and behaviour. In this experiment, it has been demonstrated that the reducible ceria support plays a crucial role in the catalytic process by providing new active sites strongly affecting both the physical and chemical properties of the metal nanoparticles which, in turn, have a strong effect on the catalytic performance. This work constitutes one of the few examples reported in the literature where the surface and sub-surface of a real catalyst has been characterized by XPS by using different photon energies under controlled atmospheres closely reproducing working conditions.

SCIENTIFIC RESULTS

MAGNETISM



ENGINEERING $\text{LaAlO}_3/\text{SrTiO}_3$ QUANTUM WELLS BY SELECTIVE ORBITAL OCCUPANCY

Two-Dimensional Electron Gases at $\text{LaAlO}_3/\text{SrTiO}_3$ Interfaces: Orbital Symmetry and Hierarchy Engineered by Crystal Orientation. *Physical Review Letters* 113, 156802 (2014)

D. PESQUERA,¹ M. SCIGAJ,^{1,2} P. GARGIANI,³ A. BARLA,⁴ J. HERRERO-MARTÍN,³ E. PELLEGRIN,³ S. M. VALVIDARES,³ J. GÁZQUEZ,¹ M. VARELA,^{5,6} N. DIX,¹ J. FONTCUBERTA,¹ F. SÁNCHEZ,¹ AND G. HERRANZ^{1*}

Over the last decade, the discovery of a highly conductive two-dimensional electron gas (2DEG) at the interface between LaAlO_3 (LAO) and SrTiO_3 (STO) has been heralded as one of the most attention-grabber topics in condensed matter¹⁻⁵. The fundamental reason is that the emergence of a high-mobility 2DEG is a rather unexpected phenomenon, given the wide-bandgap insulator character of the constituent materials. It is largely believed that the origin of these 2DEGs is due to mismatched electrostatic boundary conditions at the interface that, in turn, drive a charge-transfer a few unit cells across the interface.

Over the first years, the research was focused exclusively on (001)-oriented LAO/STO quantum wells. Yet, recent works have demonstrated that 2DEGs can also be generated along other crystal orientation and, in particular, along (110)⁶⁻⁸. This raises the question of how the electronic band structure is reconstructed when the quantum well orientation is changed, as this would enable novel pathways to tailor the electronic properties of oxide quantum wells.

To understand how the electronic subband structure is modified with the crystal orientation, either along (001) or (110), experiments were done at the BOREAS beamline of the ALBA Synchrotron. Room-temperature X-ray absorption spectroscopy (XAS) was carried out at the $\text{Ti-L}_{2,3}$ edges in total electron yield (TEY) mode. The main peaks featured in the XAS spectra result from transitions from $\text{Ti-2p}_{1/2}$ (L_2) and $\text{Ti-2p}_{3/2}$ (L_3) core levels to unoccupied Ti 3d states and have a contribution from t_{2g} (d_{xz} , d_{yz} , and d_{xy}) and e_g ($d_{3z^2-r^2}$ and $d_{x^2-y^2}$) levels. Figure 8 shows a schematic description of the relationship between the photon beam linear polarization and the orbital symmetries. In all cases, the linear polarization vector E_a (red) was always kept in plane, i.e., $E_a \parallel [100]$ for (001) and $E_a \parallel [001]$ for (110) samples, respectively. Instead, polarization E_b (blue) was either in plane (normal incidence) or out of plane (grazing incidence). The orientation of E_b with respect to the crystal axes is given in Figs. 8(a)–8(d) for each case. X-ray induced electronic transitions to the d orbitals have an intensity that depends on the orbital symmetry of the available d final states, the interaction being strongest when light polarization is along the direction of the orbital lobes. The sketch in the inset of Fig. 8 graphically depicts the different possibilities of electric field projection onto the orbital lobes. The TEY intensities I_a and I_b were recorded for the two orthogonal E_a and E_b polarizations, and the XLD signal was defined as the difference $\text{XLD} = (I_a - I_b)$. Taking into account the aforementioned description of the experiment, spectra were measured at grazing incidence (60° away from the normal), which, in turn, allowed to quantify the splitting between the t_{2g} and e_g substates and, thus, unveil the details of the reconstructed electronic structures. The

AFFILIATION

¹Institut de Ciència de Materials de Barcelona (ICMAB-CSIC), Campus de la UAB, Bellaterra E-08193, Catalonia, Spain

²Departamento de Física, Universitat Autònoma de Barcelona, E-08193 Bellaterra, Barcelona, Catalonia, Spain

³ALBA Synchrotron, Cerdanyola del Vallès, Barcelona, Spain

⁴Istituto di Struttura della Materia, ISM CNR, Area Science Park Basovizza (Ts), Trieste I-34149, Italy

⁵Departamento Física Aplicada III, Universidad Complutense de Madrid, Madrid, 28040 Spain

⁶Materials Science and Technology Division, Oak Ridge National Laboratory, Oak Ridge, Tennessee 37831, USA

ACKNOWLEDGEMENTS

This work was supported by the Spanish Government through MAT2011-29269-C03, and NANOSELECT CSD2007-00041 projects and the Generalitat de Catalunya (2009 SGR 00376 project). J. G. acknowledges the Ramon y Cajal programme (RYC-2012-11709). These experiments were performed at the Boreas beamline of the ALBA Synchrotron with the collaboration of ALBA staff. Microscopy work was conducted in the STEM Group of the Oak Ridge National Laboratory (ORNL), and in the Laboratorio de Microscopías Avanzadas at the Instituto de Nanociencia de Aragón—Universidad de Zaragoza. Research at ORNL was supported by the U.S. Department of Energy (DOE), Basic Energy Sciences (BES), Materials Sciences and Engineering Division (MV). Research at UCM was supported by the ERC Starting Investigator Award STEMOX 739239.

experiments were done for STO substrates capped with LAO thin films with thickness 8 MLs (≈ 3 nm) for [001] and 9 MLs (≈ 24 nm) for [110].

From these experiments, it was found that d_{xy} and $d_{x^2-y^2}$ states were lower in energy for the (001) interface, whereas the lowest energy t_{2g} and e_g orbitals had mostly d_{xz}/d_{yz} and $d_{3z^2-r^2}$ character for confinement along [110]. The authors thus observed that the degeneracy within the t_{2g} and e_g subbands is broken in opposite directions depending on the crystal orientation. For a quantitative description of the reconstructed bands, atomic model calculations were performed using the CTM4XAS software⁹ using typical crystal field and charge transfer parameters for Ti^{4+} in octahedral coordination to fit the experimental XLD curves. The simulated spectra are included in Figs. 9(c)–9(d) (red lines). Figure 9(e) summarizes all the information extracted from CTM4XAS simulations. The first conclusion is that in (001)-oriented interfaces d_{xy} orbitals are lower than d_{xz}/d_{yz} levels by ~ 15 meV, whereas $d_{x^2-y^2}$ states are shifted down with respect to $d_{3z^2-r^2}$ by about 20 meV. Secondly, the orbital energy hierarchy of (110)-oriented 2DEGs is reconstructed in an inverted way; i.e., d_{xz}/d_{yz} and $d_{3z^2-r^2}$ states are lower than d_{xy} and $d_{x^2-y^2}$ by 30 meV and 50 meV, respectively. The authors thus conclude that the 2DEG along the (110) orientation has an unambiguously genuine band structure, completely different from that of the (001) 2DEG, being the hierarchy of states with different symmetry totally reversed.

In summary, the results establish crystal symmetry as an extra degree of freedom to realize different 2DEG band reconstructions at the LAO/STO interface, thus allowing a selective occupancy of states of different symmetry. These results open up new opportunities for 2DEG band engineering and are crucial to extend our current understanding of the link between orbital symmetry and complex correlated states at these interfaces, such as magnetism or superconductivity. For instance, a connection has recently been established between d_{xy} orbitals and magnetism¹⁰. This issue can be further investigated in a controlled experiment, during which electrostatic fields can be adjusted to fill selectively— at low doping levels—the d_{xy} or d_{xz}/d_{yz} states in (001) or (110) interfaces, respectively, while the magnetism is probed. By the same token, selective orbital occupancy combined with electrostatic gating would extend our present knowledge on intra- and interband pairing mechanisms of 2D superconductivity¹¹ as well as on the observed universal Lifshitz transition, by which a switch from one- to two-carrier transport takes place at a universal charge carrier density¹². These, and other fascinating experiments, are possible by the crystal symmetry reconstruction of 2DEGs at the LAO/STO interfaces.

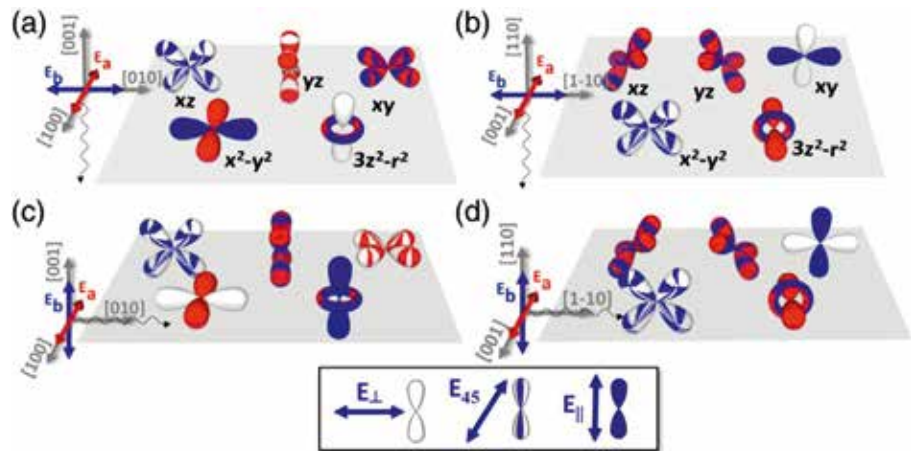


Figure 8: Schematics of the interaction of linearly polarized light with d orbitals for normal incidence of X-rays on (001)-oriented samples (a) and (110)-oriented samples (b); same schematics for the case of grazing incidence on (001) samples (c) and (110) samples (d). The color shading code is shown in the box.

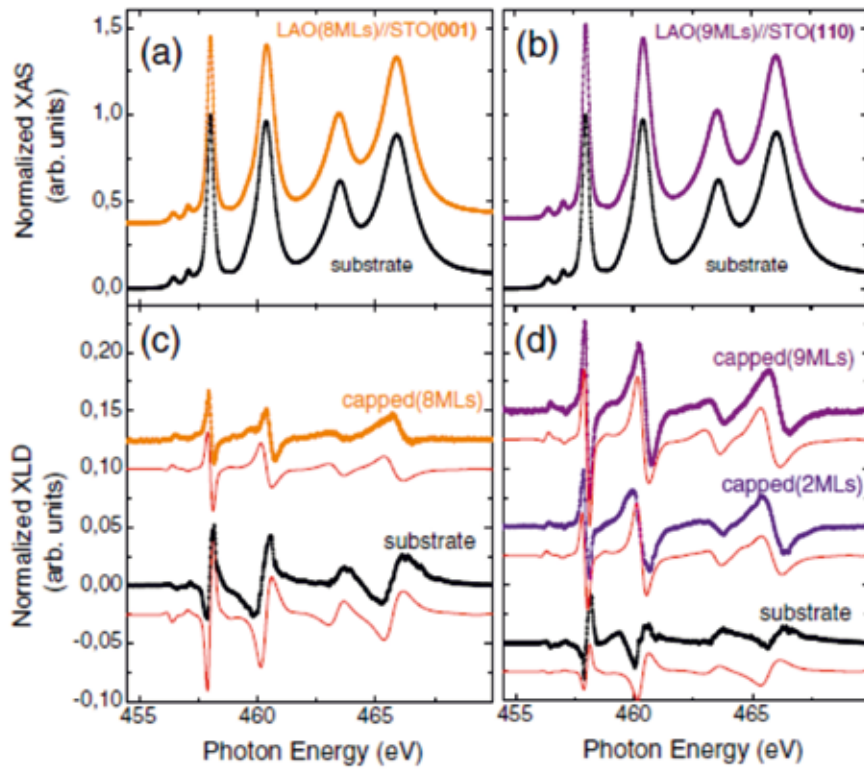
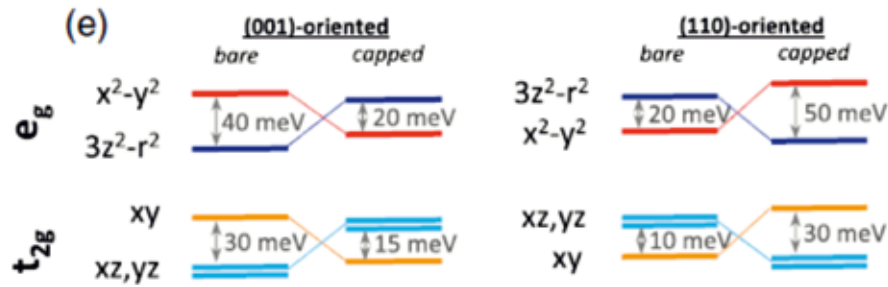


Figure 9: Normalized XAS spectra measured at grazing incidence are plotted for bare STO surfaces as well as LAO/STO interfaces for orientation along (a) [001] and (b) [110]. The LAO thickness is 8 MLs for (001) and 9 MLs for (110) interfaces. The corresponding XLD spectra are shown for (001)- and (110)-oriented samples in (c) and (d), respectively. Red lines, corresponding to XLD simulations using CTM4XAS, are shifted for clarity. Finally, the energy splittings for (001)- and (110)-oriented samples are sketched in (e).



REFERENCES

- ¹ Ohtomo, A. & Hwang, H. Y. A high-mobility electron gas at the LaAlO₃/SrTiO₃ heterointerface. *Nature* 427, 423–426 (2004).
- ² Jang, H. W. et al. Metallic and insulating oxide interfaces controlled by electronic correlations. *Science* 331, 886–889 (2011).
- ³ Reyren, N. et al. Superconducting interfaces between insulating oxides. *Science* 317, 1196–1199 (2007).
- ⁴ Caviglia, A. D. et al. Electric field control of the LaAlO₃/SrTiO₃ interface ground state. *Nature* 456, 624–637 (2008).
- ⁵ S. Thiel, G. Hammerl, A. Schmehl, C. W. Schneider, J. Mannhart, *Science* 2006, 313, 1942.
- ⁶ G. Herranz, F. Sánchez, N. Dix, M. Scigaj, and J. Fontcuberta, *Sci. Rep.* 2, 758 (2012).
- ⁷ A. Annadi et al., *Nat. Commun.* 4, 1838 (2013).
- ⁸ G. Herranz et al., *Nat. Commun.* 6, 6028 (2015).
- ⁹ E. Stavitski and F. M. F. De Groot, *Micron* 41, 687 (2010); F. M. F. de Groot, J. C. Fuggle, B. T. Thole, and G. A. Sawatzky, *Phys. Rev. B* 41, 928 (1990); M. Matsubara, T. Uozumi, and A. Kotani, *J. Synchrotron Radiat.* 8, 393 (2001).
- ¹⁰ J.-S. Lee, Y.W. Xie, H. K. Sato, C. Bell, Y. Hikita, H. Y. Hwang, and C.-C. Kao, *Nat. Mater.* 12, 703 (2013).
- ¹¹ R. M. Fernandes, J. T. Haraldsen, P. Wolfle, and A. V. Balatsky, *Phys. Rev. B* 87, 014510 (2013).
- ¹² A. Joshua, S. Pecker, J. Ruhman, E. Altman, and S. Ilani, *Nat. Commun.* 3, 1129 (2012).

THE SURFACE MAGNETIC MOMENT OF MAGNETITE (001)

Spin and orbital magnetic moment of reconstructed $\sqrt{2}\times\sqrt{2}R45$ magnetite(001).
Phys. Rev. B (Rapid Comm) 91 020408(R). (2015)

Laura Martín-García¹, Raquel Gargallo-Caballero¹, Matteo Monti¹, Michael Foerster², José F. Marco¹, Lucía Aballe², and Juan de la Figuera^{1*}

Magnetite, an iron oxide with formula Fe_3O_4 , is the oldest (and namegiving) magnetic material known to mankind. However, still today its surface magnetic properties are not fully known and understood. On one hand, the surface and interface magnetic moments may differ from the volume values. On the other hand, the surface and interface properties are key for using materials in modern spintronic and nanotechnology with steadily increasing surface to volume ratio, for instance in spin valves which are used as magnetic sensors in magnetic data storage like hard disk drives.

A collaboration between researchers from the Instituto de Química Física "Rocasolano" and the ALBA Synchrotron, employed the high surface sensitivity and multi-technique capabilities of the CIRCE low-energy electron and photoelectron microscope, to characterize the magnetic moment at the magnetite surface and correlate it with the surface reconstruction, i.e. the specific local atomic structure of the surface.

The (001) surface of a magnetite single crystal is studied by an approach combining photoemission electron microscopy with X-ray photoelectrons with *in situ* preparation monitored by low-energy electron microscopy and diffraction. The crystal surface is prepared by repeated cycles of sputtering and annealing in UHV with additional annealing in an 10^{-6} mbar oxygen atmosphere until a high quality low-energy electron diffraction pattern is observed, indicating that the surface is $\sqrt{2}\times\sqrt{2}R45^\circ$ reconstructed¹. Imaged with low energy electron microscopy, the surface of the crystal shows then typical square "mesas", structures of 1–2 μm width, aligned along the $\langle 110 \rangle$ in-plane directions as shown in Figure 10 (a). In dark field imaging mode, two equivalent surface terminations but rotated 90° between them, are shown to cover the whole surface area (Figure 10 (b)).

Illuminating the sample with polarized X-rays tuned to the iron absorption L edge and imaging the spatial distribution of the secondary electrons emitted by the X-ray absorption process, the magnetic domains are detected in complementary ways. While circular dichroism (XMCD, Figure 10(c)) is sensitive to the magnetic component along the X-ray beam direction, linear dichroism (XMLD Figure 10(d)) is sensitive to the magnetic component along the electric field direction. Combining these modes under different azimuthal sample rotation angles, the orientation of the magnetization was confirmed to be fully in the surface plane, along two in-plane easy axis directions of the $\langle 110 \rangle$ type. These easy axes are different from the volume $\langle 111 \rangle$ type, but represent the projections of the volume easy axes onto the surface.

AFFILIATION

¹Instituto de Química Física "Rocasolano" (CSIC), Madrid, Spain

²ALBA Synchrotron, Cerdanyola del Vallès, Barcelona, Spain

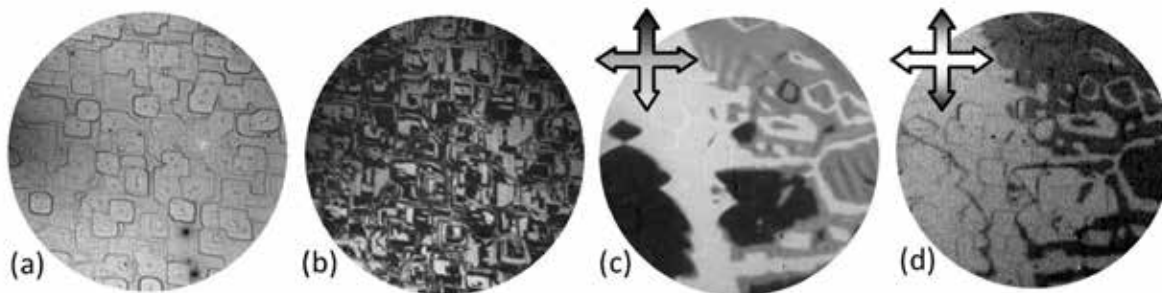


Figure 10: (a) Low-energy electron microscopy image of the *in situ* prepared surface of magnetite with (001) orientation. (b) Dark field electron microscopy image using diffracted electrons showing the two different surface terminations. (c) X-ray circular magnetic dichroism image showing the magnetic domains present at the magnetite surface. The grayscale magnetic contrast (inset arrow symbol) reflects the four-fold easy axis of the surface. (d) X-ray magnetic linear dichroism image, grayscale magnetic contrast according to the inset arrow symbol. All four images show the very same area, with field of view 20 μm .

Full XMCD spectro-microscopy stacks were acquired scanning the photon energy across the iron absorption edges with opposite circular polarizations in order to extract the spin and orbital magnetic moments of the magnetite surface by application of the XMCD sum rules. In order to vary the sampling depth, two different energies of the secondary electrons were selected to acquire the XMCD images: a very low kinetic energy (about 2 eV, equivalent to the total electron yield measurements in integrated XMCD), and 50 eV. Both measurements are very surface sensitive, and in the latter case there is agreement that the electron mean free path should be especially small, as it is near the minimum of the universal mean free path curve. In both cases, a reduced total moment of $3.3 \mu_B$ and a ratio of about 0.10 between orbital and spin moment was found. This reduction is attributed to the Fe^{2+} deficient surface reconstruction. The total magnetic moment for the volume was $4.07 \mu_B$. The ratio between orbit and spin moment for the volume “vanishing” and error bar at $3.3 \mu_B: \pm 0.07$.

In summary, the magnetic properties of the magnetite (001) surface have been measured and shown to be different from volume properties. In a first step, the surface of a magnetite single crystal with (001) orientation was prepared by sputtering/annealing cycles providing the $\sqrt{2} \times \sqrt{2} R45^\circ$ reconstruction. The distribution of magnetic domains on the surface was imaged by X-ray magnetic dichroism in a photoemission microscope, with the easy axes along the surface in-plane $\langle 110 \rangle$ directions. The near-surface magnetic moment was determined by applying the sum rules to XMCD spectra obtained with different kinetic energies of the secondary electrons. The reduced total magnetic moment of $3.3 \mu_B$ of the near surface material is in agreement with expectations for the Fe_{2+} deficient surface reconstruction. In order to obtain these results, the combination of surface preparation and different characterization techniques has been key.

REFERENCES

1 R. Bliem, G. S. Parkinson et al., *Science* 346, 1215 (2014)

ACKNOWLEDGEMENTS

This research was supported by the Spanish Ministry of Economy and Competitiveness through Project No. MAT2012-38045-C04-01. These experiments were performed at the CIRCE beamline of the ALBA Synchrotron with the collaboration of ALBA staff. For their contribution to the CIRCE beamline, J. Nicolas, E. Pellegrin, S. Ferrer, V. Pérez-Dieste, and C. Escudero are especially acknowledged. Fruitful discussions regarding the magnetic moment determination with E. Pellegrin and A. K. Schmid's help with and loan of the magnetite crystal are also acknowledged.

A SOFT X-RAY MAGNETIC CIRCULAR DICHROISM STUDY OF FERROMAGNETIC SrRuO₃

Electronic and spin states of SrRuO₃ thin films: An X-ray magnetic circular dichroism study.
Physical Review B 91, 075127 (2015)

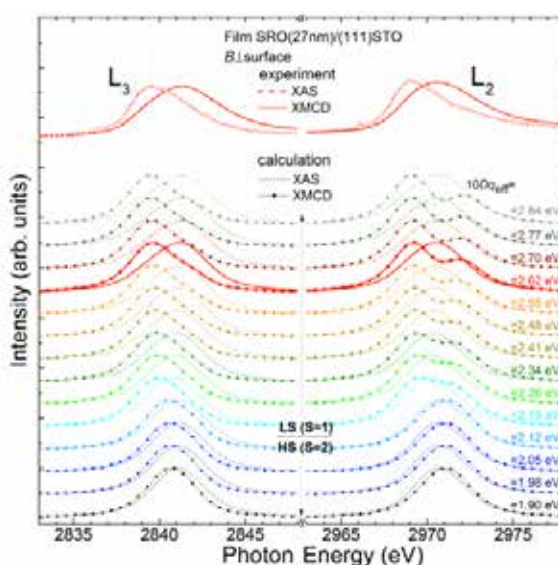
S. AGRESTINI¹, Z. HU¹, C.-Y. KUO¹, M. W. HAVERKORT¹, K.-T. KO¹, N. HOLLMANN¹, Q. LIU¹, E. PELLEGRIN^{2*},
S. M. VALVIDARES², J. HERRERO-MARTIN², P. GARGIANI², P. GEGENWART³, M. SCHNEIDER⁴, S. ESSER³,
A. TANAKA⁵, A. C. KOMAREK¹, AND L. H. TJENG¹

SrRuO₃ is one of the few known 4d transition-metal oxide ferromagnets with a Curie temperature as high as 160 K. Its rare physical properties have raised the interest of the scientific community during the last fifty years and recently also of the applied science sector due to its capacity for being used as an electrically conducting layer within heterostructured magnetic devices as used in storage technologies.

In this study, researchers have grown strained SrRuO₃ thin layers on (001)- and (111)- oriented SrTiO₃ substrates and compared them with unstrained SrRuO₃ single crystals. The technology for growing SrRuO₃ thin layers on (001) oriented SrTiO₃ substrates is well known. However, the systematic growth of thin films on (111)-oriented SrTiO₃ substrates is very recent.

Using synchrotron light from the BOREAS beamline, researchers wanted to determine if the compressive strain from the SrTiO₃ substrate can indeed induce a spin state transition of the Ru⁴⁺ cations (i.e., from S=1 to S=2) and if the Ru orbital magnetic moment is quenched (i.e., close to zero). Although the latter orbital magnetic moments are usually small, they can have a considerable influence on the anisotropic properties of magnetic systems. To this end, X-ray magnetic circular dichroism (XMCD) studies of the Ru L_{2,3} absorption edges were performed. Results show that for the strained as well as the unstrained samples the Ru orbital moment is close to zero and that the Ru spin (and thus the associated spin magnetic moment) is close to the low-spin value of S=1, as could be verified using theoretical calculations on the shape of the Ru L_{2,3} absorption spectra (see Fig. 11).

Figure 11: Experimental (top) and simulated (bottom) Ru L_{2,3} X-ray absorption (XAS) and X-ray magnetic circular dichroism (XMCD) spectra (the sign of the experimental L₃ XMCD spectrum has been reversed for clarity). The latter theoretical spectra show a transition from the S=2 high spin (HS) to the S=1 low spin (LS) state of the Ru atoms as a function of the ligand crystal field. The best agreement between experiment and theory is obtained for a Ru crystal field strength of 2.62 eV (solid and dotted red lines in bottom part).



AFFILIATION:

¹ Max Planck Institute for Chemical Physics of Solids, Nöthnitzerstrasse 40, 01187 Dresden, Germany

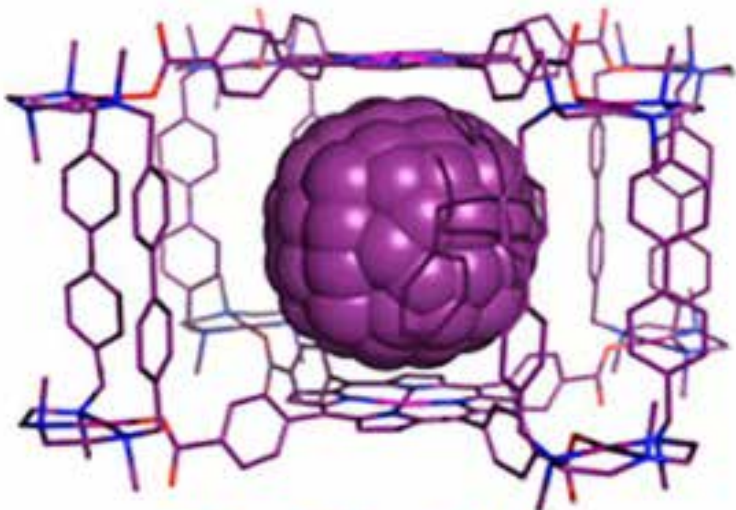
² ALBA Synchrotron, Cerdanyola del Vallès, Barcelona, Spain

³ Experimental Physics VI, Centre for Electronic Correlations and Magnetism, University of Augsburg, 86159 Augsburg, Germany

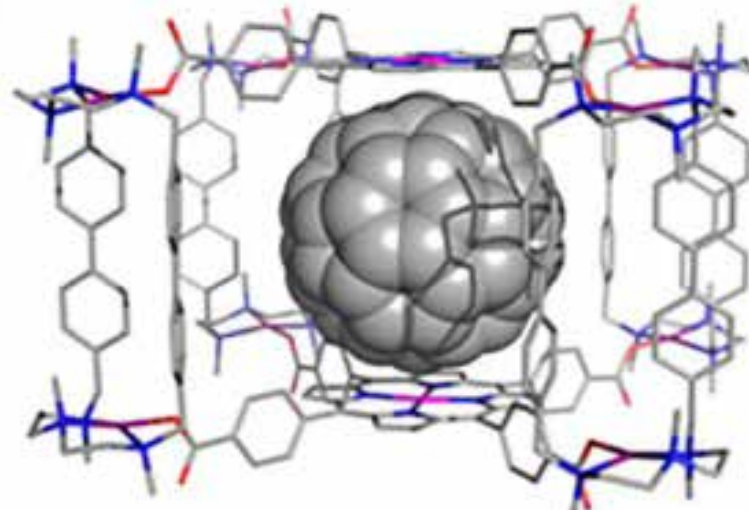
⁴ I. Physikalisches Institut, Georg-August-Universität Göttingen, D-37077 Göttingen, Germany

⁵ Department of Quantum Matter, ADSM, Hiroshima University, Higashi-Hiroshima 739-8530, Japan

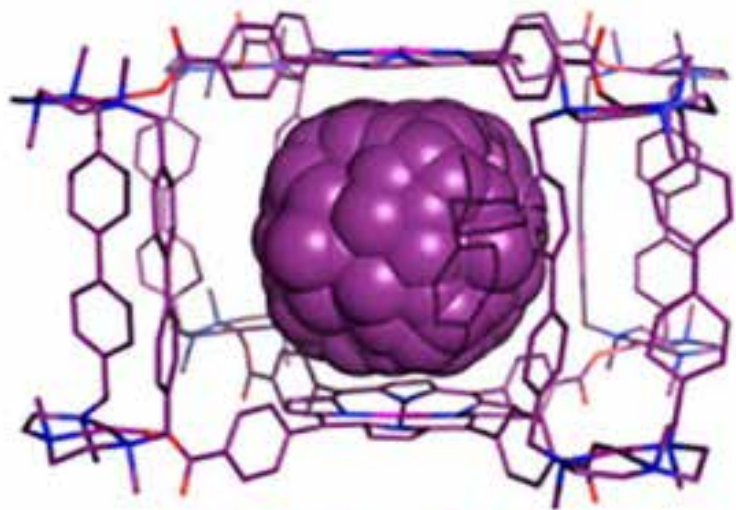
SCIENTIFIC RESULTS
MATERIALS SCIENCE



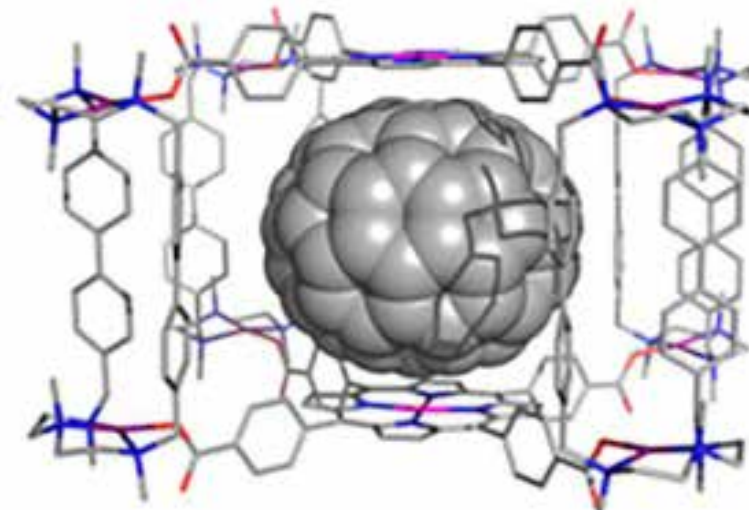
Zn...Zn = 13.1



Zn...Zn = 12.8



Zn...Zn = 13.7



Zn...Zn = 13.3

A SPONGE-LIKE MOLECULAR CAGE FOR PURIFICATION OF FULLERENES

Sponge-like molecular cage for purification of fullerenes. *Nature Communications*. 5, 5557. (2014)

CRISTINA GARCÍA-SIMÓN¹, MARC GARCIA-BORRÀS¹, LAURA GÓMEZ¹, TEODOR PARELLA², SÍLVIA OSUNA¹, JORDI JUANHUIX³, INHAR IMAZ^{4*}, DANIEL MASPOCH^{4,5}, MIQUEL COSTAS¹ & XAVI RIBAS¹

A fullerene is a molecule made of carbon that can be found in many shapes, such as spheres or tubes. They have a wide range of applications, highlighting their extensive use as electroactive materials in solar cells and with new uses continuously appearing in medicine. Any application, however, is limited in origin by tedious solid-liquid extractions (usually in toluene) and time-expensive chromatographic separations. Even the extraction of small amounts of purified fullerenes for research purposes becomes a complex process. Here the authors present a supramolecular nanocage synthesized by metal-directed self-assembly, which encapsulates fullerenes of different sizes.

The research has provided direct experimental evidence for the 1:1 encapsulation of C60, C70, C76, C78 and C84, fullerene molecules consisting of 60, 70, 76, 78 and 84 carbon atoms respectively (Fig. 12). Solid-state structures for the caged fullerenes with C60 and C70 have been obtained using X-ray synchrotron radiation. With a washing-based strategy it is possible to exclusively extract pure C60 from a solid sample of cage charged with a mixture of fullerenes.

This tetragonal prismatic supramolecular cage with a high affinity for the inclusion of fullerenes, and a facile ability to release them by solvent washing of the solid inclusion compound, is an attractive methodology to selectively extract C60 and, with a lower efficiency, C70 from fullerene mixtures. Although the method cannot be used to produce big amounts of purified fullerenes, it provides an experimental platform to design tuned cages for selective extraction of higher fullerenes. The solid-phase fullerene encapsulation and liberation represent a twist in host-guest chemistry for molecular nanocage structures.

AFFILIATION

¹ Institut de Química Computacional i Catàlisi and Departament de Química, Universitat de Girona, Campus Montilivi, Girona, Spain.

² Servei de RMN and Departament de Química, Facultat de Ciències, Universitat Autònoma de Barcelona (UAB), Campus UAB, Bellaterra, Spain.

³ ALBA Synchrotron, Cerdanyola del Vallès, Barcelona, Spain.

⁴ Institut Català de Nanociència i Nanotecnologia, ICN2, Campus UAB, Bellaterra, Catalonia 08193, Spain.

⁵ Institució Catalana de Recerca i Estudis Avançats (ICREA), Pg. Lluís Companys 23, Barcelona, Spain.

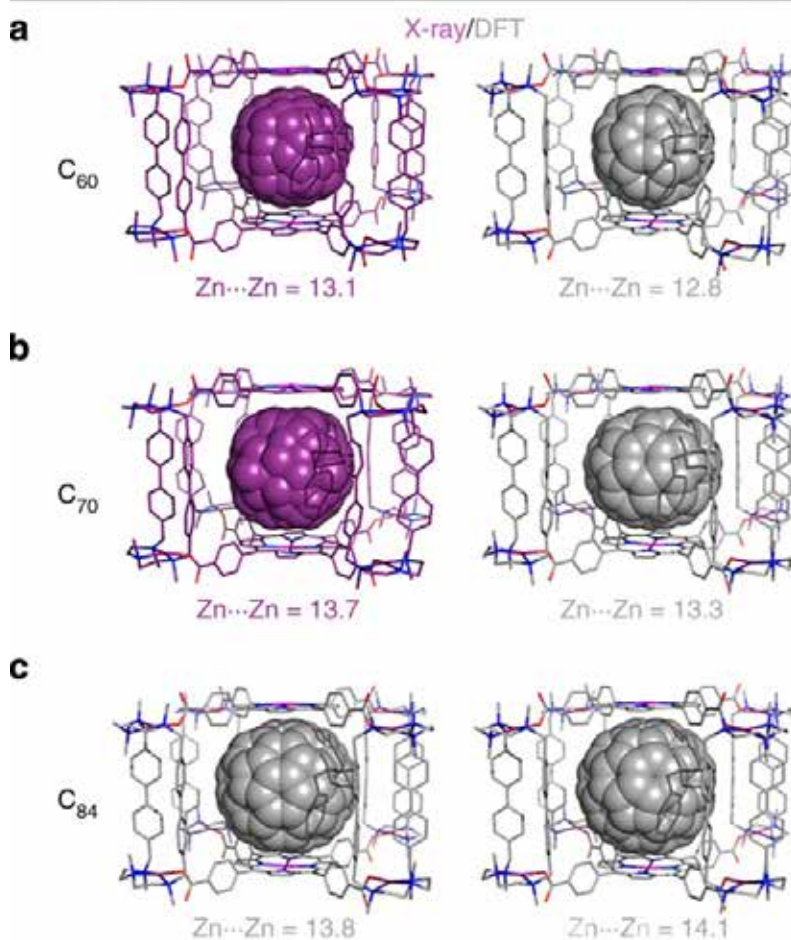
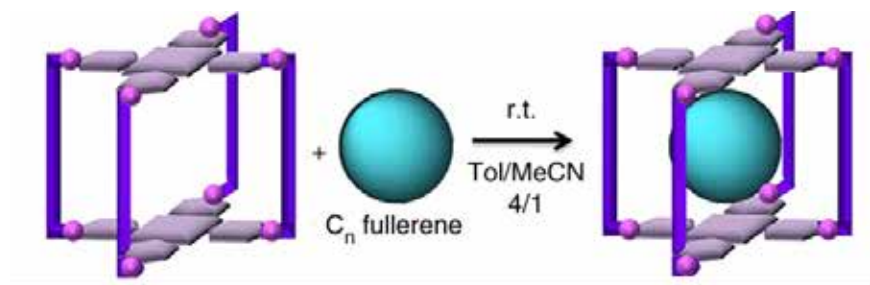


Figure 12: Above, schematic illustration of the encapsulation of fullerenes by the molecular cage C_4 . Below, X-ray diffraction and Density Functional Theory (DFT) analysis of fullerene host-guest compounds. Crystallographic data (purple) and DFT structures (grey) for cationic fullerene inclusion compounds (a) $C_{60}C_{48}^+$ and (b) $C_{70}C_{48}^+$; and (c) DFT calculation for $C_{84}C_{48}^+$ isomers IPR (D₂)-22 and IPR (D_{2d})-23 ($Zn \cdots Zn$ distances in Å). r.t., room temperature.

ACKNOWLEDGEMENTS

This work was supported by grants from the European Research Council (Starting Grant Projects ERC-2011-StG-277801 and ERC-2009-StG-239910), the Spanish MICINN (CTQ2012-37420-C02-01/BQU, CTQ2012-32436, CTQ2011-23156/BQU, CTQ2011-25086/BQU, Consolider-Ingenio CSD2010-00065, INNPLANTA project INP-2011-0059-PCT-420000-ACT1, MAT2012-30994, an RyC contract to I.I., a JdC contract JCI-2012-14438 to SO and a PhD grant AP2010-2517 to M.G.B.) and the Generalitat de Catalunya (2009SGR637 and a PhD grant to C.G.S.). Dr J.M. Luis and Professor M. Swart are acknowledged for fruitful discussions on DFT calculations, Dr C. Whiteoak for English grammar corrections, and Professor P. Ballester for providing the authors access to fluorescence spectroscopy measurements. X.R. and M.C. also thank the ICREA-Acadèmia awards.

NANOSTRUCTURED FIBRE SENSORS: *IN SITU* STUDY OF LIQUID INFILTRATION IN HIERARCHICAL CARBON NANOTUBE FIBRES

Electric Field-Modulated Non-Ohmic Behaviour of Carbon Nanotube Fibers in Polar Liquids.
ACS Nano, 8(8), 8497-8504 (2014)

J. TERRONES¹, J. A. ELLIOTT¹, J. J. VILATELA^{2*}, A. H. WINDLE¹

Liquid sensors benefit from a large surface area and minimal resistance to the flow of signals (current) once the external stimulus is detected. The potential of nanomaterials, and in particular carbon nanotubes, lies in their exceptionally high surface area and electrical conductivity. The authors have a process to assemble millions of these carbon nanotube “molecules” into a continuous fibre with a diameter similar to a human hair and extending over kilometres. Its complex structure consists of a network of multiple carbon nanotubes preferentially aligned parallel to each other, but with sufficient space between them to form pores accessible to gas and liquid molecules. Upon infiltration of these molecules the material experiences a change in electrical properties, thus giving out a signal indicating the presence of a foreign molecule. Of the many challenges to exploit the potential of these fibres as sensors, one of the most important is to accurately observe the structure of the material from the nano to the micro-scale, and how this hierarchical network changes in the presence of liquids. X-ray diffraction experiments at ALBA’s NCD beamline enabled the authors for the first time to observe such effects *in situ* and understand the relation between capillary forces and electrical sensor signals.

The experiments consisted of simultaneous 2D WAXS and SAXS at BL11-NCD. Typical examples of 2D diffractograms and an optical micrograph of a CNT fibre are shown in Figure 13. From WAXS data, information about the orientation of CNTs in the fibre can be extracted, for example by calculation of the FWHM azimuthal profile from radial integration of the (002) graphite reflection. In addition, the structure of the catalyst used during the synthesis process as FCC iron was determined. This finding has been critical in understanding how to control the Chemical Vapor Deposition (CVD) reaction and tailor the diameter and number of layers of the CNTs that make up the fibre. SAXS measurements allow to obtain the orientation distribution of the bundles, manifested as a streak perpendicular to the fibre axis (i.e. equatorial fibre streak). This scattering arises from the imperfect packing of CNTs, and closely corresponds to the pores accessible to foreign molecules such as liquids and polymers.

The authors observed that infiltrated fibres have non-ohmic electrical behaviour, whereby electrical resistance decreased at higher voltage bias. This suggested that an important component of electron transport in the infiltrated material occurred through tunnelling between adjacent

AFFILIATION

1. Department of Materials Science, University of Cambridge, UK.
2. IMDEA Materials Institute, Madrid, Spain.

Fibre vertically oriented, with CNTs
Preferentially aligned in fibre direction

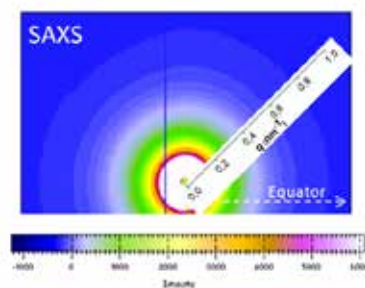
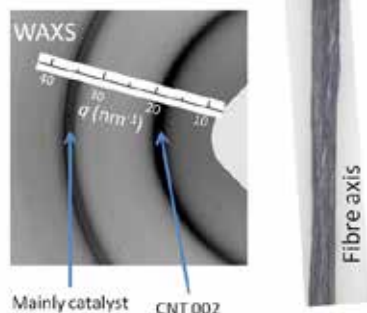


Figure 13: 2D WAXS & SAXS patterns of CNT fibres as-made showing multiscale structural information. The inner WAXS ring correspond to carbon nanotubes stacked at separations close to 0.34nm. The higher intensity at the equator reflects predominant alignment of the CNTs parallel to the fibre axis. The SAXS pattern corresponds to scattering from pores between CNT bundles, with size in the range of 1 to tens of nm.

elements, with the probability of tunnelling increasing in the presence of the liquid on account of its higher dielectric constant compared to air. On the other hand, the formation of surface charges (capacitance) at such junctions also implied that at higher bias voltages the equilibrium separation could be reduced. This hypothesis was for the first time demonstrated at BL11-NCD. The voltage supplied was of 1-15V so as to produce a current of 1-5mA. The effect of voltage on the shape of the network of conductive elements that make the fibres was determined by *in situ* SAXS measurements on fibres immersed in capillaries filled up with N-Methyl-2-pyrrolidone (NMP) and subjected to different voltages. The full-width at half-maximum (FWHM) of the azimuthal profile in the q range of 0.2-1.2 nm^{-1} provides a measure of the degree of orientation of CNTs and bundles in the fibre. The FWHM values against applied voltage are plotted in Figure 14, which also includes a typical pattern and a SEM image of the fibre. The plot shows an overall drop in the FWHM with increasing applied voltage, maintained even after the voltage was switched off and indicating an increase in CNT alignment parallel to each other and to the fibre axis. Such an improvement in orientation implies a closer contact between elements in the fibre through better packing and a reduction in the distance between them, and is thus consistent with the similar drop in electrical resistance.

Non-ohmic resistive behaviour in macroscopic CNT fibres infiltrated with polar liquids or polymers has been demonstrated. This behaviour is ascribed to the much higher dielectric constant of these media relative to air or nonpolar liquids. When using low-viscosity epoxy as infiltrating medium, authors find that the temperature dependence of both resin viscosity and electrical resistance lead to very similar activation energies. This suggests that the non-ohmic behaviour in infiltrated fibres is due to the reshaping of the CNT network in the fibre, induced by the electric field at the capacitive bundle junctions and detectable as an increase in bundle orientation as measured by synchrotron SAXS. The combination of resistive and capacitive behaviour in the fibre is confirmed by impedance spectroscopy on dry and infiltrated fibres. The non-ohmic behaviour in CNT fibres is ultimately a manifestation of nanoscale effects, for example conduction by interjunction tunneling, detectable on a macroscopic length scale. Results discussed here will apply to a variety of emerging hierarchical structures made up of other nano-building blocks assembled into macroscopic materials, such as graphene fibres, nanowire membranes, self-assembled metamaterials, and various other macroscopic hybrid materials.

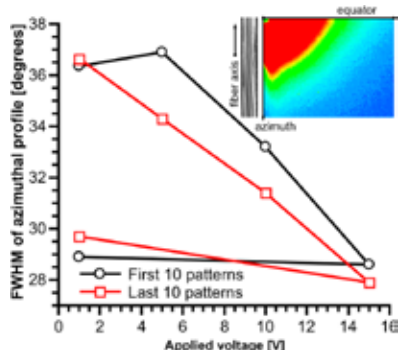


Figure 14. FWHM of the azimuthal profile of 2D SAXS patterns of a fibre immersed in NMP at different voltages. The decrease in FWHM is due to the electric field bringing bundles closer and therefore more aligned. The inset shows an electron micrograph of a CNT fibre and a section of the 2D SAXS pattern.

REFERENCES

1. V. Reguero, B. Alemán, B. Mas, J. J. Vilatela; Controlling Carbon Nanotube Type in Macroscopic Fibers Synthesized by the Direct Spinning Process; Chemistry of Materials; 2014, 26(11), 3550-3557;
2. B. Aleman, V. Reguero, B. Mas, J. J. Vilatela; Strong Carbon Nanotube Fibers by Drawing Inspiration From Polymer Fiber Spinning; ACS Nano; 2015, 10.1021/acs.nano.5b02408;
3. J. Qiu, J. Terrones, J. J. Vilatela, M. E. Vickers, J. A. Elliott, A. H. Windle; Liquid Infiltration into Carbon Nanotube Fibers: Effect on Structure and Electrical Properties; ACS Nano; 2013, 7(10), 8412-8422;

ACKNOWLEDGEMENTS

The authors are grateful to H. Yue and J. P. Fernandez for their assistance with synchrotron and rheological measurements, and to T. Gspann for the SEM image. J.T. acknowledges generous financial support from The Cambridge Commonwealth European and International Trust, CONACyT (Mexico), Dyson Ltd, and Pembroke College Cambridge. J.J.V. acknowledges support from MINECO (Spain) and FP7-People-Marie Curie Action-CIG. Synchrotron XRD experiments were performed at NCD beamline at ALBA Synchrotron with the collaboration of ALBA staff.

IN SITU SYNCHROTRON DIFFRACTION STUDIES ON SUBSTITUTED M_n -BASED SPINEL CATHODE MATERIALS DURING ELECTROCHEMICAL CYCLING

Influence of Iron on the Structural Evolution of $\text{LiNi}_{0.4}\text{Fe}_{0.2}\text{Mn}_{1.4}\text{O}_4$ during Electrochemical Cycling Investigated by *in situ* Powder Diffraction and Spectroscopic Methods. *Zeitschrift Für Anorganische Und Allgemeine Chemie*. 640, 3118-3126, (2014)

MURAT YAVUZ^{1,2,3}, NILÜFER KIZILTAS-YAVUZ¹, AISWARYA BHASKAR¹, MARCO SCHEUERMANN^{1,2}, SYLVIO INDRIS^{1,2}, FRANCOIS FAUTH⁴, MICHAEL KNAPP^{1,2,*}, HELMUT EHRENBURG^{1,2,3}

Lithium-ion batteries are rising energy storage systems which require high volumetric and gravimetric energy and power densities for their applications such as electric vehicles (EVs) and hybrid electric vehicles (HEVs). Since most of the commercial Li-ion batteries operate cathode-limited, to increase the battery performance, it is essential to develop more suitable cathode materials¹.

$\text{LiNi}_{0.5}\text{Mn}_{1.5}\text{O}_4$ (LNMO) is a highly promising cathode material, which shows an impressive electrochemical performance. In the ideal case, the structure has no Mn in the trivalent state, which is well-known as Jahn-Teller ion causing structural instability. However, usually a small amount of Mn^{3+} remains in the compound as a result of oxygen deficiency after the high temperature synthesis process². Partial substitution with Fe could increase the structural stability of the system during cycling and improve the thermal stability.

In battery research, *in situ* synchrotron powder diffraction is one of the most powerful tools to investigate structural changes such as the de/insertion of lithium from/into electrode materials, formation of crystallographic phases or tracking of microstructural changes and site occupancies. Short exposure times during the electrochemical cycling are necessary to observe changes in the materials on the same time scale as during charge and discharge in a battery.

Ex situ and *in situ* diffraction experiments were performed at beamline BL04-MSPD using synchrotron radiation with an energy of 30 keV and an exposure time of 40 s. The diffraction patterns are obtained using a MYTHEN 1D Position Sensitive Detector. The initial powders were filled into glass capillaries with a diameter of 0.5 mm for *ex situ* XRD, and a new *in situ* cell design was used for *in situ* diffraction experiments³.

The cell housing is made of stainless steel. The windows of the cell for the beam are sealed with thin glass discs ($\approx 100 \mu\text{m}$), fixed with a high-density polyethylene foil by heating up to 180°C. The cells were prepared in an Ar-filled glovebox and consist of a stack of a contact stainless steel spring, nickel current collector, lithium foil (Alfa Aesar) as counter electrode,

AFFILIATION

1 Karlsruhe Institute of Technology (KIT), Institute for Applied Materials (IAM) Hermann-von-Helmholtz-Platz 1 76344 Eggenstein-Leopoldshafen, Germany
 2 Helmholtz Institute Ulm for Electrochemical Energy Storage (HIU) P. O. Box 3640 76021 Karlsruhe, Germany
 3 Technische Universität Darmstadt Materials Science Alarich-Weiss-Strasse 2 64287 Darmstadt, Germany
 4 ALBA Synchrotron, Cerdanyola del Vallès, Barcelona, Spain

two pieces of glass fibre (Whatmann®-GF/D) separator with 12 mm diameter size soaked in LP30 electrolyte (Merck, 1M LiPF₆ in ethylenecarbonate (EC): dimethylcarbonate (DMC) = 1:1) and the working electrode (coated cathode).

The sample holder can hold four *in situ* cells that can be automatically interchanged allowing cycling of 4 cells in parallel (Fig. 15). All electrodes were electrochemically cycled with a VMP3 multi-channel potentiostat (Bio-Logic, France) at 25°C in the voltage range of 3.5-5.3 V for LiNi_{0.4}Fe_{0.2}Mn_{1.4}O₄ (LNFMO) at a current rate C/2 (i.e. complete discharge within 2 h) with galvanostatic cycling.

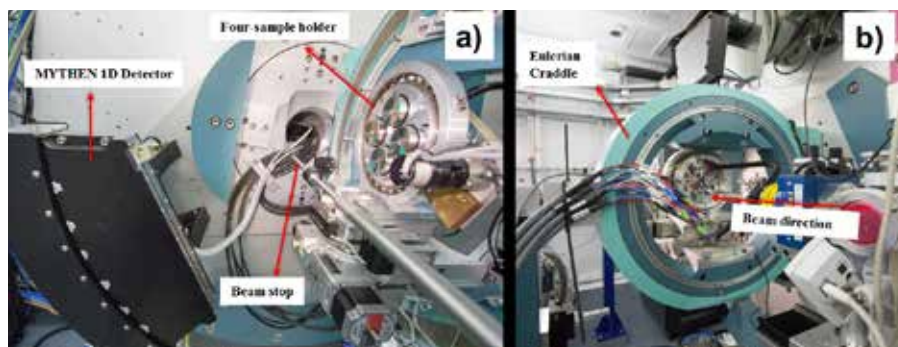


Figure 15: (a) Overview of the MSPD beamline at ALBA with MYTHEN 1D Detector, (b) the four-sample holder in the beam direction with cradle.

The initial powder sample has a cubic spinel structure with space group $Fd\bar{3}m$ without any impurity phase (Figure 16). The electrochemical mechanism of LNFMO cathode material (cycled within the voltage range of 3.5-5.3 V with C/2 current rate) is very similar to a solid solution mechanism (see Figure 17), where mainly a single cubic spinel phase remains throughout the complete cycle. However, there is a phase separation into a second cubic spinel phase ($Fd\bar{3}m$). Moreover, the obtained lattice parameters for the two cubic spinel phases are very close to each other (see Figure 18). Apparently, the formation of this second phase is reversible because it disappears at the end of the discharging process. The micro-strain analysis obtained by Rietveld refinement is shown in Figure 19. An increase in lattice strain was observed at the voltage points where the Ni²⁺/Ni⁴⁺ and Fe³⁺/Fe⁴⁺ redox couples are active. The overall strain as well as the change in lattice strain that occurs during cycling is lower than in undoped LiNi_{0.5}Mn_{1.5}O₄. The existence of huge lattice strain or changes of it in the structure during cycling leads to cracks and eventually results in loss of electrical contact and finally to quick capacity fading. Therefore, the improved structural stability of LNFMO during cycling also improves cycling performance.

REFERENCES

- 1 A. Bhaskar, D. Mikhailova, N. Kiziltas-Yavuz, K. Nikolowski, S. Oswald, N. N. Bramnik, and H. Ehrenberg, '3d-Transition metal doped spinels as high-voltage cathode materials for rechargeable lithium-ion batteries', *Progress in Solid State Chemistry*, 2014.
- 2 N. Kiziltas-Yavuz, A. Bhaskar, D. Dixon, M. Yavuz, K. Nikolowski, L. Lu, R.-A. Eichel, and H. Ehrenberg, 'Improving the rate capability of high voltage Lithium-ion battery cathode material LiNi_{0.5}Mn_{1.5}O₄ by ruthenium doping', *Journal of Power Sources*, 267, 533–541, 2014.
- 3 M. Herklotz, 'Advances in *in situ* powder diffraction of battery materials – a case study of the new beamline P02.1 at DESY Hamburg', *Journal of Applied Crystallography*, 46, 1117 – 1127, 2013.

ACKNOWLEDGEMENTS

This work has benefitted from beamtime allocation at the Materials Science and Powder Diffraction beamline (MSPD) at ALBA. This research has received funding from the BMBF, project grant number 03SF0477B (DESIREE). The authors thank Wilhelm Boldt for helping to synthesize the samples.

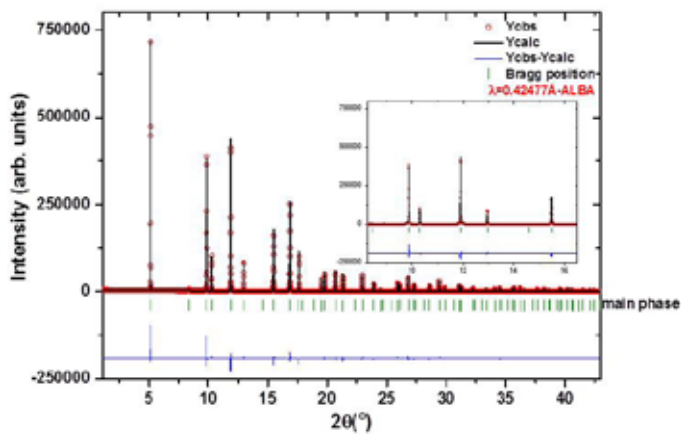


Figure 16: Synchrotron diffraction pattern of as-prepared LNFMFO measured in 0.5 mm capillaries.

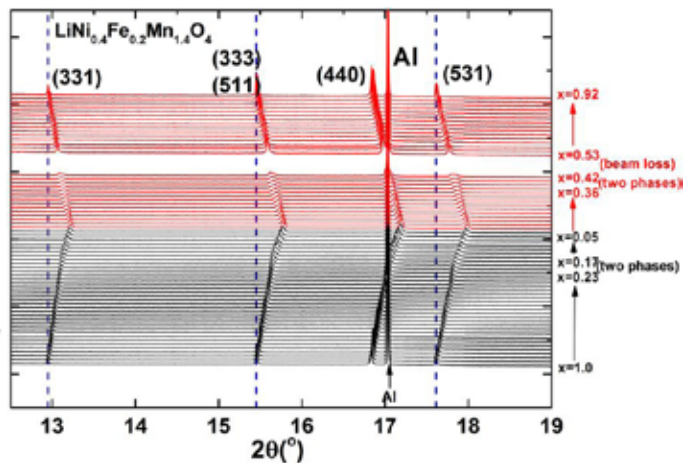


Figure 17: Selected 2θ regions of the *in situ* synchrotron diffraction patterns of LNFMFO cathode material.

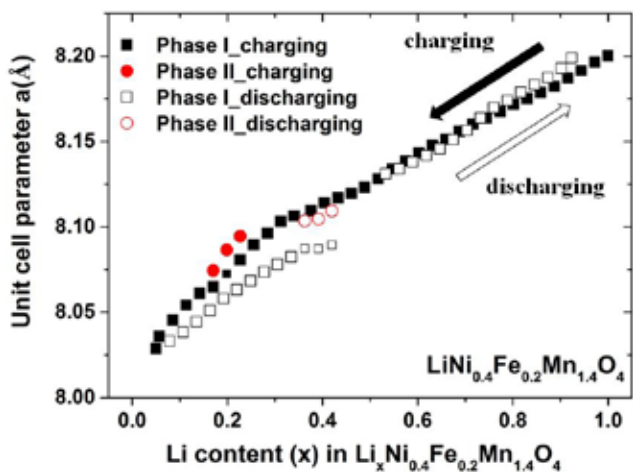


Figure 18: Change in the unit cell parameter as a function of nominal number of moles of Li (x) remaining in the structure.

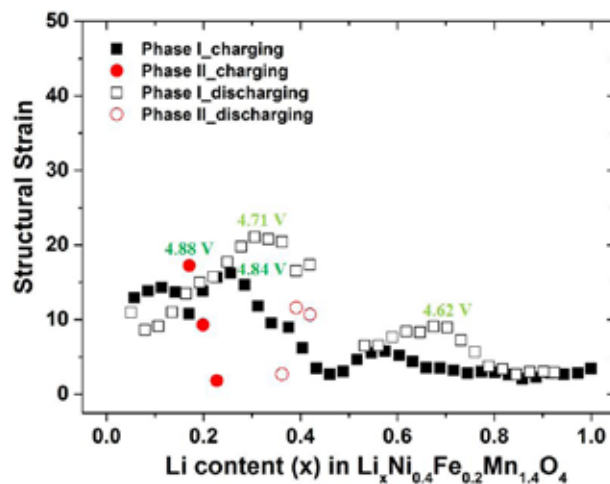


Figure 19: The micro-strain analysis. The maximum strain as given in the Fullprof microstructural output file as $\frac{\Delta d}{d} \times 10^{-4}$.

INDUSTRIAL LIAISON OFFICE

THE ALBA COMMITMENT IS TO DEVELOP COLLABORATIONS AND TO MAKE THE ADVANCED SYNCHROTRON TECHNIQUES AVAILABLE TO THE INDUSTRY, WHICH ENHANCES ITS R&D CAPABILITIES AND INCREASES ITS COMPETITIVENESS.



The Industrial Liaison Office acts as a single contact point for the interested industries to facilitate as much as possible access to the ALBA services. Even though it is a relatively new activity at the ALBA Synchrotron, industries are becoming more and more familiar with the current techniques and innovations. In 2014, the Industrial Liaison Office has almost triplicated the industrial beamtime used by industries (see Fig. 20) and set up the procedures and started the activity referred to intellectual property and technological transfer. Different types of services have been provided to private companies, ranging from punctual ones to longer term collaborations. Not only new companies have become ALBA users but also some companies have become routine users meaning that the services offered are crucial for their research or developments. Being conscious of its importance, a big effort has been carried out in terms of outreach activities to disseminate the synchrotron techniques among industries and to attract more industrial customers.

One of the main achievements of the year 2014 is the increase of the industrial beamtime usage as well as the number of customers, both local and international. Moreover, four out of seven beamlines hosted industrial experiments during last year: CLAES and MSPD were the most used beamlines followed by NCD and BOREAS. The type of experiments were diverse, covering different research areas such as chemistry, pharmaceuticals, environmental studies or automotive. Long-term collaborations with industries continued in 2014 and are also of great interest for ALBA as they have been really successful both in terms of good and abundant results and in terms of defining the future new techniques required by ALBA to keep offering a good portfolio of services. Sometimes these long collaborations involve industrial postdoc personnel, funded by the companies, working at ALBA and at the company premises. Figure 21 shows two pie charts with the beamlines and the research fields of the industrial activities carried out during 2014.

Besides the beamtime usage, other laboratories such as the magnetic measurements lab and the RF lab were also offered for proprietary access to external

users. These types of laboratories are particularly suited for equipment supplier companies. In this sense, discussions on long-term collaborations in the area of cleaning of optical components have also been held.

Another relevant achievement during the year 2014 is the start of the technological transfer activities and the intellectual property protections. Most of them are related with innovations developed at ALBA, others are in collaboration with other institutions. One patent for the magnetic measurements bench, two utility models of a new viewport compatible with high vacuum and a KB motion system compatible with ultra-high vacuum have been registered in the Spanish patent office. All these developments may be of interest for the industrial community and may be offered for licensing.

Also in the direction of innovation and the marketing of academic developments, ALBA has been involved in the pilot programme called EDI (Innovation Teams), promoted by the Fundació Catalana per a la Recerca i la Innovació, with two different projects, one in the engineering area and the other one in the computing and controls area. The aim of the programme was to promote relations between the research and business sectors. The ALBA teams took advantage of the training offered during the programme as well as the funding for the development characterization and technological transfer studies.

Outreach and marketing activities play a central role in the Industrial Liaison Office, which is essential for such a young facility like ALBA. In 2014 an industrial workshop focusing on the chemical and materials science sectors was held at the ALBA premises. Polymers, plastics developments, chemical raw material industries as well as health care, pigments, coating, and petrochemical industries attended the meeting making a total of nearly 30 companies. Among other outreach activities, an invited presentation about the ALBA industrial capabilities was performed at EXPOQUIMIA 2014, an International Chemical Exhibition, with more than 500 industrial exhibitors.

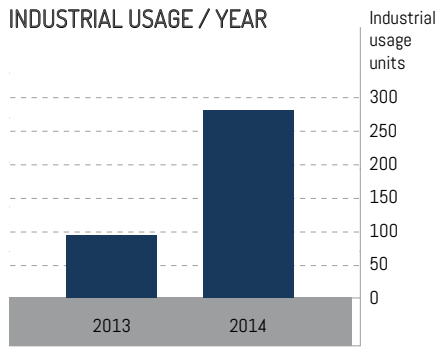


Figure 20: Bar chart showing the industrial usage during the periods 2013 and 2014.

Networking activities have been performed within the CALIPSO project, funded by the European Commission, where most of the Industrial Liaison Offices from synchrotron facilities across Europe and selected companies gathered and shared their experience and knowledge.

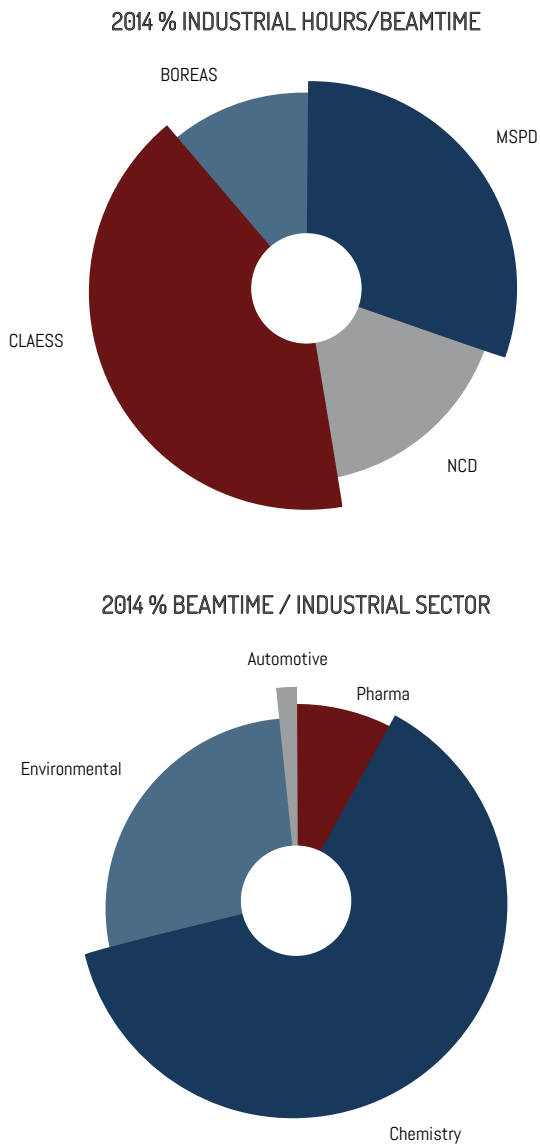


Figure 21: pie charts with the beamlines (top) and the research fields (bottom) of the industrial activities carried out along 2014.



Networking session during the industrial workshop for chemical and materials science companies held at ALBA in April 2014.

ACTIVITY REPORTS BY DIVISION

ACCELERATORS

THE ACCELERATOR DIVISION OPERATES THE ALBA ACCELERATORS. IT ALSO DESIGNS AND IMPLEMENTS IMPROVEMENTS AND UPGRADES. ALBA HAS THREE ELECTRON ACCELERATORS. THE LINAC IS A LINEAR ACCELERATOR IN WHICH ELECTRONS ARE GENERATED AND ACCELERATED UP TO 100 MEV. THESE ELECTRONS ARE THEN INJECTED INTO THE BOOSTER WHERE THEY ARE FURTHER ACCELERATED TO 3.0 GEV AND FINALLY TRANSFERRED TO THE STORAGE RING, WHERE THEY PRODUCE THE SYNCHROTRON RADIATION FOR USERS. IN THE FOLLOWING PAGES A SUMMARY OF THE MAIN ACTIVITIES PERFORMED DURING 2014 BY THE ACCELERATOR DIVISION IS PROVIDED.



OVERVIEW

During 2014 the ALBA accelerators have operated for more than 5000 h with a 96.8% of beam availability. Table II shows the main parameters of the Storage Ring.

Energy	3 GeV
Circumference	268.8 m
Operating current	110 mA
Emittance	4.6 nm-rad
Coupling	0.5%

Table II: Main Storage Ring characteristics

The Accelerators division has been working in several projects during 2014 in order to further improve the quality of the beam provided to the users and to get a deeper knowledge of our Storage Ring, which should later translate into operational improvements. Hereafter is a short status report on the different projects in which the machine has been working during 2014.

TOP-UP INJECTION: FROM DECAY TO TOP-UP

The ALBA Storage Ring has been designed to operate in top-up mode. In this injection mode, the current in the Storage Ring is kept constant at a level of 1% or less, by doing frequent injections. The advantage of these frequent and short injections is that the Front Ends (FEs) remain open and the beamlines receive an almost constant heat load, avoiding thus thermal drifts that are detrimental to their performance, as shown in figure 22.

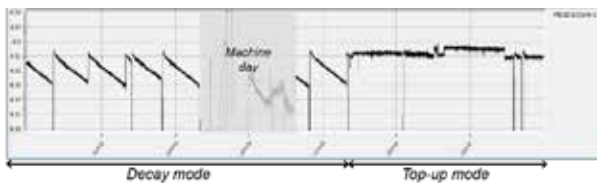


Figure 22: Vertical position of the photon beam in decay and top-up modes for BL09. We can observe the improvement in stability in top-up mode due to the constant current that eliminates the thermal drift observed in decay mode.

There are several issues that need to be considered before a facility like ALBA switches from decay mode injection into top-up injection: the first one is radiation safety, since in top-up, injection is done with FEs ends open and it must be ensured that the injected electrons cannot reach any beamline under any circumstance. In addition, under top-up injection the injector is almost in

continuous operation. Its reliability and performance are also issues to be addressed.

Safety simulations were addressed by particle tracking simulations. The simulations were performed to determine if there were any realistic scenarios that could bring an injected beam of electrons down an open beamline FE. Realistic magnetic field, trajectory, aperture and energy errors were taken into account over a large range of faulty conditions.

For the Insertion Device (ID) beamlines simulations, an aperture boundary enclosing all FE apertures was defined by enlarging by a safety margin of 20% the second mask aperture of the FE with the largest aperture. If top-up is demonstrated to be safe for this configuration, then all other ID beamlines must also be safe. The bending magnet beamline (BL09) required an additional simulation. The simulations demonstrated that the stored beam condition is sufficient to guarantee that neither a single error nor more combined events could lead to a top-up accident. Therefore, top-up injection is only allowed if there are at least 20 mA in the Storage Ring with a nominal lifetime.

To ensure that injection conditions are good, for each injection cycle a Linac-to-Storage-Ring injection efficiency is calculated. This number for cycle (i-1) is then used to estimate the time an injection at cycle (i) would take under the same conditions. An extra margin of 10% is added, and if the injection in cycle (i) takes longer than the calculated time, then top-up is stopped and, before starting again, a corrective action by the operator is required.

In addition to the simulations, experimental tests were conducted for each beamline during injection with FEs under different working conditions, i.e. different injection efficiencies, different settings of slits at the FEs and also as a function of the ID position. For 6 out of 7 beamlines there has been no detectable increase of radiation measured outside the optical hutches. However, for BL29, which uses an elliptical undulator as a photon source, an increase in the radiation dose around the optical hatch has been measured under bad injection conditions (injection efficiency less than 50%) together with a closed ID gap and closed masks. In any case, the integrated dose has always stayed below 2 μSv in 4 h, which is the public dose limit. On this specific FE, due to space restrictions, the movable masks were placed in the optical hatch. Under these circumstances any misaligned/blow-up photon beam coming from the Storage Ring will be stopped first at the optical hatch. An additional shielding has been designed and installed. Therefore the

experimental hall continues to be a public area also during top-up injection.

Because it is extremely difficult to have an injection process which is fully transparent, the beamlines have been provided with software signals that indicate the different steps during an injection cycle. The beamlines may use these signals to gate the top-up injection.

At ALBA, top-up has started with injection cycles every 20 min, in which about 1% of the beam is re-injected. This number is flexible and could be changed at any time as required by the beamlines. Figure 23 shows a four-weeks run in top-up. It is important to notice that, under this operation mode, the injector, even if it is running more often, runs for less time, and that no detrimental effect on the injector has been observed by working with this new injection mode.



Figure 23: Storage Ring current during one run operating in top-up. Note the 100% beam availability over a 2 weeks period.

TURN-BY-TURN MEASUREMENTS

To meet the required performance, modern synchrotron light sources demand a fine control over lattice parameters. Until now, lattice measurement and correction methods have been based on low orbit data acquisition (LOCO). The possibility to retrieve linear model information from turn-by-turn (TbT) beam position data has been proven at ALBA, as shown in figure 24. Agreements down to 1-2% RMS beta beating and 5-7 mrad RMS phase error have been achieved between LOCO

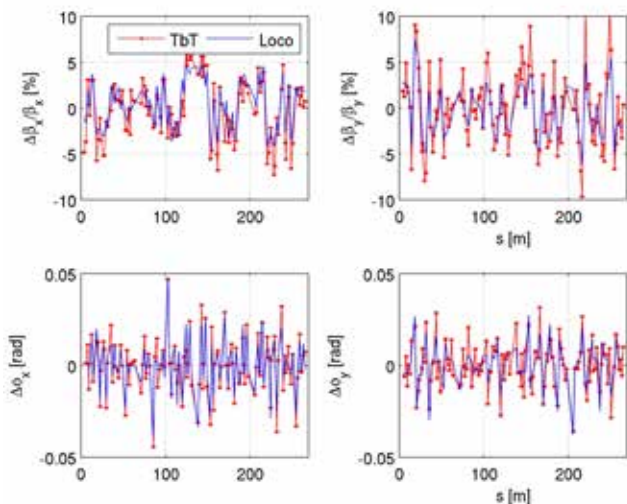


Figure 24: Beta beat and phase error with respect to the model measured using both LOCO and TbT data.

and TbT, which is close to the simulated LOCO accuracy. TbT measurements have opened as well the possibility to measure and correct non-linear properties of the Storage Ring lattice.

NEW MAGNETIC MEASUREMENT BENCH FOR CLOSED STRUCTURES

At the Insertion Device Lab a new bench for measuring large and closed structures has been designed, built and is now being tested. The bench consists of a Hall probe head with a weight of only 0.75 g, containing 3 miniature Hall sensors and a PT100, to measure the magnetic field in the 3 space directions and the temperature. The Hall probe head is fixed in the middle of a flexible belt, made of carbon fibre that can easily be introduced inside a closed magnetic system. The edges of the belt are attached to an external mechanical bench to position the Hall probe with a high degree of accuracy. The positioning error of the Hall probe head with respect to the encoder is below $10 \cdot 10^{-6}$ mm.

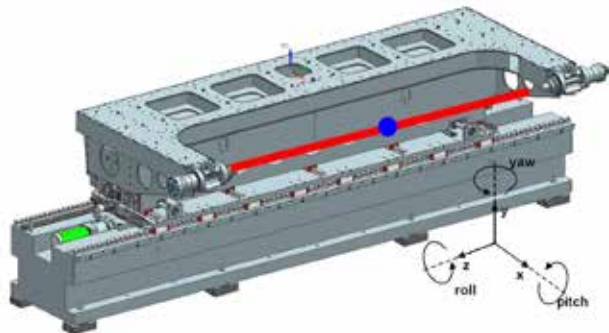


Figure 25: General view of the new Hall probe bench and reference system. Stretched belt is red and Hall probe is marked with a blue dot.

INTERFEROMETRY AT ALBA TO MEASURE VERTICAL BEAM SIZE

Vertical beam size in 3rd generation light sources cannot be determined by using a simple image system because the beam size is diffraction limited. Measurement of the vertical beam size at the Storage Ring (typically 24 μm) is routinely performed using an x-ray pinhole camera. In order to have a 2nd reliable measurement of this parameter, a double-slit synchrotron radiation interferometer technique has been developed. In this technique the degree of spatial coherence of the synchrotron radiation produced by the beam is measured, and then the beam size can be inferred. Figure 26 shows the optical setup at the diagnostics beamline.

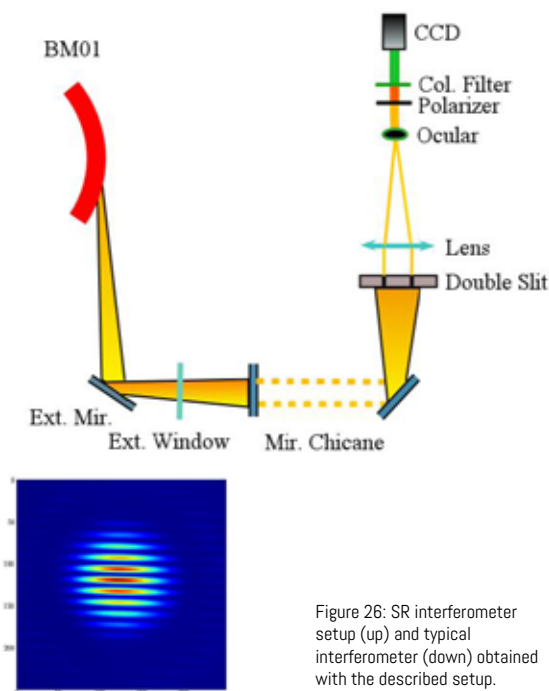


Figure 26: SR interferometer setup (up) and typical interferometer (down) obtained with the described setup.



Pinger magnets under assembly.

The double-slit system has been replaced by a double-pinhole system to obtain reliable data. Special care has been taken to block any air turbulence in the optical path as well as to optimize the CCD settings. First results indicate a good agreement between the pinhole and the interferometer.

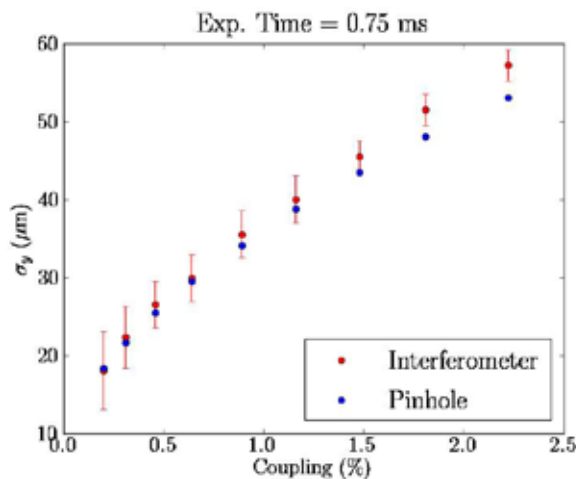


Figure 27 : Vertical beam size for different machine couplings as measured with the pinhole and the interferometer.

PINGER MAGNET

Two pulsed magnets, called pinger magnets because they ping (kick) the beam over one turn, have been designed, built and tested in-house. During the summer shutdown they were installed in the Storage Ring and have since been used to probe the non-linear regime of beam dynamics in the Storage Ring. This study is aimed at optimizing the Storage Ring dynamic aperture and the beam lifetime.

FAST ORBIT FEEDBACK (FOFB)

The ALBA slow orbit feedback system (SOFB) stabilizes the photon beam in a position and angle of less than 10% the beam size and beam divergence, which is the minimum requirement for a 3rd generation synchrotron light source. But the SOFB has a bandwidth limit of about 1 Hz. In order to stabilize the beam at higher frequencies, up to 100 Hz, ALBA started the development of a fast orbit feedback system (FOFB) in 2013. During 2014 the FOFB has been extensively tested, including during user operation.

The FOFB system uses 88 beam position monitors. The Libera Brilliance BPM electronics provide a continuous data flow of position values at a 10 kHz rate through their high-speed serial connection ports. The correction computation, based on the widely-used SVD algorithm, runs on 16 distributed CPUs to which the BPMs data is transferred and which calculate the new set points for the corrector power supplies.

For the correction, 88 vertical and 88 horizontal corrector magnets are used. The corrector coils are extra windings in the sextupole magnets. To minimise eddy current effects, the vacuum chamber has a 1 mm thickness reduction where the sextupoles are located. Also the thickness of the laminations of the sextupoles is only 0.5 mm in order to reduce eddy currents in the core of the sextupoles.

The commissioning tests have been done using a preliminary Graphical User Interface from where the feedback system can be started/stopped and the different parameters involved can be tested and optimized. The last version of the correction code has separated PI loops for the horizontal and the vertical

plane, since the feedback requirements and the beam noise are different depending on the plane.

The RF frequency control will be implemented as a routine on the high-level FOFB device server. The routine will monitor the dispersive pattern on the horizontal correctors and change the RF accordingly. The minimum frequency step and the correction periodicity are parameters that can be modified in the FOFB GUI.

The current activities are dedicated to optimise the user-friendly interface and to provide a robust system for operation.

With the new system, the orbit is corrected up to frequencies of 200 Hz and the rms value of the residual

orbit has decreased almost by one order of magnitude. It is now 0.08 μm in the horizontal plane and 0.04 μm in the vertical plane.

By sampling the beam position data at 10 kHz, the integrated power spectral density (PSD) has been calculated in both planes. Figure 28a compares the PSD in the horizontal plane with and without the FOFB on, and figure 28b does the same for the vertical plane.

It is noticeable that the FOFB completely dumps the 3 Hz noise of the BO when injection is on. The signal at 3 Hz is, together with the 50 Hz signal, the largest source of noise on the measured spectrum when the FOFB is off. The distortion at 50 Hz does not disappear completely but it is damped by a factor of 2.

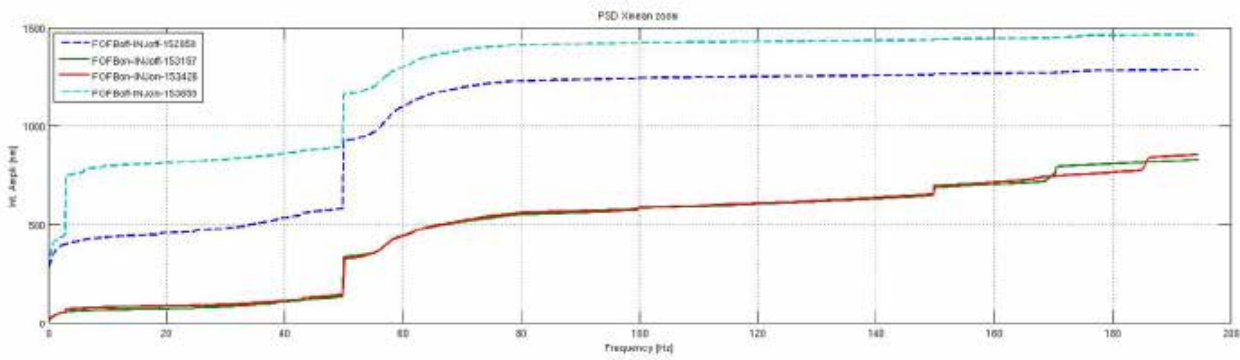


Fig 28a: Integrated spectra for the horizontal plane. Up to 200 Hz the integrated noise is below 1 μm when the FOFB is running. The colours correspond to spectra taken under different working conditions. Blue: FOFB off, injection off; green: FOFB on, injection off; red: FOFB on, injection on; and light blue: FOFB off, injection on.

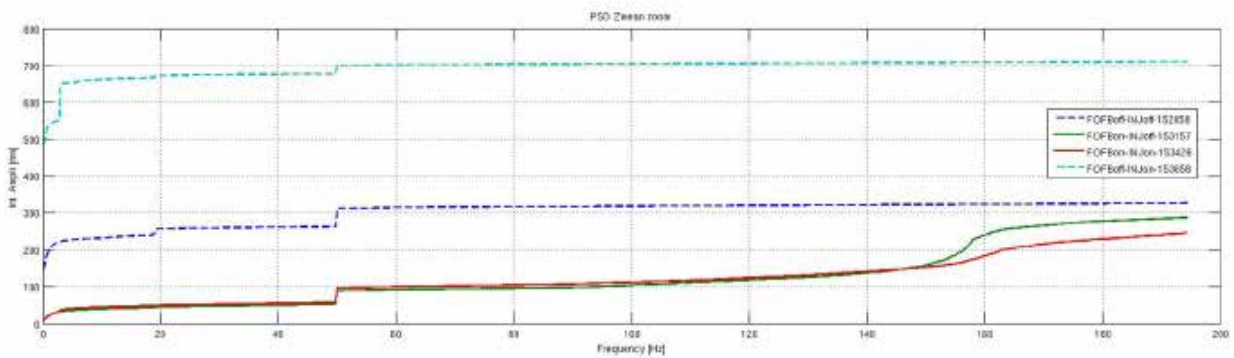
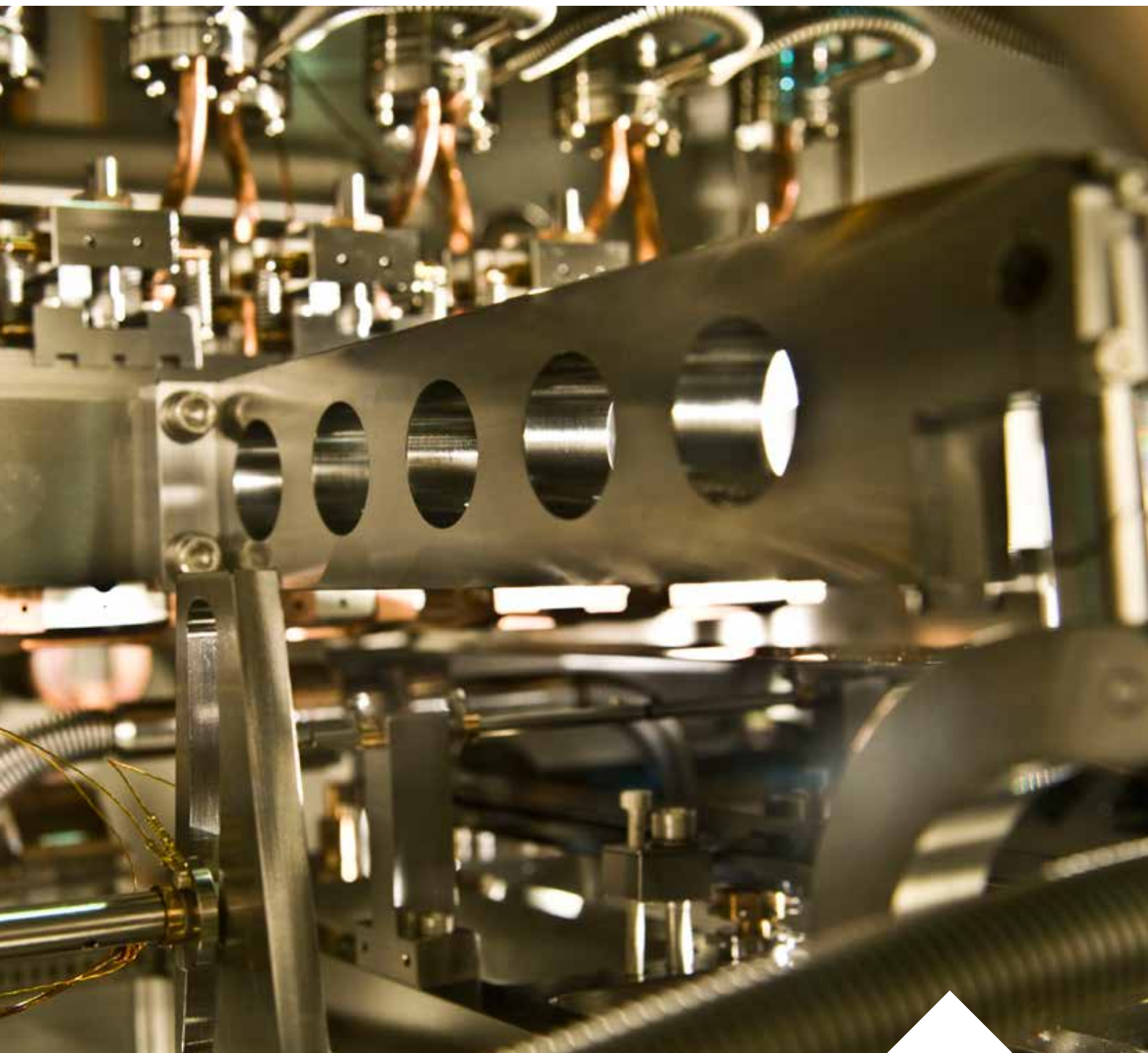


Fig 28b: Power spectral density for the vertical plane. Up to 200 Hz the integrated noise is below 0.3 μm when the FOFB is running. The colours correspond to spectra taken under different working conditions. Blue: FOFB off, injection off; green: FOFB on, injection off; red: FOFB on, injection on; and light blue: FOFB off, injection on.

ACTIVITY REPORTS BY DIVISION

ENGINEERING

THE ENGINEERING DIVISION IS MADE UP OF A TEAM OF 32 MULTIDISCIPLINARY ENGINEERS AND TECHNICIANS THAT GIVE SUPPORT TO THE OTHER DIVISIONS IN ALBA (MAINLY TO EXPERIMENTS AND ACCELERATORS) AND TO THE ALBA FACILITY ITSELF. IT CONSISTS OF TWO SECTIONS: THE INFRASTRUCTURES SECTION AND THE TRANSVERSAL SECTION.



The Infrastructure Section is devoted to civil engineering projects and the maintenance of facilities and processes. The Transversal Section has several groups that provide transversal engineering services (mainly design of instrumentation) to the beamlines and the Accelerator, and some groups that provide support to the operation on Vacuum, Cryogenics and Logistics.

In what follows, a description of the activities in 2014 will be given. Besides this, the division has started to offer new services: a "vibration service" which provides help to the engineers to know the real performances of the structures and components they design. It is also a powerful tool to know the behaviour of any instrument, including the stability of slab of the experimental hall allowing to predict and optimize the expected

stability and vibrations of future beamlines, as well as the post processing of the measured data is included in the service.

INFRASTRUCTURES SECTION

NEW HUMIDITY, TEMPERATURE AND PRESSURE CONTROL SYSTEM AT BIOLOGY LAB BIO II+

A new humidity control system has been successfully implemented at our Biology Laboratory classified BIO II+. Specifications required treating and renewing air while keeping relative humidity below 40% and a temperature of 22 +/- 2 °C with 12 Pascal of negative pressure. The

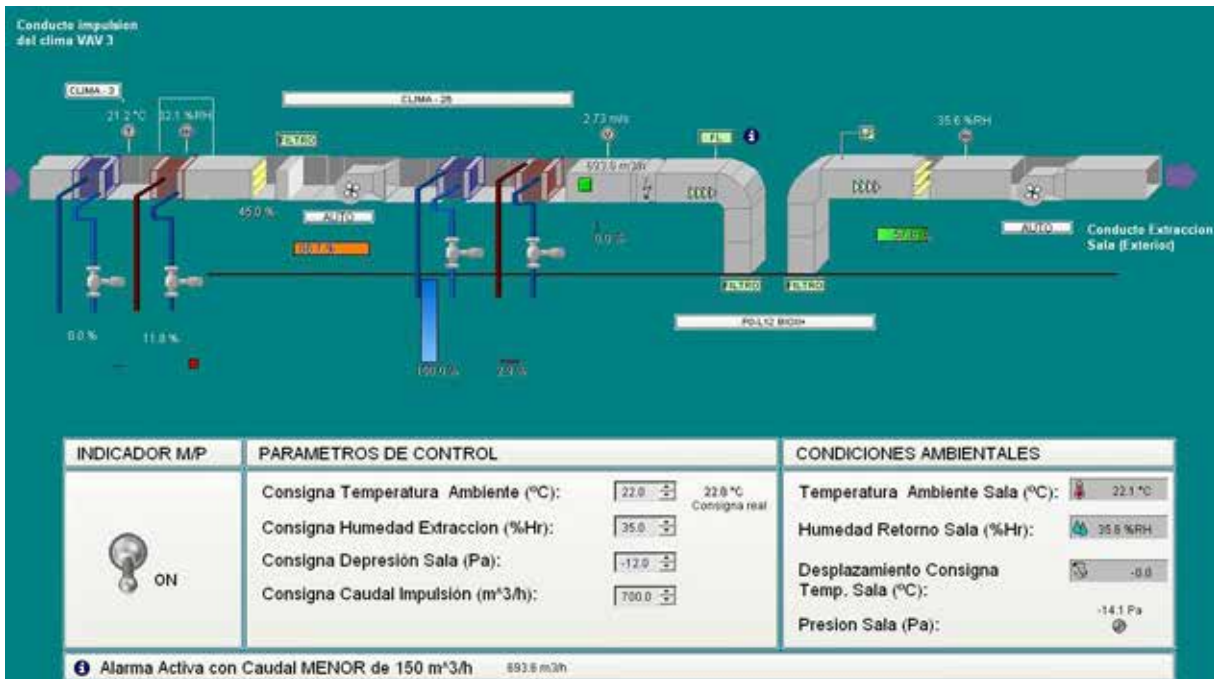


Figure 29: Sinoptic diagram of the new system.

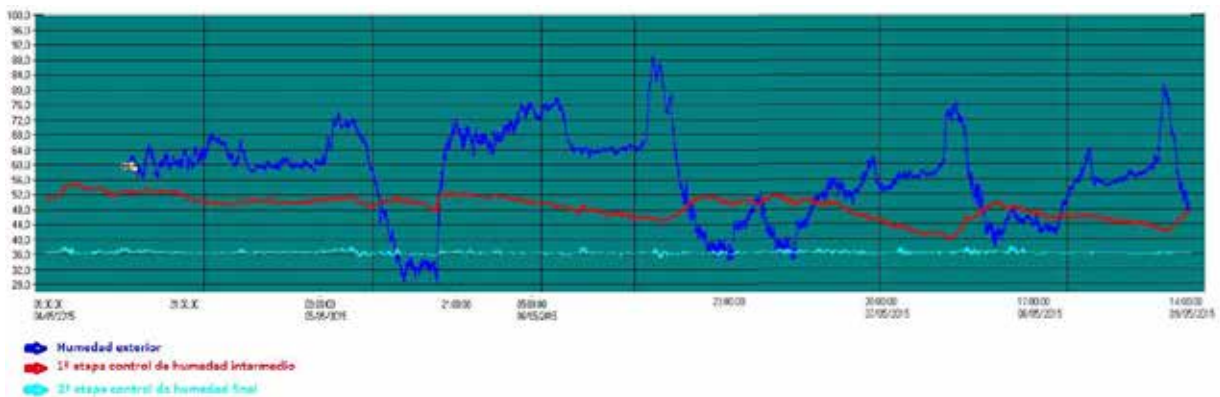


Figure 30: Measured humidity vs. time at the Bio II+ Lab. (dark blue=outdoor; red=controlled after 1st stage; light blue=controlled after 2nd stage).

temperature and humidity control is performed by two air treatment units with cooling and post heating phases each one, supplying fresh air treated and filtered at a rate of 750 m³/h while an adjustable extractor that aspires up to 1000 m³/h giving under pressure conditions (Fig. 29). The control system is based on the implementation of a MIMO (multiple input, multiple output) open loop system. The system uses the information on temperature, humidity, pressure, flow and speed of treated air provided by sensors. As shown in figure 30, the exterior humidity fluctuations have a peak-to-peak variation of about 50%, that reduces to 20 % in the first stage (red curve) and to less than 4% in the second stage.

SF₆ GAS RECOVERY AND REFILL FACILITY

The 3 GHz radiofrequency produced by each one of the two Klystrons (KA1 and KA2) located at the Service Area is transmitted to the cavities of the Linac, through waveguides that are filled with SF₆ gas, used as an insulator. The SF₆ gas recovery and refill facility has been designed and implemented in order to satisfy the following needs:

- Recovery and storage of the SF₆ gas emptied in gas cylinders, due to the high potential of fluorinated gases to produce greenhouse effect if released into the atmosphere. The storage of the used gas allows correct and sustainable waste management.
- Emptying and filling the SF₆ gas when a waveguide needs to be repaired or due to a scheduled maintenance.
- The volumes filled with SF₆ gas, at a pressure of 4 bar (absolute), are 34.7 liters and 20.8 liters for the waveguides from KA1 and KA2 to cavities respectively.

SF₆ gas cylinders for the refilling of the waveguides are connected to a gas panel equipped with internal gas purging to avoid contaminant entering the line after changing the cylinders. The purging system consists of a pressure regulator, inlet and outlet pressure gauges, a relief valve and shut-off valves for the process gas and for the purge gas. SF₆ gas recovery cylinders for the recovery of the used gas are connected to a gas booster that multiplies the low inlet gas pressure in the Booster to obtain a high outlet pressure needed to insert the gas inside the recovery cylinders. All tubing and fittings are AISI 316 L joined with orbital welding.

TRANSVERSAL SECTION

UPGRADES AND INSTRUMENTATION DEVELOPMENT AT XALOC BEAMLINE

1) NEW HUMIDITY AND TEMPERATURE CONTROL SYSTEM.

In order to assure the proper environment conditions at XALOC Experimental Hutch, a humidity and temperature control system was required. The equipment has been located out of the experimental hutch, hanging from the stairs structure so that no vibration is transmitted to the beamline. Based on a *Munters* ML420 dehumidifier device, the performance reached is: relative humidity better than 40% in any case, with a regulation range from 25% to 40%, and with a stability of ±5%. Temperature control performances are: range from 20°C to 25°C with a set point of 23°C & a stability of ±0.5°C.

2) NEW CRYOSTREAM. The N₂ gas cryostream gun located at the XALOC endstation maintains the samples to be analyzed under cryogenic temperatures. The new Cryostream provides an In-out fast 10 mm linear movement in 1 s (based on a stepper motor actuated guided system) and a Near-far 45deg rotatory movement based on a pneumatic actuator and a cross-roller bearing.

3) NEW DEGASSER (PHASE SEPARATOR). The new Degasser is fully vacuum-insulated and is able to increase the liquid nitrogen quality by separating gas from the liquid nitrogen consumed. A new degasser was installed to avoid the leak of cold nitrogen gas in XALOC Hutch.

NEW UHV MOTION SYSTEM FOR CIRCE AND BOREAS

An all new UHV motion system has been designed to replace the current KB mirror motors which have performance problems (up to failure). All the parts of the new design are fully UHV-compatible, avoiding exotic housings. All movements are rolled avoiding dry frictions, thus making it a maintenance-free mechanics. The new device has been patented and it is already working into two CIRCE KB mirror system movements. Performances for this frictionless mechanism are 5 mm range for a 250 N payload, long duty cycles, 0.1 μm resolution, 2.7 μm backlash, < 0.5 μm repeatability.

NEW WATER COOLING MOTOR PUMP BENCHES

The current common return pump for the ALBA water cooling system has a too short operating life due to the fact that the mechanical structure has eigenfrequencies that couple

to the 50 Hz of the mains. A new design has been done by means an accurate FEA which even includes the concrete steel reinforcement and the concrete anisotropy. With the new design, the two independent pumps' first resonance mode is located at 172 Hz.

HALL PROBE BENCH PROTOTYPE FOR CLOSED MAGNETIC STRUCTURES

The concept prototype proposed, as described in further detail in the Accelerators division report, is based on a floating arc structure with a tensioned strip where a Hall effect sensor is mounted. All this assembly is displaced and positioned on the three axes. A small prototype bench with 1200 mm of measuring range has been developed and is under commissioning. The aim of this development is to learn empirically about this concept in order to construct a bigger bench of 3000 mm range. The prototype has been validated and can be extrapolated for a longer measuring range of 3000 mm.

NCD FLIGHT TUBE DOWNSTREAM WINDOW PROTECTION

At NCD beamline, a new automatic protection system has been developed to protect ALBA staff and users of a vacuum implosion due to the Flight Tube window break (because of lifetime limitations and material degradation of the kapton foil). The new device consists of a steel plate actuated with a pneumatic cylinder that covers the kapton window when someone is inside the experimental hut. Red and green lights placed outside Experimental Hutch next to both doors, display the corresponding access permissions.

UPGRADES AND INSTRUMENTATION DEVELOPMENT AT MSPD BEAMLINE

- 1) WATER COOLING SYSTEM ANALYSIS AND UPDATE WORKS. Since the beginning of the operations, the MSPD beamline has been suffering problems in its water cooling system with insufficient water flow in some of its components. In order to get a better understanding and improvement of operation, an analysis and a simulation of different configurations of the system have been performed. The system has been re-optimized, and a global increase of water flow from 100 to 110 l/min has been reached. Enough to solve the interlock problems at the beamline.
- 2) DIFFRACTOMETER CABLE CHAINS. HUBER Diffractometer in MSPD has three rotation discs with independent movement, an outer disc with a MAD detector installed, a middle disc with a MYTHEN detector installed and finally

an inner disc with the Eulerian Cradle installed. In order to save the relative rotations between the middle disc and the outer disc, and between the outer disc and the cable trays installation, a system of cable chains has been designed to collect and route all cables in the diffractometer to protect and ensure its correct operation.

UPGRADES AND INSTRUMENTATION DEVELOPMENT AT MARES, BOREAS

- 1) CRYOMAGNET TOOL. MARES endstation has a cryomagnet (Fig. 31, left) that must be moved vertically inside the vacuum chamber during normal operation. This must be done with $1\mu\text{m}$ resolution and a tilt angle independent from the support or the vacuum chamber. Performances are: vertical range up to 520mm, operation range of 265mm, resolution $1\mu\text{m}$, tilt adjustment, option to remove magnet.
- 2) ENDSTATION SUPPORT. MARES is a complex multicomponent instrument for soft X-ray scattering in a UHV environment (see Figs. 31 and 32). The whole system is supported by a stable support with an accurate transverse beam movement. The goal of the design was to achieve both high stability and high resolution movements, and for a big massive and tall setup. The concept is based on a first fixed stage of support composed of four angled natural granite columns acting as a pyramid with a frame where the transverse movement is mounted. In spite of the big mass (about 2 tons) the system can be moved perpendicularly to the beam with $0,2\mu\text{m}$ resolution keeping the first resonance mode over 40Hz (thus, far from floor excitations). Performances of this support are: range of transverse beam movement $\pm 20\text{mm}$; movement resolution $0,2\mu\text{m}$; X,Y, Z fully adjustable.
- 3) ENDSTATION DETECTORS. MARES endstation has a Θ , 2Θ rotary feedthrough that allows the positioning of some detectors and samples in the appropriate configuration to perform the experiment. Two mechanical arms have been developed (one for an in-vacuum camera and the other, for some diodes with slits, Fig. 33). Performances reached are: movement resolution of $1\mu\text{m}$, bakeable, self-supported and highly stable (resonance modes over 35Hz).

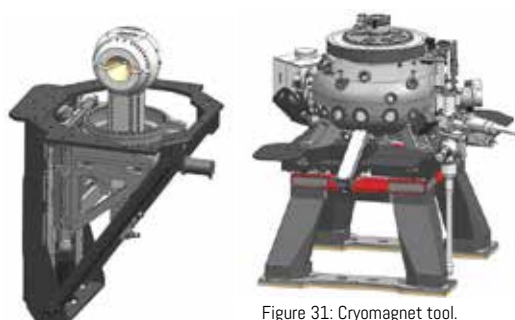


Figure 31: Cryomagnet tool.

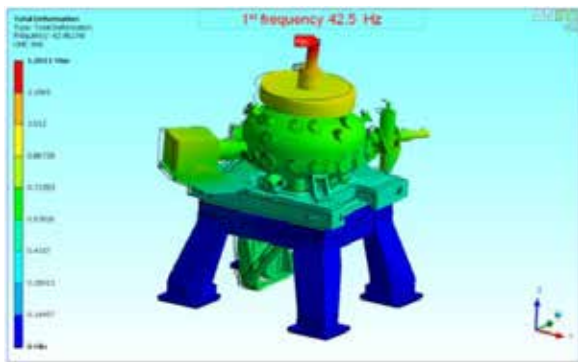


Figure 32: Static Analysis. First eigenmode shown as a qualitative map of relative displacements.

4) SAMPLE TRANSFER. The Sample Transfer system of BOREAS (Fig. 34) allows exchanging samples between the two beamline endstations: Hector and Mares. The system is composed of three UHV vacuum chambers provided with two rack-and-pinion components that move the samples. The central chamber is the distribution chamber that can be used as a load-lock and external docking system. Everything is mounted on a high-rigidity support.



Figure 33: Endstation detectors



Figure 34: Sample Transfer

THE NEW INFRARED BEAMLINE MIRAS

1) VACUUM PROFILE. MIRAS, one of the two new phase-II beamlines at ALBA, will be dedicated to infrared microspectroscopy experiments. This beamline will be directly connected to the Storage Ring, and as a consequence, the vacuum will be shared. Being that a critical issue to the proper operation of the machine, the vacuum profile has been calculated and optimized with the insertion of MIRAS in the simulation model (Fig. 35). The simulation has been done by means of the MolFlow+ software. The following two steps described in Fig. 35 have been followed.

2) THERMAL-MECHANICAL STUDIES OF THE EXTRACTION MIRROR FOR MIRAS. The thermal-mechanical behaviour of the extraction mirror for MIRAS has been quantitatively analysed. Using the software package SynRad+, the trajectory of the Storage Ring photons coming from the

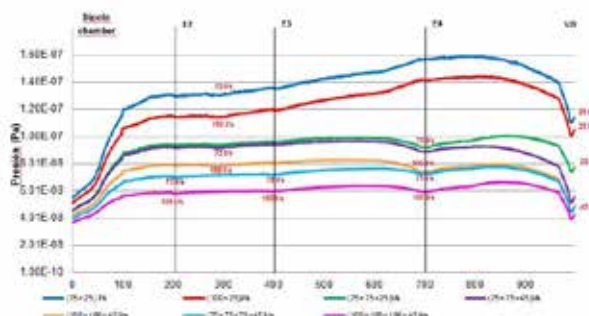


Figure 35: 1) Creation and calibration of a simulation model for the sector of the storage ring where MIRAS will be attached. 2) Dimensioning of the vacuum system of the inside tunnel part of MIRAS ensuring no affect negatively the vacuum level of the Storage Ring. Vacuum profile: Chamber pressure for different pumping configurations (75 l/s + 25 l/s) vs (100 l/s + 25 l/s) vs etc. along the vacuum chamber from the dipole chamber up to the Diamond window (path length in mm).

upstream bending magnets is calculated and traced through the mirror until their reflection and absorption. This allows to obtain the power density as boundary condition and to simulate by using ANSYS the thermal-mechanical behaviour of the extraction mirror. For the worst conditions (Beam Current = 400 mA, Thermal Contact Conductance Aluminium - Copper = 2000 W/m²C, and air free convection) the maximum temperature reached at the centre of the mirror is 76.6°C and the surface deformation is <2μm.

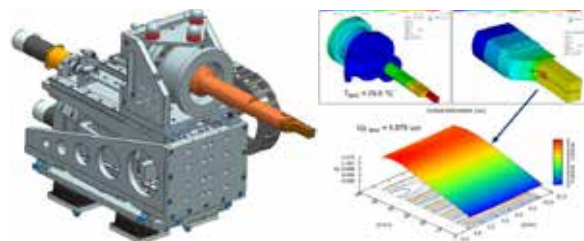


Figure 36: Analysis of the thermal-mechanical behaviour of the MIRAS extraction mirror.

3) THERMAL-MECHANICAL DESIGN OF THE CUSTOMIZED ABSORBER FOR MIRAS. In order to protect the extraction mirror for MIRAS, a customized copper absorber has been designed. The power boundary conditions are calculated by SynRad+, and the maximum temperature, stress and strain have been simulated with ANSYS. The model has been optimized for the maximum beam current = 400 mA. The maximum values for the stress, strain, temperature and wall-cooling water are in a safe region (35.3 MPa, 0.031%, 145°C and <65°C respectively).

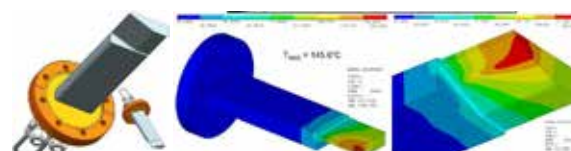
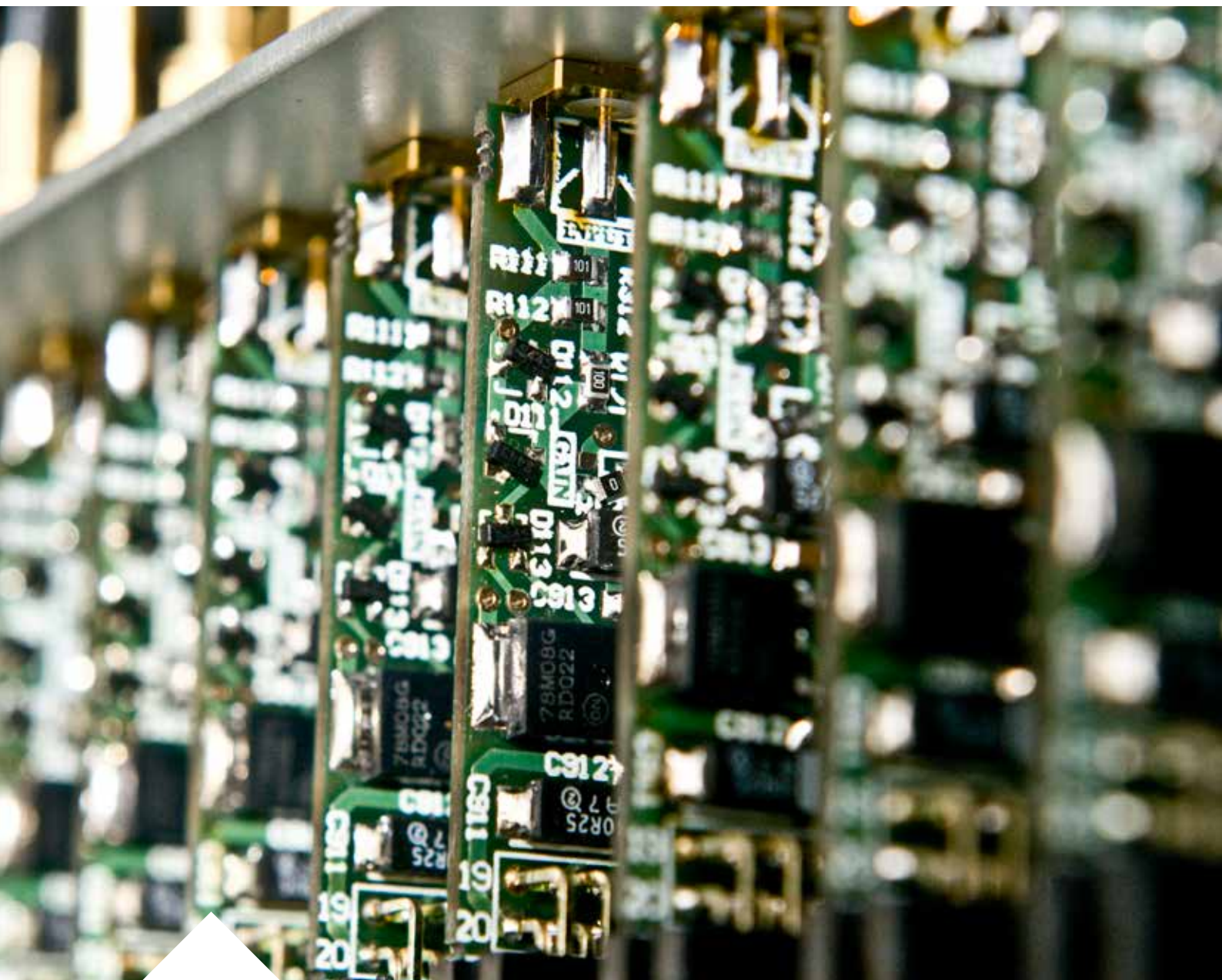


Figure 37: Design of the customized absorber for MIRAS.

ACTIVITY REPORTS BY DIVISION

COMPUTING AND CONTROLS

THE MISSION OF THE COMPUTING AND CONTROLS DIVISION IS TO SUPPORT USERS' RESEARCH AND EXPERIMENTS BY PROVIDING RELIABLE, HIGH-PERFORMANCE, EASY-TO-USE AND HIGHLY AVAILABLE HARDWARE AND SOFTWARE SOLUTIONS FOR CONTROL SYSTEMS, PERSONAL SAFETY, EQUIPMENT PROTECTION, DATA ACQUISITION, DATA ANALYSIS, IT SERVICES AND SYSTEMS WITH A LARGE PORTFOLIO OF SERVICES. THE ENDEAVOUR IS GROUNDED IN A CLOSE RELATIONSHIP WITH SCIENTISTS AND ACTIVE COLLABORATIONS WITH OTHER EUROPEAN SYNCHROTRONS AND RESEARCH FACILITIES TO DEVELOP NEW SOLUTIONS. MORE INFO: [HTTP://COMPUTING.CELLS.ES](http://computing.cells.es)



COMPUTING & CONTROLS PORTFOLIO MANAGEMENT

The division manages projects and services following the PRINCE2 methodology and ITIL best practices, by means of web applications. These management tools enable a proactive quality management, which produces valuable information for the provision of purpose-fitting services and continuous service improvement. For instance, the graph in Fig. 38 below summarizes the efforts of the whole year classified by customer. Complete monthly and annual reports are available on <http://computing.cells.es>. The project management follows PRINCE2, and in the case of software development is combined with an iterative and incremental agile software development approach using SCRUM. While both emphasize the importance of customer involvement, PRINCE2 centres on the customer benefits, business justification and project control, whereas SCRUM offers an agile and systematic approach to the daily tasks, through constant re-prioritizations and frequent releases.

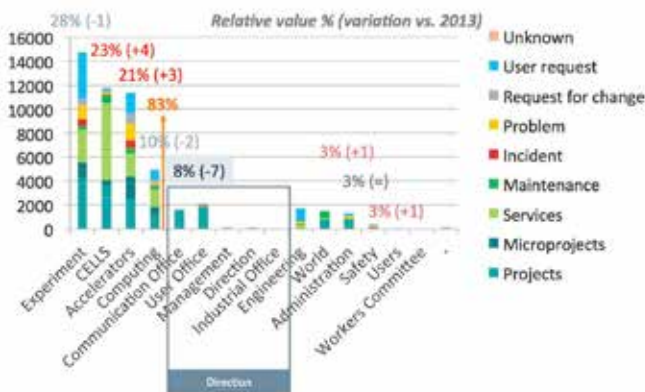


Figure 38: 2014 distribution of the Computing division manpower in hours per internal customer and compared with the previous year (2013).

COMMISSIONING OF FAST ORBIT FEEDBACK AND UPGRADE OF TOP-UP

In 2014, the first version of ALBA Fast Orbit FeedBack (FOFB) has been commissioned using MRF PMC EVR boards and changing its FPGA firmware to implement the

functionality of BPM data sniffers. The calculations are carried out by Linux Operating system running on quadruple core processors. This project leverages the installed hardware and required the upgrade of sixteen cPCI crates with new CPUs and new PMC carriers with "sniffer boards". The next version of the FOFB will include new FPGA boards that have already been provisioned and will allow FOFB calculations to be performed at 10 kHz sampling rate. The top-up system was upgraded to allow injection on a single bunch, enabling hybrid and complex filling modes.

ACCELERATORS AND BEAMLINES OPERATIONS AND NEW PHASE-II BEAMLINES SUPPORT

The Computing and Controls division carries out a large number of activities to support the operation and/or construction of accelerators and beamlines. All requests are logged and tracked in project and service management tools with detailed information from which executive reports are produced. Figure 39 shows the distribution of hours per service and type of issue as registered in the service desk. Other activities at the accelerators include the study of the thermal inertia of the power supplies of the Booster aiming to increase the injection efficiency, the new Taurus GUI for the Linac, the use of low-cost silicon photomultipliers for measuring the bunch charge, the integration of the pinger magnets in the control system or the cabling and control of the new hall probe measurement bench for insertion devices. The works on the new phase-II beamlines MIRAS and LOREA are combined with projects on the beamlines in operation. For instance, in BL11-NCD, more detectors (imXPAD) are being commissioned and integrated into the data acquisition; in BL22-CLAESS the CLEAR spectrometer has a new temperature control for the motors and the Mythen detector installed; in BL29-BOREAS both experimental stations have been upgraded, with HECTOR completed and MARES near completion.

SARDANA AND TANGO

Tango started at the ESRF, soon joined by Soleil and later Elettra and ALBA in 2004. The community grew quickly and

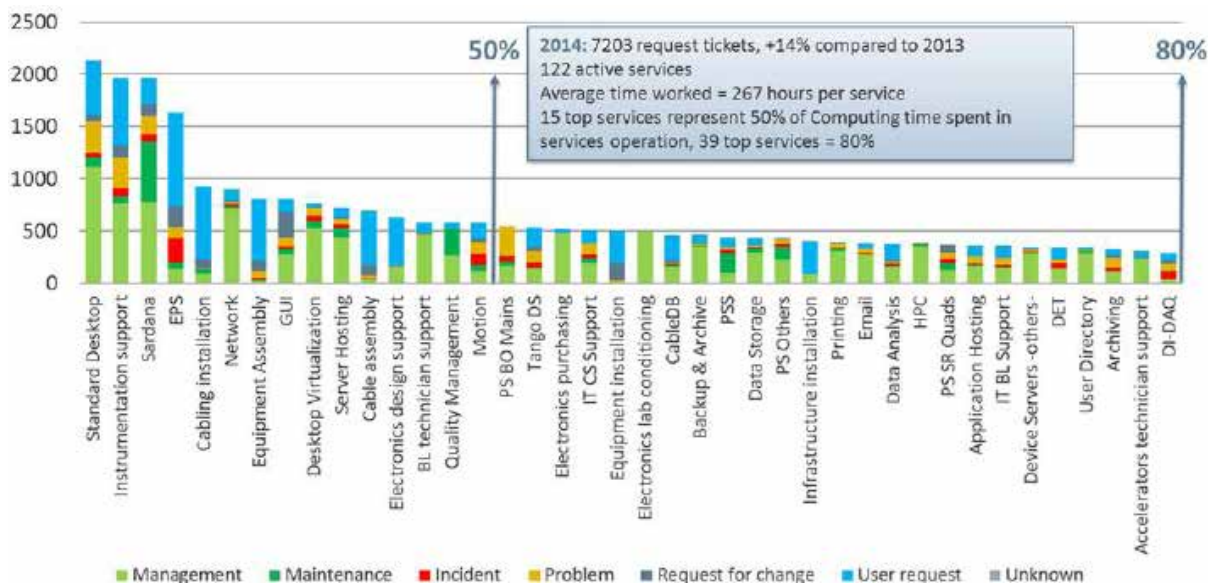


Figure 39: The Computing and Controls division has had 7203 tickets registered in the service desk in 2014. This means an increase of 14% with respect to the previous year.

now includes more than 20 institutions (see the new web page <http://www.tango-controls.org>). Tango is an Open Source solution for creating Distributed Control Systems (DCS). Sardana is a Supervision, Control And Data Acquisition (SCADA) system oriented to experimental stations using Tango as the communication bus. The Sardana project (and subprojects as Taurus) started at ALBA in 2006 and since 2013 is the fruit of collaboration among several institutes (ALBA, DESY, MaxIV and Solaris). Sardana is an Open Source project hosted by Sourceforge with Git as the version control system. Recently the documentation has been moved to "Read the Docs" (see <http://sardana-controls.org>, and <http://taurus-scada.org>).

CONTINUOUS SCANS

Currently, most of the experiments in four beamlines benefit from Continuous Scans. Since the last report, the most important improvement has been the possibility to include in the continuous scan any channel available in the control system, which can be slower than the rest of the acquisition, addressing the need for flexibility required for demanding experiments in a few beamlines. However, step scans are still used in many cases, and remain the standard data acquisition technique in some beamlines. Dead times and software overheads were significantly reduced in step scans, in particular in cases where complex movements of combinations of "pseudomotors" are involved.

ELECTRONIC DESIGNS: THE ALBA ELECTROMETER AND THE PHOTODIODE X-RAY DETECTOR

The development of the new electrometer is progressing well, becoming a larger project involving all teams in the Computing and Controls division. As of today, it has turned into a versatile platform featuring the electrometer as one possible use, and a broad range of other potential applications such as encoders, etc. It enhances the triggering and buffering capabilities combined with a well-characterized current amplifier and an 18-bit SAR ADC. A Single Board Computer running an embedded Linux handles the configuration, the buffering and the interfaces with the control systems.

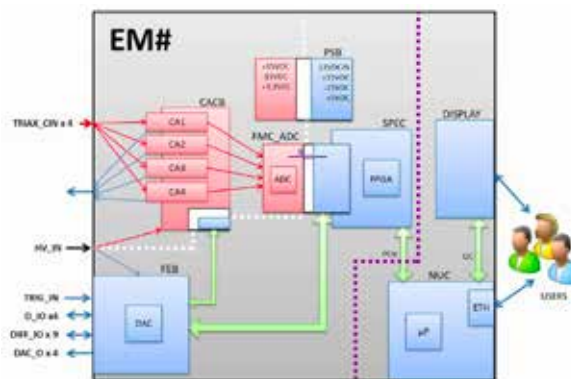


Figure 40: Block diagram of the new Electrometer Em#

The prototype is planned for the last quarter of 2015. Figure 40 shows the block diagram of the Electrometer.

The collaboration with the CNM-CSIC for producing 10µm thickness photodiodes was completed successfully. These silicon based photodiodes are designed as beam monitors as they show little absorption at energies of few keV. The business plan was carried out in collaboration with the FCRi (Fundació Catalana per la Recerca i la Innovació, Equips d'Innovació), and the project concluded with a utility model and the product commercialized by Alibava (<http://www.alibavasystems.com>), a CNM-CSIC spin-off. Encouraged by this success, we started a new project with the CNM-CSIC and the ESRF to add position monitoring capabilities to the intensity monitoring. The new project aims to produce four quadrant thin diodes both in silicon (Si) and in Silicon carbide (SiC).

INFORMATION TECHNOLOGIES AND MANAGEMENT INFORMATION SYSTEMS

While directly supporting user research at the beamlines and accelerators, IT Systems and Management Information

Systems teams also provision a portfolio of more than 60 transversal services, including the IT infrastructure, computing, user support, server hosting, and a wide variety of web applications for the management of experiments, safety, logistics, recruitment, finance, communication, etc. A novelty in 2014, MIS development team selected Django (Python) and AngularJS (Javascript) platform to build its new applications around syntactic web service paradigm, providing a more robust and versatile architecture. The new electronic invoicing service has been developed on this platform, and old applications are slowly being migrated to it. In 2014, we also replaced the old Document Management Systems (DMS) with Alfresco and introduced a Central Authentication System (CAS) for websites and web applications.

Figure 41 shows an illustration of the benefits brought by the new architecture.

In 2014, we also released the **ALBA new public website** with renewed contents and a new corporate image. The new site, based on the latest Plone 4, provides better security, performance and content management, as well as multiple-language support and responsive design for mobile devices.

In production since 2011, the **User Office Portal** has since been the most important MIS service in terms of

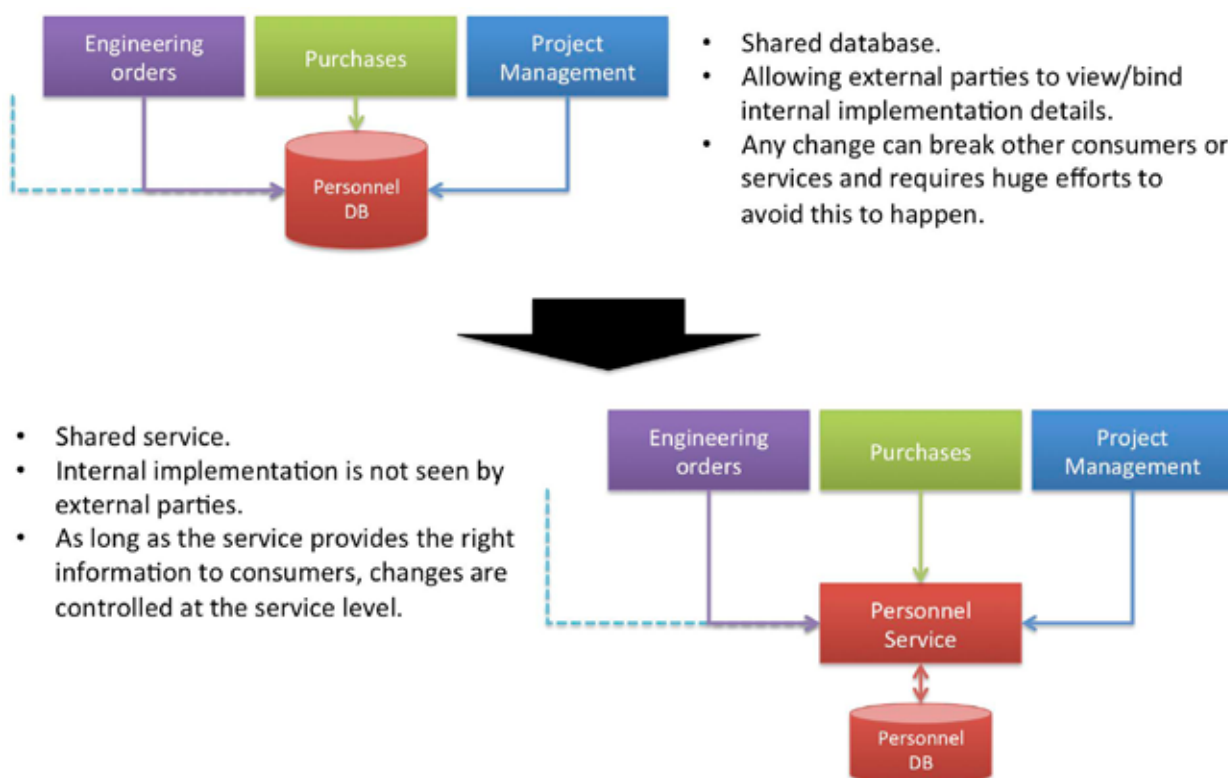


Figure 41: Benefits of the service-oriented approach (REST - JSON)

support and development hours. In 2014, we introduced the management of publications produced in ALBA, new management procedures related to safety-level tracking for user experiments, and a better handling of last minute changes in the experiments. In 2015, the phase 5 of the project will include improvements in the management of ALBA publications and the adaptation of existing management processes to industrial and in-house experiments.

The **Ethernet Data Network** is both the main connection to the Public Internet and to the intranet IT resources, and the main fieldbus used by the distributed controls systems of accelerators and beamlines. The service is continuously improved with infrastructure upgrades, more redundant topologies and hardware configurations, as well as increased capacities where they are needed.

The **Remote Access** to experimental data was enhanced in 2014 with a new SFTP server. ALBA users can now access their experimental data from the public Internet using the credentials of each proposal's user without file transfer size restrictions.

At the end of 2014, the data centre was provisioned with 11 new servers, increasing the computing power available for new server and application hosting, machine virtualization, and **High Performance Computing (HPC)**. The HPC cluster is being commissioned and tested running radiation shielding simulations among others.

New virtualization farms have also been introduced to increase the availability and the capacity of the most critical systems. The Virtualization is one of the key IT Systems disciplines as most controls and central servers are hosted as virtual machines, e. g. Tango control system databases, web portal, email, CAD, virtual desktops or network services among others.

New deployment and configuration management tools are being introduced to simplify both the HPC and the virtual servers' orchestration efforts.

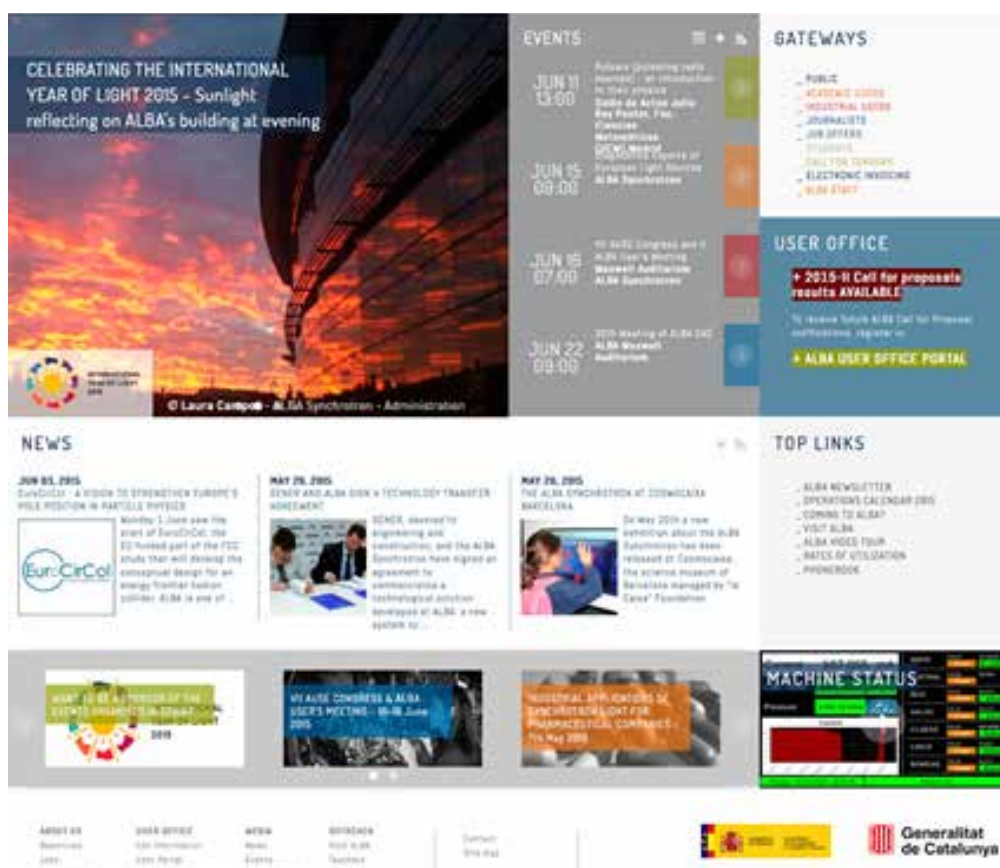
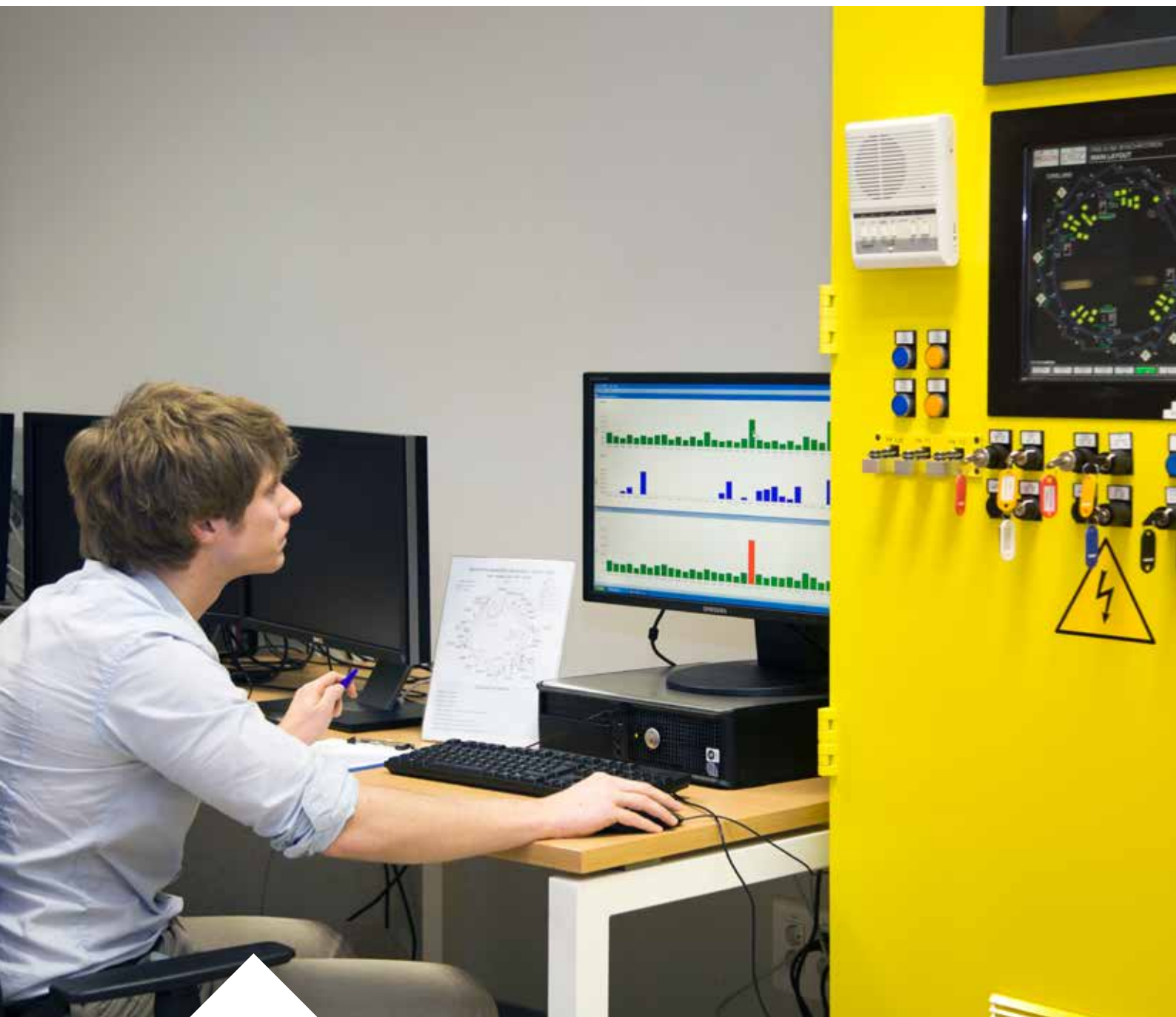


Figure 42: Snapshot of the new main webpage.

ACTIVITY REPORTS BY DIVISION

HEALTH AND SAFETY

THE HEALTH AND SAFETY OFFICE MANAGES TWO DIFFERENT AREAS: THE OCCUPATIONAL HEALTH & SAFETY AND THE RADIATION PROTECTION SERVICE, AND REPORTS DIRECTLY TO DIRECTION. DURING 2014, THE HEALTH AND SAFETY OFFICE HAS WORKED ON ALL THE SAFETY ISSUES AT ALBA IN ORDER TO IDENTIFY AND REDUCE HAZARDS IN THE FACILITY.



RESULTS OF THE 2014 DOSIMETRY AND NEW ACCESS RULES CLASSIFICATION

More than 3000 area ThermoLuminescence Dosemeter (TLD) official readings have been registered inside ALBA in 2014 and none of them overpassed an accumulated dose of 0.00 mSv during the year. In addition, the accumulated doses of all the 190 occupationally exposed workers have also been 0.00 mSv during 2014.

In 2014, and since ALBA accelerators started to work in 2009, the radiation levels measured outside the bunkers have never surpassed the public zone classification. As a consequence, at the end of 2014 the Health and Safety Office reclassified the occupationally exposed personnel and presented new access rules applicable as of 1st January 2015 (Fig. 43) in a seminar for all the ALBA staff and external companies.

TOP-UP MODE AND RADIATION MEASUREMENTS

Since June 2014, ALBA accelerators are operating in top-up mode, injecting the 3 GeV electron beam from the Booster to the Storage Ring with open Front Ends. Radiation measurements and shielding studies have been done by the Radiation Protection Service to ensure that the working areas outside the shielding (Experimental Hall and Service Area) remain available to the public when operating in top-up mode.

CALIBRATION AND VERIFICATION OF RADIATION DETECTORS AT ALBA

In 2014, the radioprotection group has performed a campaign of calibration of all the radiation detectors at ALBA together with the annual verification of all the radiation detectors. In particular, the 34 Gamma probes and the 15 Neutron probes of the Radiation Monitors, forming part of the Personal Safety System (PSS) have been calibrated and verified with success.



Figure 44: Image of calibrated and verified radiation detectors at ALBA.

USERS' VISITS MANAGEMENT

In 2014 ALBA receives 318 user visits to perform their experiments at ALBA facility. In total, 211 of these visits belong to the 2014 Call and 107 to the 2013 Call.

	PUBLIC AREA	WATCHED AREA	CONTROLLED AREA	PROHIBITED ACCESS AREA
SIGNALLING				
ACCESS PUBLIC	Free	with EPD	Not allowed	Not allowed
NON EXPOSED WORKER CATEGORY A	Free with TLD	with EPD with TLD	Not allowed with TLD	Not allowed

Figure 43: New access rules at ALBA from 1st of January 2015.

	Total white flags	Total green flags	Total yellow flags	Total red flags	
BL04-MSPD	10	28	9	2	49
BL09-MISTRAL	11	14	7	0	32
BL11-NCD	19	22	2	0	43
BL13-XALOC	43	71	1	0	115
BL22-CLAEISS	11	9	4	5	29
BL24-CIRCE	6	10	6	4	26
BL29-BOREAS	7	16	1	0	24
TOTAL	107	170	30	11	318
	January - April '14 Call 2013	April - December '14 - Call 2014			

Table III: List of users' visits in 2014.

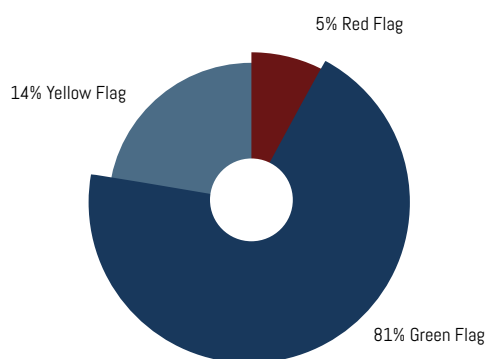







Figure 45: Distribution of 2014 experiments according to their flag identification.

NEW PROPOSAL FOR A CLASSIFICATION SYSTEM

A new classification system has been established to label the proposals according to the risk assessment performed for each experiment.

In the following table you can see the established criteria:

	Criteria: Safety information is missing
	Criteria: The experiment does not need any further supervision
	Criteria: The experiment needs initial supervision by Safety or Experiments with ALBA Lab access request
	Criteria: The experiment needs initial supervision by Safety and permanent supervision WHEN the risk is present
	Criteria: The experiment is not accepted

EXTERNAL COMPANIES AT ALBA

During 2014 a total of 147 external companies were performing works at ALBA requested by all the different divisions of our institution (see figure 46).

The Occupational Health and Safety Group has verified that the business coordination activity of each external contractor has been carried out in accordance with the Spanish regulations, and has also performed a risk assessment of the work done by each external contractor in order to identify and solve any potential risk situation.

NEW EXTERNAL PREVENTION SERVICE

A new external prevention service has been chosen following a public call for tenders.

WORKSHOPS AND CONFERENCES

The Occupational Health & Safety group participated in September 2014 in the International Technical Safety Forum held in Fermilab with the presentation: *"Handling hazardous and greenhouse gases at ALBA Synchrotron facility"*.

The radioprotection Health & Safety group took part in July 2014 in the 9th International Topical Meeting on Industrial Radiation and Radioisotope Measurement Applications (IRRMA-9) in Valencia, Spain presenting an oral contribution about *"A comparative shielding"*

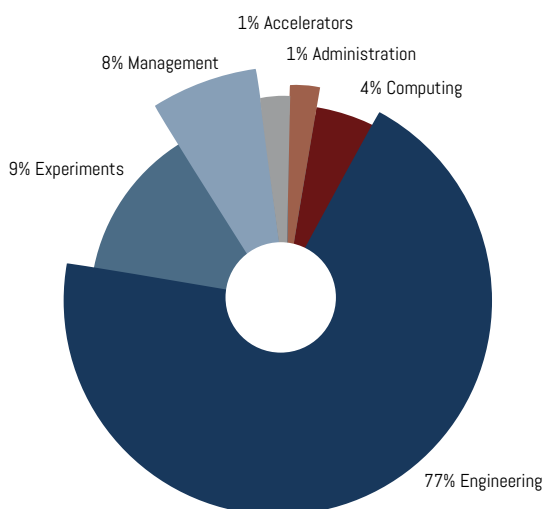


Figure 46: Distribution of 2014 external companies works required by ALBA's divisions.

study at ALBA Synchrotron facility between Monte Carlo modeling and radiation monitor dosimetry measurements”.

The paper is a detailed study of the origin of the radiation produced at BOREAS Beamline, giving the characteristics of an additional shielding, installed in BOREAS together with the Engineering division, to ensure the classification of the outside of the optical hutch as a public zone during top-up operation that started at ALBA in June 2014.

SAFETY TRAININGS DONE AT ALBA DURING 2014

More than 50 safety trainings were organised for ALBA staff and external contractors, about a wide range of Health & Safety issues:

- Newcomers (17)
- Pressurized Gas Bottles Manipulation (3)
- Occupational H&S – 50h (1)
- Laser Risks (3)
- Electrical (2)
- Chemical Risks (1)
- Biosafety (1)
- Operation Procedure for PSS Beamlines (11)
- Operation Procedure for Users Trainers PSS Beamlines (3)
- Specific Training for Operators of IRA-3075 (2)
- Use of Radioactive Sources at ALBA (1)
- General Annual Training for Operators and Supervisors of IRA-3075 (1)
- Training of Operator of Radioactive Installations (3)
- Annual Seminar on Health and Safety (1)



COLLABORATION WITH EXTERNAL INSTITUTIONS

IN 2014 ALBA HAS CONTINUED ITS CLOSE COLLABORATION WITH OTHER NATIONAL AND INTERNATIONAL INSTITUTIONS. BELOW ARE SOME SPECIFIC COLLABORATION PROJECTS CHOSEN FOR THEIR STRATEGIC VALUE AND THEIR SCIENTIFIC RELEVANCE.





ALBA and CIEMAT have been collaborating in the field of accelerators to perform tests, the set-up and installation of radiofrequency cavities. The ALBA facility and its experts are providing these services under the IFMIF project, the International Fusion Materials Irradiation Facility under construction in Japan.



A new collaboration between ALBA and I3M-UPV has been established for magnetic measurements using ALBA laboratories. The Instrumentation Institute for Molecular Imaging (I3M) is a research group created in 2010 by the Polytechnic University of Valencia (UPV), the Spanish National Research Council (CSIC) and the CIEMAT.



ALBA is also collaborating with the CIEMAT in the design, fabrication, validation and installation of a magnetic measurement bench of closed magnetic systems of up to 1.3 metres in length.



The successful collaboration between ALBA and CLPU started last year and has been extended during 2014 for the installation of the vacuum chamber for a 1 Petawatt laser system.



ALBA and CERN are collaborating in the design, development, construction and validation of components and systems in the field of accelerators. In particular, magnetic measurements for the dipole magnets for the SESAME synchrotron will be performed.



ALBA is collaborating with the INFN in the areas of diagnostics, radiofrequency, control systems and commissioning of the Extreme Light Infrastructure for Nuclear Physics – High Intensity Gamma Beam System to be built in Romania.



Since 2004, ALBA has been an active contributor to the TANGO open-source control systems for accelerators and synchrotron radiation applications. The consortium involves more than 20 research institutes, including ANKA (Germany), DESY (Germany), ELETTRA (Italy), ELI-ALPS (Hungary), ESRF (France), FRM II (Germany), INAF (Italy), MAX-IV (Sweden), SOLARIS (Poland), SOLEIL (France) and University of Szeged (Hungary).



LIMA (Library for Image Acquisition) is a collaborative project for the unified control of 2D detectors, developed by a community of detector users and manufacturers. ALBA is using this library at the beamlines and contributes with feedback, proposals, and new functionalities.



Sardana is an open-source software suite for Supervision, Control and Data Acquisition in scientific installations. Its development was started at the ALBA Synchrotron and is now supported by a larger community which includes several other laboratories such as ALBA, DESY, MAX-IV, Solaris and ESRF.



IcePAP is a motor controller developed in collaboration with the ESRF and largely deployed in ALBA to control pumps, robots, etc. It is optimised for high-resolution position applications in synchrotron radiation experimental beamlines.



Formed in 2008, PANdata - the Photon and Neutron data infrastructure initiative - brings together thirteen major world-class European research infrastructures, including ALBA, to create a fully integrated, pan-European, information infrastructure supporting the scientific process.



ALBA and CNM have been collaborating in the design and characterization of semiconductor-based diagnostic devices capable of being highly transmissive at high X-ray energies. A project to make them commercially available by Alibava (a CNM-CSIC spin-off) has been finished via a FCRI programme (EDI).

STUDENT TRAINING ACTIVITIES

ALBA HAS CONTINUED DURING 2014 ITS INTENSE EFFORT ON CONTRIBUTING TO THE TRAINING OF STUDENTS OF DIFFERENT LEVELS AND PROFILES. UNIVERSITY STUDENT ACCESS TO ALBA HAS BEEN ORGANIZED VIA PERIODIC PUBLIC CALLS, WHEREIN STUDENTS FROM ANY UNIVERSITY COULD OPENLY APPLY TO A WIDE RANGE OF SCIENTIFIC AND TECHNICAL POSITIONS IN ORDER TO DO AN INTERNSHIP. IN ADDITION, A NEW SPECIFIC PROGRAM FOR TECHNICAL STUDENTS HAS ALSO BEEN INITIATED.



Year 2014 has been very important for the ALBA student training activities. Indeed it has seen the onset of two systematic student programmes, which have the vocation of staying with us for a long time: one for university undergraduate students and a second one for technical students (in vocational training).

The ALBA university undergraduate student programme stems from the experience of the last few years, in which student internships were promoted and dealt with case by case. The experience accumulated has led to the conclusion that students can actually benefit in a very relevant way from doing such internships, and that ALBA can also profit from the students' enthusiastic contribution to a number of technical and scientific areas. Therefore, in April 2014, ALBA opened the first public call for university undergraduates, with 39 applications received, wherein 10 students could do an internship at ALBA. Training activities took place at very different areas: scientific applications of synchrotron light, mechanical design, outreach and communications, controls. Later along the year, in September, a second call was issued, with very similar results. Internships arising from this second call have been mainly allocated to start during the first months of 2015. Altogether ALBA has received 20 university undergraduate students along 2014, a remarkable success to be sustained in the future.

Complementing the effort with university undergraduates, during 2014 we decided to find the best possible options to contribute as well to the training and education of technical students (in vocational training). Recently the Catalan autonomous government had started applying a new scheme for this type of students, called dual education system, consisting in having a close coordination between a technical school and a collaborating company or institution, in order to train a technical student for a whole academic year (ten months). The student has two tutors (at the school and at the collaborating institution) and shares his/her time between the classroom and hands-on training. After a systematic survey of the possibilities at different technical areas of ALBA, a formal agreement was signed with the Education department of the Catalan autonomous government, contemplating the training of 8 students per year, from different technical profiles and from 7 different technical schools, with the aim of repeating the same profiles with the same schools every year. Students arrived gradually and finally up to nine of them could start doing their dual education training at ALBA in 2014. The programme has worked very well and the plan is to extend it to nine profiles (from eight different schools) in 2015-16.

Once the two programmes mentioned above have been launched, ALBA is working on the establishment of a PhD student programme as well. Initial steps in this direction were already taken via European funding programmes and cooperation agreements with external institutions and industries. The outcome is promising: three students have started or continued PhD internships fully based at ALBA during 2014.

It is also worth mentioning the teaching activities developed by members of the ALBA staff for university students. We'd like to highlight our participation in the official master of the Universitat Autònoma de Barcelona "Advanced Nanoscience and Nanotechnology", where a total of 42 hours were delivered by scientists of the Experiments division. At the same university, Caterina Biscari taught the subject "Accelerators' Physics" (optional 6 credit subject, Physics degree). The Accelerators' division regularly collaborates with the Universitat Politècnica de Catalunya in the tutoring of final grade and PhD projects.

Some other relevant contributions to student education at large are briefly mentioned elsewhere in this report: numerous visits by student groups, some specific short stays of selected high school students, a two-day training course for high school teachers, etc. A very complete year indeed, gradually moving upwards, towards a systematic training system based on three pillars: university undergraduates, dual education technical students and PhD programme. The challenge is to further develop and consolidate these three pillars.

WORKSHOPS AND SEMINARS

DURING 2014 THE ALBA SYNCHROTRON HAS ORGANIZED 41 WORKSHOPS AND SEMINARS TO SHARE THE STATE-OF-THE-ART SYNCHROTRON-BASED RESEARCH AND TECHNOLOGY AMONG ITS STAFF AND THE SCIENTIFIC COMMUNITY.





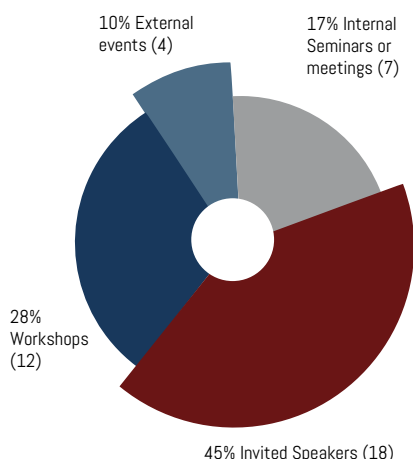
Promoting scientific and technical debates and exchanging points of view are the main reasons why ALBA continued its effort in organizing, hosting and participating in workshops and seminars. A total of 41 activities have been held across the year: 18 invited speakers from national and international synchrotron facilities and research centres, 12 workshops or courses, 7 internal seminars or meetings addressed to ALBA staff and 4 external events.

Regarding the workshops and courses, some of them were aimed at showing the analytical capabilities of ALBA to the scientific community and the industry while others focused on the discussion and generation of best practices. The ALBA Phase-III workshop and 19th ALBA Scientific Advisory Committee were devoted to the proposal and evaluation of the future ALBA beamlines.

LIST OF WORKSHOPS ORGANISED OR HOSTED BY ALBA

- 10/04/2014 - ALBA Phase-III workshop
- 15/04/2014 – Industrial meeting "Applications of the ALBA Synchrotron for the Chemical and Materials industries"
- 01-02/07/2014 – 18th ALBA Scientific Advisory Committee Meeting
- 29-30/09/2014 - BioStruct-X 3rd Annual Meeting
- 01/10/2014 - SAXS Workshop
- 06-09/10/2014 - Introductory course: Synchrotron EXAFS & XANES for Chemical Specification on Environmental Systems
- 15-17/10/2014 – Specialization course for high school teachers
- 03-04/11/2014 - European Users Offices Meeting
- 05-06/11/2014 - CALIPSO Annual Council Meeting
- 12-14/11/2014 - Hands-on Course on the Pair Distribution Function method
- 13-14/11/2014 - ALBA Synchrotron: new tools for material characterization
- 03/12/2014 – 19th ALBA Scientific Advisory Committee Meeting

2014 EVENTS



Poster session of the workshop "ALBA Synchrotron: new tools for material characterization".

Group photo of the attendees to the Hands-on Course on the Pair Distribution Function method, organised by MSPD beamline.



Caterina Biscari's presentation during the 19th ALBA Scientific Advisory Committee.



Presentation of Laura Simonelli, responsible of CLAESS beamline, during the Industrial meeting "Applications of the ALBA Synchrotron for the Chemical and Materials industries".



COMMUNICATIONS AND OUTREACH

IN 2014, THE ALBA SYNCHROTRON HAS CONSOLIDATED THE COMMUNICATIONS AND OUTREACH ACTIVITIES, IMPROVING AND ENABLING NEW CHANNELS AND TAKING PART IN INITIATIVES LIKE THE EUROPEAN RESEARCHERS' NIGHT AND THE BARCELONA SCIENCE FESTIVAL.

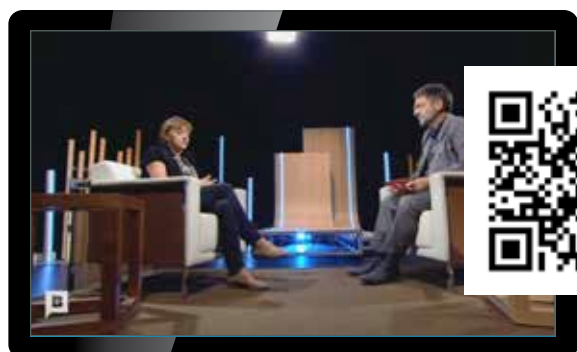
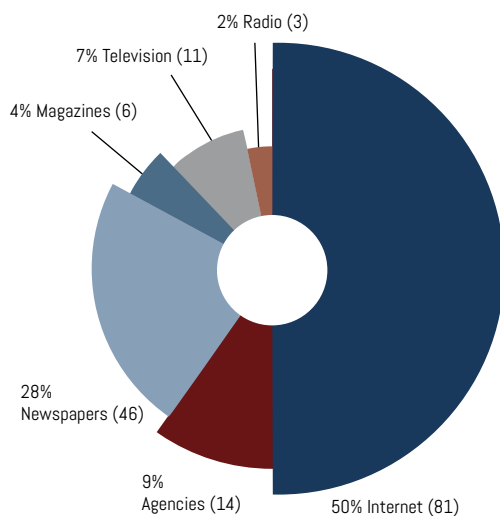


ALBA IN THE MEDIA

Working closer with media and informing them about ALBA's endeavours has been one of the main tasks inside the Communications and Outreach office. As a result, ALBA has obtained 161 direct impacts in mainstream media, distributed equally between offline (80) and online (81) platforms. Some of the most successful examples have focused on the results of users' experiments developed at ALBA. However, it is important to mention the participation of the ALBA facility in documentaries such as *"Inversió de futur"* in the Catalan television or the movie *"Barcelona, la rosa de fuego"* from Manuel Hueriga.



MEDIA APPEARANCE: NUMBER OF IMPACTS



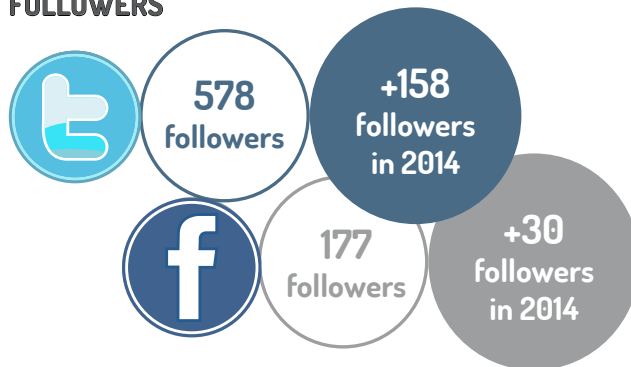
UPGRADE AND IMPLEMENTATION OF ALBA'S COMMUNICATIONS CHANNELS

In collaboration with the MIS section inside the Computing and Controls division, a new public website has been released in 2014, as explained in further detail in the Computing and Controls division report above. With the aim of easing website navigation and allowing quick access to information, we designed a new content architecture and layout. In order to achieve a higher impact on the national public, the new public website has been translated into Spanish and Catalan.

In parallel, the presence in social media has continued growing in 2014, increasing the number of followers in Facebook and Twitter.



FOLLOWERS



Two issues of the ALBA News magazine were published in 2014, including new sections and articles, and expanding the reach of the magazine.



OPENING DOORS

Since its inauguration in 2010, ALBA has attracted the interest of the general public to know its facilities, the equipment and applications of the synchrotron-based research.

The number of visitors has considerably increased, reaching more than 5,250 visitors in 2014. Guided tours are organized in groups of 20 people who visit the experimental hall and some beamlines. Almost half of our visitors (49%) came from high schools, followed by institutional bodies (14%), universities and research centres (12%), general public (14%) and associations (11%).

In 2014, ALBA organized a successful edition of the ALBA Open Day. It took place on Saturday 9th October 2014 with the participation of 1,630 people who enjoyed the circuit around the experimental hall, the explanations from ALBA volunteers and games and audiovisual material.

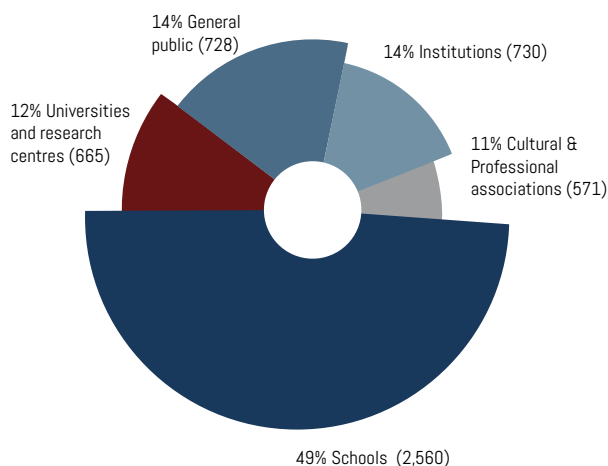


ALBA has also enlarged its external outreach activities. On September 26th ALBA brought science into the city centre of Cerdanyola del Vallès celebrating the European Researchers' Night. From 18:00 till 23:00, participants were able to attend conferences from ALBA scientists, have a look at the exhibition "Synchrotrons and crystallography: a perfect couple", take part in demonstrations and games and attend the final show of science monologues. These activities were related to the celebration of the International Year of Crystallography.

For the first time, the ALBA Synchrotron was present at the 2014 Barcelona science festival, where it showed how to create a homemade Van der Graaf accelerator.



VISITORS 2014



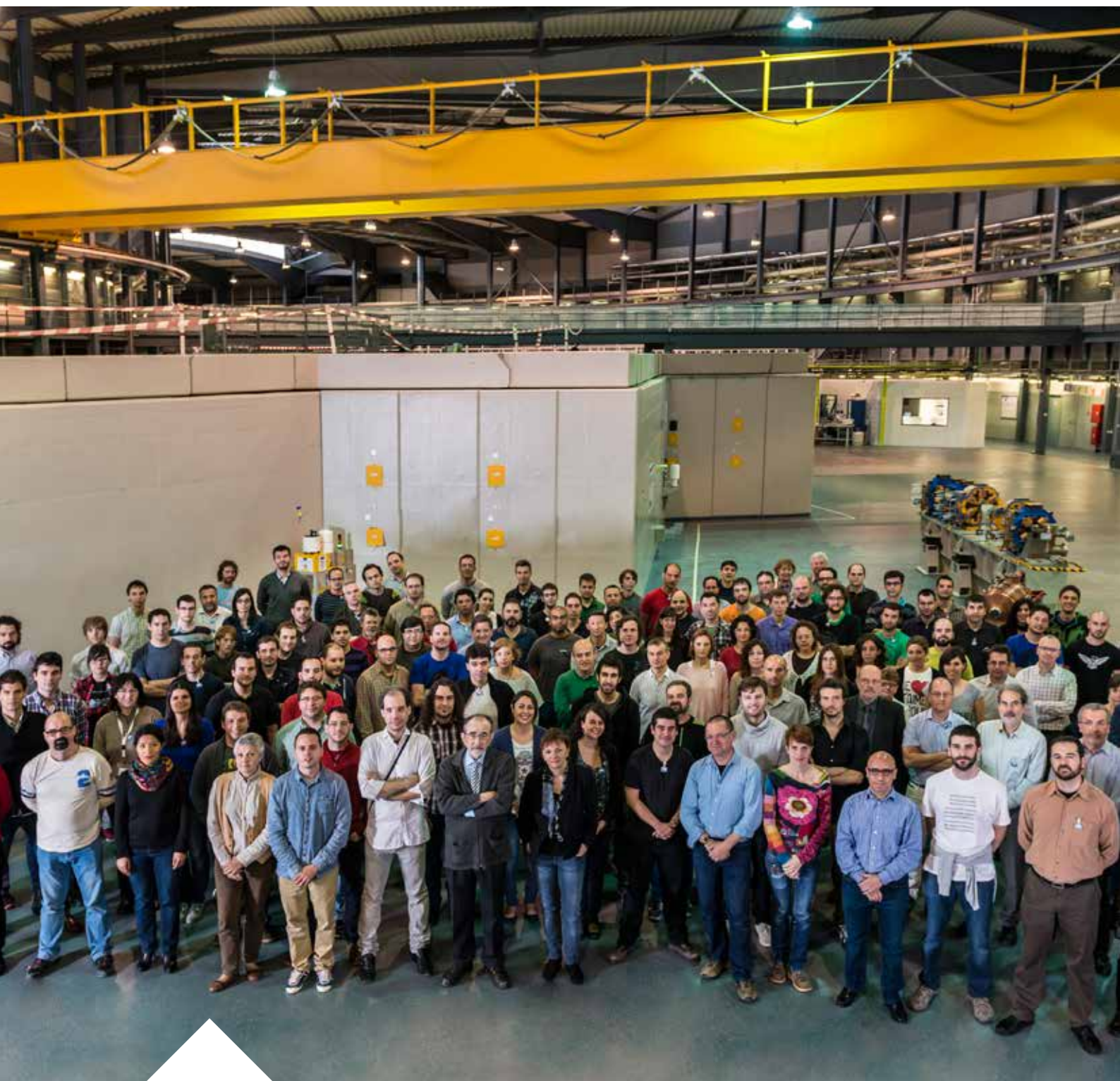
MATERIALS AND RESOURCES FOR TEACHERS

Teachers are key to disseminate science among young students and to encourage scientific vocations. This is why in 2014 ALBA and the Catalunya-La Pedrera Foundation have organized for the second time a two-day seminar for Physics and Chemistry high school teachers with the aim of increasing their knowledge about synchrotron light. Some outreach materials (posters and informative dossier) have been also developed to be used at classroom with students.



FACTS & FIGURES

IN THIS FINAL SECTION, WE SUMMARIZE THE MAIN FACTS AND FIGURES OF THE ALBA SYNCHROTRON ACTIVITY IN 2014.



USERS

The 2014 ALBA call for proposals was launched to allocate experiments from April to December 2014. Experiments from January to March 2014 came from the 2013 call for experiments.

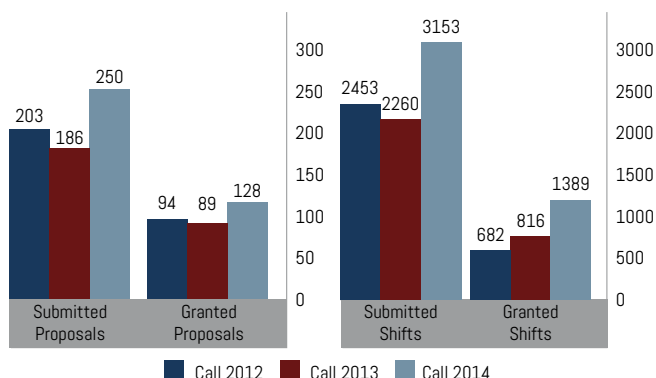
In comparison with previous calls, the number of proposals and shifts in this period increased. A total of 250 proposals (3,153 shifts) were submitted. Proposals were evaluated by a panel, composed of international experts from different research areas. As a result of a ranking based on scientific excellence criteria, 128 proposals (1,389 shifts) were granted, representing an overbooking factor of 2.3.

According to the number of proposals, the most demanded beamline was the Materials Science and Powder Diffraction (MSPD). However, according to the number of shifts requested, the Photoemission Spectroscopy and Microscopy beamline (CIRCE) was the most demanded. The biggest number of granted proposals and shifts were for the macromolecular X-ray crystallography beamline (XALOC), followed by the Materials Science and Powder Diffraction beamline (MSPD).

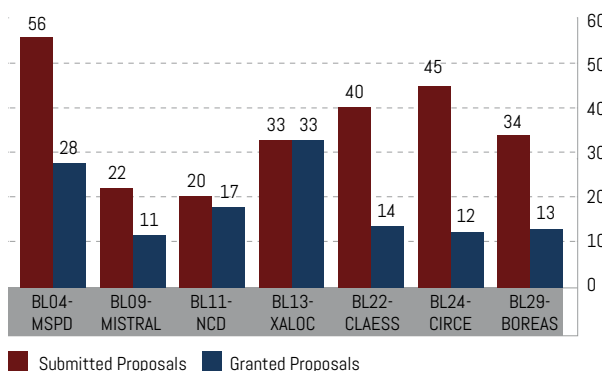
Most of the granted proposals correspond to Spanish institutions (73%) while European countries represent 25% and non-European countries only 2%. If we go deep into the Spanish granted proposals, we can see that 41% corresponds to institutions from Catalonia, 25% from Madrid, 13% from Valencia, 8% from the Basque Country, 6% from Aragon and the remaining 7% from other areas of Spain.

Experiments from Materials Science and Structure have been the most granted (31%), followed by Hard Condensed Matter and Electronic and Magnetic properties (18%), Chemistry (14%), Biology (14%), Macromolecular Crystallography (13%), Soft Condensed Matter and Biomaterials (9%) and Environment and Cultural Heritage (1%).

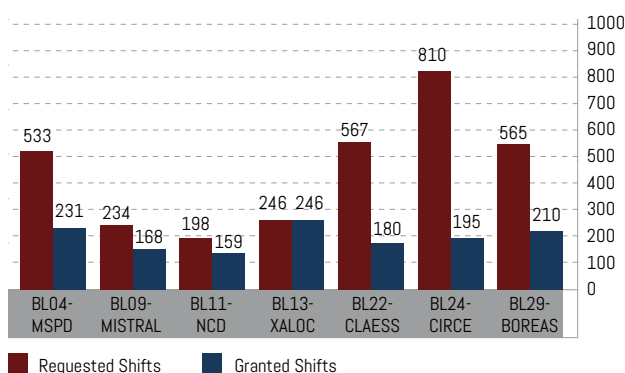
COMPARISON OF SUBMITTED AND GRANTED PROPOSALS AND SHIFTS



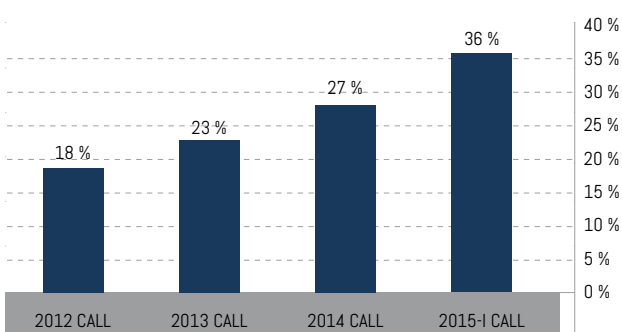
2014 CALL FOR PROPOSALS



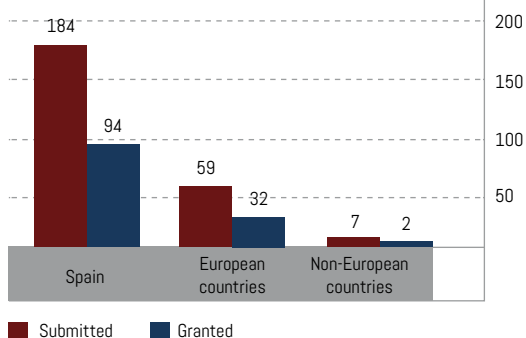
2014 CALL FOR PROPOSALS



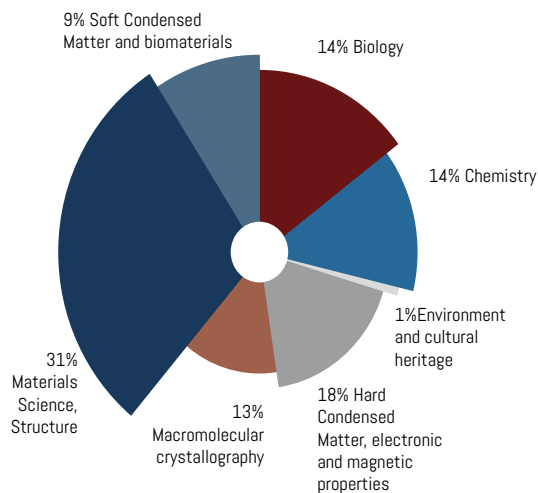
EVOLUTION OF INTERNATIONAL USERS %



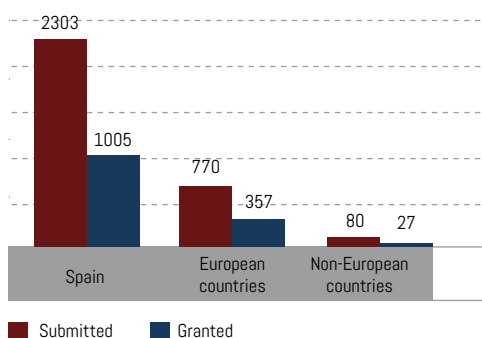
COUNTRY OF ORIGIN OF 2014 PROPOSALS



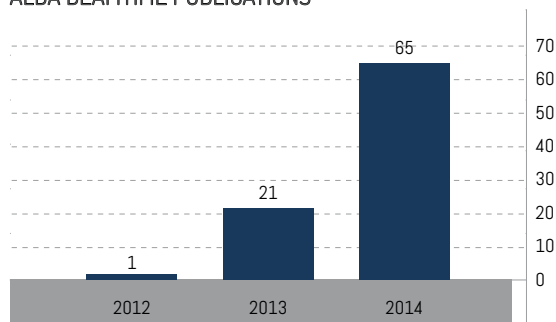
2014 CALL: RESEARCH AREAS OF ALL GRANTED SHIFTS



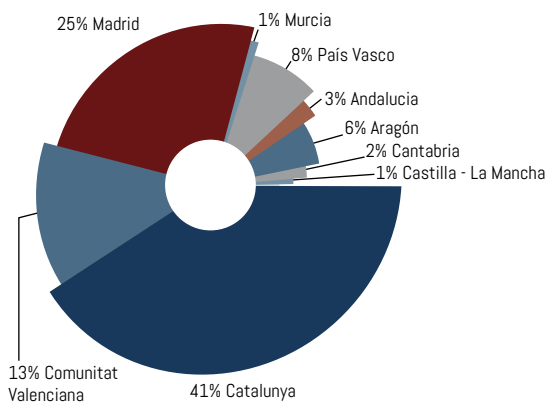
COUNTRY OF ORIGIN OF 2014 SHIFTS



ALBA BEAMTIME PUBLICATIONS



2014 CALL: SPANISH GRANTED SHIFTS BY REGION



MACHINE PERFORMANCE

2014 scheduled and delivered hours have increased by 22% with respect to 2013.

	2012	2013	2014
Scheduled hours for BLs	2821.6 h	3539.5 h	3740.5 h
Delivered hours for BLs	2387.3 h	2971.5 h	3621.2 h
Beam availability	84.6%	83.8%	96.8 %
Hours for machine development	1128 h	1368 h	1352 h
Mean Time Between Failures	20.75 h	24.95 h	33.7 h
Mean time to be back	1.0 h	0.8	1.1 h

HUMAN RESOURCES

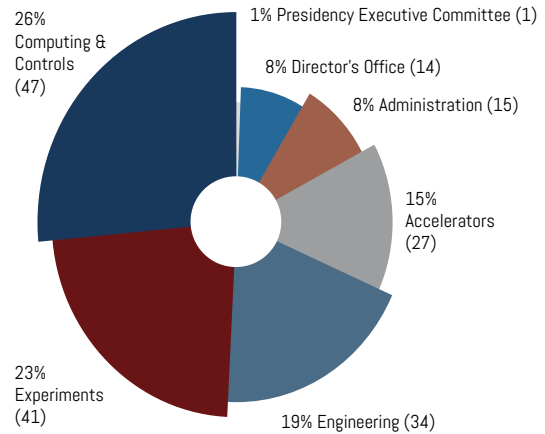
As of 31st December 2014, the ALBA Synchrotron has 179 employees, organized in five different divisions: Accelerators (15%), Administration (8%), Computing & Controls (26%), Experiments (23%), Engineering (19%); in addition, there is a director's office (8%) and the president of the ALBA Executive Committee.

The ALBA staff consists of 60% technologists, 43% scientists, 13% administrative & management staff and 3% health & safety staff.

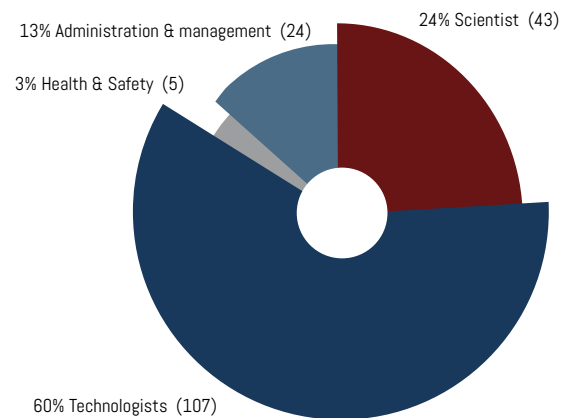
Gender distribution is not proportional. Women represent 25% of ALBA staff. In some specific areas, women have more representation (80% administration and 57% director's office). However, in technical divisions, like Engineering and Computing and Control, women are only 18% and 4%, respectively.

81% of staff is composed of Spanish people – in many cases people who have come back from foreign countries -, 17% of staff is from other European countries and 2% from non-European ones.

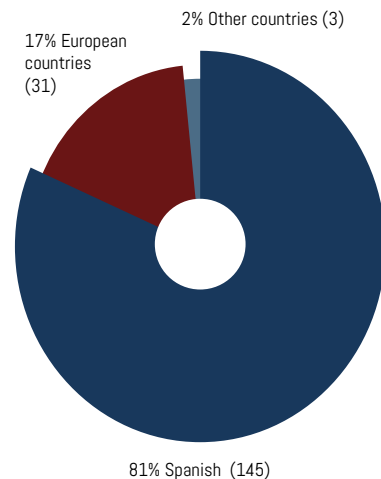
ALBA STAFF - DISTRIBUTION OF DIVISIONS



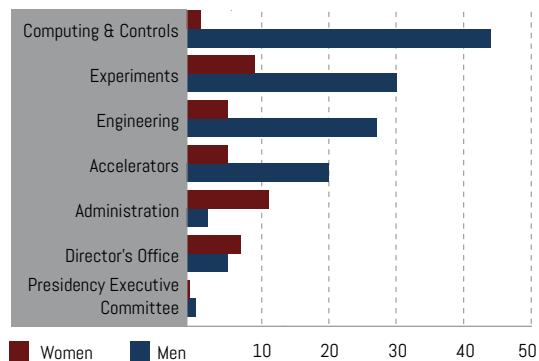
ALBA STAFF - DISTRIBUTION OF CATEGORIES



ALBA STAFF - DISTRIBUTION OF NATIONALITIES



ALBA STAFF - DISTRIBUTION OF DIVISIONS AND GENDER



2014 SCIENTIFIC ADVISORY COMMITTEE

The ALBA Scientific Advisory Committee (SAC) is a board of internationally renowned experts in the field of synchrotron radiation, which participates in the strategic scientific management of the ALBA Synchrotron with the aim of ensuring the quality and relevance of the research developed in ALBA.

These are its members in 2014:

JOHN HELLIWELL, CHAIR

.....
Professor of Structural Chemistry at the University of Manchester (UK).

OLIVER BUNK

.....
Head of Laboratory for Macromolecules and Bioimaging of the Swiss Light Source (PSI), Switzerland.

ANDY FITCH

.....
Head of ID31 beamline High-resolution Powder Diffraction Beamline of the European Synchrotron Radiation Facility (ESRF), France.

PETER GUTTMANN

.....
X-ray microscopy beamline scientist at U41-XM (BESSY II), Germany.

ANDREAS JANKOWIAK

.....
Director of the Institute of Accelerated Physics at the Helmholtz Zentrum Berlin, Germany.

AMOR NADJI

.....
Director of Sources and Accelerators Division at Soleil Synchrotron (France).

SAKURA PASCARELLI

.....
Head of ID24 beamline Energy dispersive X-ray Absorption Spectroscopy of the European Synchrotron Radiation Facility (ESRF).

ENRIQUE ORTEGA

.....
Full permanent professor of the Universidad del País Vasco, Department of Applied Physics I, Spain.

IAN ROBINSON

.....
Full permanent professor of the London Centre for Nanotechnology, UK.

NICK TERRILL

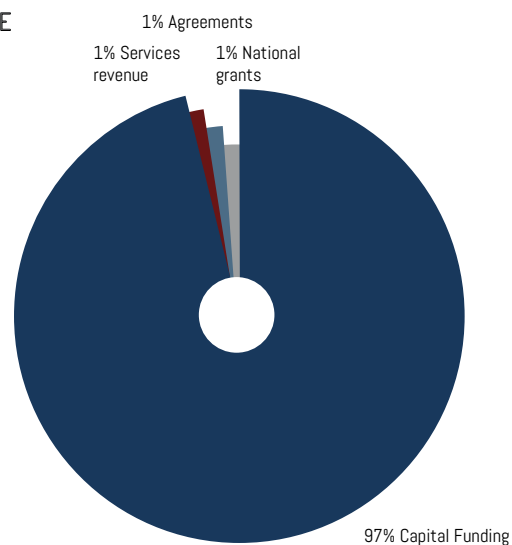
.....
Principal Beamline Scientist of the Small Angle beamline I22 of Diamond Light Source, UK.

FINANCIAL INFORMATION

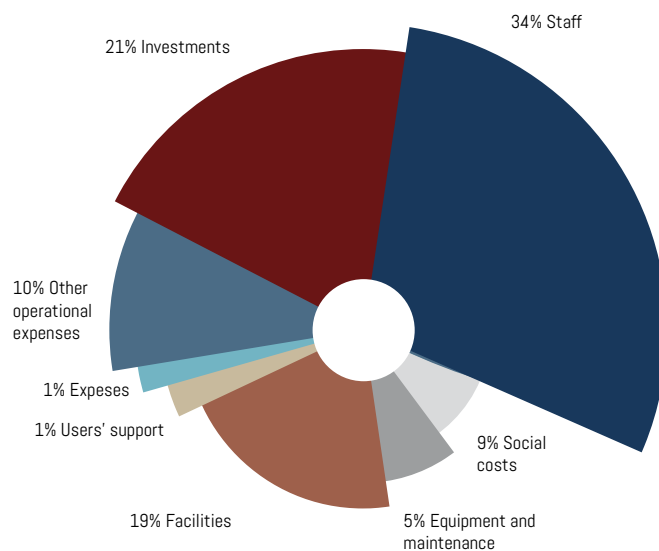
INCOME		
Capital Funding	17,514,949	96.92%
Services revenue	122,961	0.68%
Agreements	157,935	0.87%
National grants	233,145	1.29%
European grants	13,299	0.07%
Other	29,683	0.16%
TOTAL	18,071,972	100.00%
EXPENDITURE		
Staff	7,507,926	34.35%
Social costs	1,888,266	8.64%
Equipment and maintenance	1,051,845	4.81%
Facilities	4,171,988	19.09%
Taxes	40,590	0.19%
Financial costs	80,464	0.37%
Users' support	232,717	1.06%
Students grants	37,439	0.17%
Expenses	267,320	1.22%
Other operational expenses	2,062,631	9.44%
Investments	4,514,351	20.66%
TOTAL	21,855,537	100.00%

*The difference between income and expenditure is funded by previous years' remains.

2014 INCOME



2014 EXPENDITURE





ALBA Synchrotron - Carretera BP 1413, de Cerdanyola del Vallès a Sant Cugat del Vallès, Km. 3,3
08290 Cerdanyola del Vallès, Barcelona, Spain - Tel: +34 93 592 43 00 - www.albasynchrotron.es